Università degli Studi di Trento
Facoltà di Scienze Matematiche Fisiche e Naturali
Dottorato di Ricerca in Fisica - PhD in Physics

TESI DI DOTTORATO

THE STUDY OF SURFACE TENSION WITHIN THE RANDOM FIRST-ORDER THEORY OF GLASS TRANSITION

Relatore - Supervisor:
Dr. *Paolo Verrocchio*

Dottorando - Candidate:
Giacomo Gradenigo

NOVEMBRE 2009

Contents

Chapter 1

Introduction

It is well-known that a liquid is almost incompressible but it cannot support any shear stress: we can fill with it a vessel of whatever shape. Differently a solid is something with a finite shear modulus. That is, dependig on our effort, it resists any attempt to change its shape, until it eventually breaks up.
For any given material, the melting point, for fixed pressure and volume, is placed at a well-defined critical temperature T_m: when the system is cooled below this temperature, molecules or atoms organize themselves on a regular lattice. The phase transition from liquid to solid state is characterized by the onset of crystalline order.
For a wide variety of liquids it is possible —for instance quenching fast enough below the melting point— to reach solid-like behaviour continuously, i.e., without the onset of any kind of crystalline order or discontinuity in volume or energy. The system ends up in a mechanically stable but disordered state of matter: glass. It is customary to mean, by the term *laboratory glass transition*, not a thermodynamic transition, but rather temperature T_g, where the viscosity of a liquid reaches the conventional value of 10^{13} poise and the system behaves for all practical purposes like a solid. As mentioned in a review on the phenomenology of glass-forming liquids [1], empting a cup filled with a liquid just above its glass transition, i.e., with a viscosity of 10^{12} poise, would take nearly 30 years! The specific heat of a glass is similar to that of the crystal, and the only relevant degrees of freedom, much like what happens in the crystal, are the vibrations of particles around their (disordered) equilibrium positions. Nevertheless, within the glass phase two-times correlation functions are found to violate time translational invariance, which is the characteristic feature of a true thermodynamic equilibrium phase. Although glass *seems* to be at equilbrium, it is not.

Without going into greater depth in the study of the glass phase and its properties, let us focus on the supercooled liquid phase —an equilibrium phase— which can be found between melting point T_m and the glass transition T_g. Within the supercooled liquid phase, the relaxation time of the system grows by 12-14 decades under a temperature change of factor 3. The efforts of theories competing in describing the glass transition are actually devoted to deriving this huge increase of relaxation time from first principles and link it to a growing length-scale of the system.
Since Goldstein [2], the low-temperature critical slowing down of glass-forming liquids is believed to be due to the onset of a very frustrated energy landscape, characterized by an exponential number of local minima. But, is the energy landscape not always the same at all temperatures? Of course it is, but different regions of it are typically sampled by

the system at various temperatures. At low temperature, the system spends a long time near the bottom of valleys in the energy landscape, until eventually, due to thermal fluctuations, it hops to another valley. This is how the whole phase space is explored in the supercooled liquid regime. The lower the temperature, the higher the barriers between neighbouring valleys and the less the thermal drive: relaxation time in fact increases. The following questions have challenged physicists for decades:
1) Is there any real thermodynamic transition behind the *laboratory glass transition*?
2) Is there any growing length-scale in the system that can reasonably explain the increase in relaxation time?
3) How can the rather ideal picture of hopping between energy minima be translated in real space?
A belief that dates back to Goldstein is that the transition from one minimum to another is in some sense "local", i.e, *in the rearrangement process leading from one minimum to a "nearby" one, most atomic coordinates change very little, and only those in a small region of the substance change by an appreciable amount. [2].* This seminal idea has been fully developed by the Random First-Order Theory (RFOT) of glass transition [3, 4].

While the relaxation time of a supercooled liquid increases by orders of magnitude, no relevant changes are found in the Van-Hove pair correlation function, which measures the correlation between density fluctuations at different positions.
The definition of a static non-trivial length-scale in supercooled liquids had its main source of inspiration precisely in the landscape scenario first depicted by Goldstein. All the configurations belonging to the same basin of potential energy, i.e., mapped into the same minimum by following the steepest descent path, can be regarded as realizations of the same amorphous state [5]. We can then ask whether the whole system is stable in a single amorphous state. According to the Random First-Order Theory (RFOT) of glass transition, the characteristic length-scale ξ_{RFOT} of a supercooled liquid is exactly the maximum length-scale up to which a single amorphous state is stable [4]. A minimum of the potential energy is a function of the coordinates of *all* particles: it is therefore puzzling, having isolated a bunch of neighbouring particles in the liquid, to state wheater their positions are typical of one minimum or another. Let us for a moment define the order parameter of an amorphous system as a function which takes different values in the different minima of free-energy. This is true, for example, in a magnetic system: the two minima of the free energy at low temperature are characterized either by positive or negative magnetization. A measure of magnetization always tell us the amount of the two phases present in each portion of the system. Let us label each minima of the energy landscape of a liquid with a different colour. Then, let us imagine that each bunch of particles of the supercooled liquid can be coloured according to the minima from which they come, assuming that this could be recognized in some way. If such an ideal operation could be done, according to RFOT, the supercooled liquid would appear as a mosaic, with many tesserae of different colors. They would also be of different sizes, but one size would dominate, the characteristic length-scale ξ_{RFOT} of the liquid. This is the meaning of regarding ξ_{RFOT} as the maximum length-scale up to which a single amorphous state is stable.
Unfortunately, an order parameter that allows us to distinguish the amorphous configurations visited by the supercooled liquid —the colour of mosaic tesserae in the former example— is not available. The severe limitation of working with amorphous systems is that we cannot label different phases; we can only say, comparing two pieces of the system, whether they belong to the same phase or not. From this point of view, it would

be hopeless to check whether a supercooled liquid is a mosaic of amorphous phases or not. Nevertheless, there is also good news from RFOT. According to this theory, the interfaces between different phases —boundaries between mosaic tesserae— have a well-defined surface tension: the higher the surface tension, the higher the difference between the amorphous phases. That is, in the mosaic picture, the higher the colour contrast between neighbouring tesserae, the higher the surface tension. Moreover, according to RFOT, this mosaic is not *static*: new tesserae appear continuously, replacing those already existing, i.e., new droplets of amorphous phases are continuosly forming and relaxing: this is how the whole phase space is explored. The characteristic time τ of the system is that needed by a new tessera to appear within the mosaic: clearly, τ depends on size ξ_{RFOT}. A less pictorial and more rigorous definition of RFOT will be given in sec. 2.4.1.
With this picture in mind, the aim of the work presented in this thesis is to elaborate a numerical method to measure the surface tension between the amorphous phases of a supercooled liquid, in order to test the mosaic scenario. RFOT theory provides exact predictions on the relation between length-scale ξ_{RFOT} and surface tension [4, 6], which can be tested with a direct measure of the latter. Moreover, in the absence of *colours* in the mosaic, i.e., lacking an order parameter suitable for recognizing the various phases, a positive measure of surface tension can be regarded as the landmark that distinct amorphous phases truly coexist in the supercooled liquid.
Also, assuming surface tension as the order parameter signalling the co-existence of phases, it is possible to study the relaxation of amorphous droplets —the time needed by one tessera of mosaic to be replaced by a new one— and thus to check the relation between relaxation time τ and characteristic length ξ_{RFOT} provided by RFOT.

The static length-scale ξ_{RFOT} is the only one defined in the deeply supercooled regime, where the slow dynamics is ascribed to the frustrated energy landscape. At higher temperatures, the amorphous states merge into each other —the contrast between mosaic tesserae becomes more and more damped, until no border can be recognized any longer and the whole system has merged into a single state: ξ_{RFOT}, should it still exist, would be irrelevant. At these higher temperatures another length-scale appears, ξ_{DYN}, which in principle has nothing to do with the "many states" mosaic picture: it is the characteristic size of dynamically cooperative regions. That is, due to the close packing of particles in the supercooled regime, the motion of one particle over a distance comparable to its diameter should require many of its neighbours to move in concert, in order to create a space large enough for the particle to move into. It is customary to speak about this clustering of particles, into regions more or less dynamically active, using the term *dynamical heterogeneities*. The behaviour of the dynamic length-scale ξ_{DYN} is well described, e.g., by the theory of critical dynamics [7] in kinetically constrained models (CKM) [8] and also by the Inhomogeneous Mode Coupling Theory [9, 10]. These theories compete with or are at least complementary to RFOT. According to RFOT, the sluggish dynamics of supercooled liquids is the manifestation of a thermodynamic singular point below T_g, whereas, according to the dynamical theories mentioned above, the slowing down of glass-forming liquids is due to a critical point in the dynamics. Dynamic ξ_{DYN} and static length-scale ξ_{RFOT} are in principle well-defined at different temperature intervals, the lowest being that of ξ_{RFOT}. Nevertheless, there is also evidence of a small interval of temperatures, centered around the mode coupling temperature, where the two length-scales compete [11, 12].
This thesis also presents a new numerical procedure aimed at finding a common origin

for these two completely different defined lenght-scales, i.e., fixed overlap dynamics. It aims at exploiting the possibility that the dynamical length-scale behaves differently if interfaces with well-defined surface tension are present or not between dynamically cooperative regions.
On one hand, the finding of a shared similarity between static and dynamic excitations, i.e. surface tension, would be a step forward in understanding the physics of glass-forming liquids; on the other hand, a measure carried out with a different protocol, would be a different check on the existence of a finite surface tension in supercooled liquids.

All the original work on surface tension between RFOT excitations presented in this thesis is based on ideas of A. Cavagna, T. S. Grigera and P. Verrocchio. The study of surface tension by means of fixed overlap dynamics is based on an idea of G. Parisi. I owe a lot to all of them and I am happy to thank them. In particular I would like to thank C. Cammarota, with whom I collaborated to obtain here presented results.

Grateful thanks for discussion and comments to G. Biroli, E. Ferrero, I. Giardina, M. Montagna, A.C. Ribeiro-Teixeira, F. Simini, P. Sollich and G. Viliani.

Chapter 2

Glass transition in supercooled liquids

According to Random First-Order Theory (RFOT) of glass transition, the increasing time-scale observed in supercooled liquids at low temperatures is linked to the increasing length-scale of the cooperative rearrangements needed to relax the system, as noted for the first time in the Adam-Gibbs theory [13].
These rearrangements of particles are regarded as amorphous excitations separated by interfaces with a well-defined surface tension. This surface tension has never been directly observed, although it plays a crucial role in determining the typical size and time over which amorphous excitations form and relax. The work of this thesis focuses on the surface tension between the amorphous excitations of RFOT.

2.1 Glass transition

To introduce the problem of glass transition in supercooled liquids, let us first consider the data in fig.2.1: here, the low-temperature behaviour of viscosity is plotted for various glass-forming liquids. According to a phenomenological definition, glass transition takes place at temperature T_g, where the viscosity of a supercooled liquid reaches 10^{13} poise. In this regime, for all practical purposes viscous liquids behave like solids, even though they do not display any crystalline order. The increase in viscosity in these systems is directly proportional to the increase in relaxational time τ. For some glass-forming liquids (strong liquids), τ grows at low temperatures following the Ahrrenius law:

$$\tau = \tau_0 \exp(A/T), \tag{2.1}$$

where A is a factor weakly dependent on temperature (straigth lines in fig.2.1). For the majority of glass-forming liquids, the increase in τ is well fitted by a super-Arrhenius law:

$$\tau = \tau_0 \exp(A/(T - T_{VF})), \tag{2.2}$$

called the Vogel-Fulcher-Tamman law: these are fragile liquids. The viscosity of fragile liquids is shown in fig.2.1 by the curves which display a crossover in their slope just above T_g. The VFT law states the divergence of τ at finite temperature T_{VF}, the Vogel-Fulcher temperature, which can be obtained from data extrapolation and is always below T_g. One of the main problems in the physics of glass-forming liquids is wheather the divergenge

of τ at a finite temperature predicted by the VFT law is the signature of an underlying thermodynamic singularity. Leaving for a subsequent discussion the nature of the possible thermodynamic singularity at T_{VF}, let us concentrate here on the abrupt increase in relaxation time observed in fragile glass-formers above T_g. Is there any theoretical scenario which can capture this peculiar behaviour ?

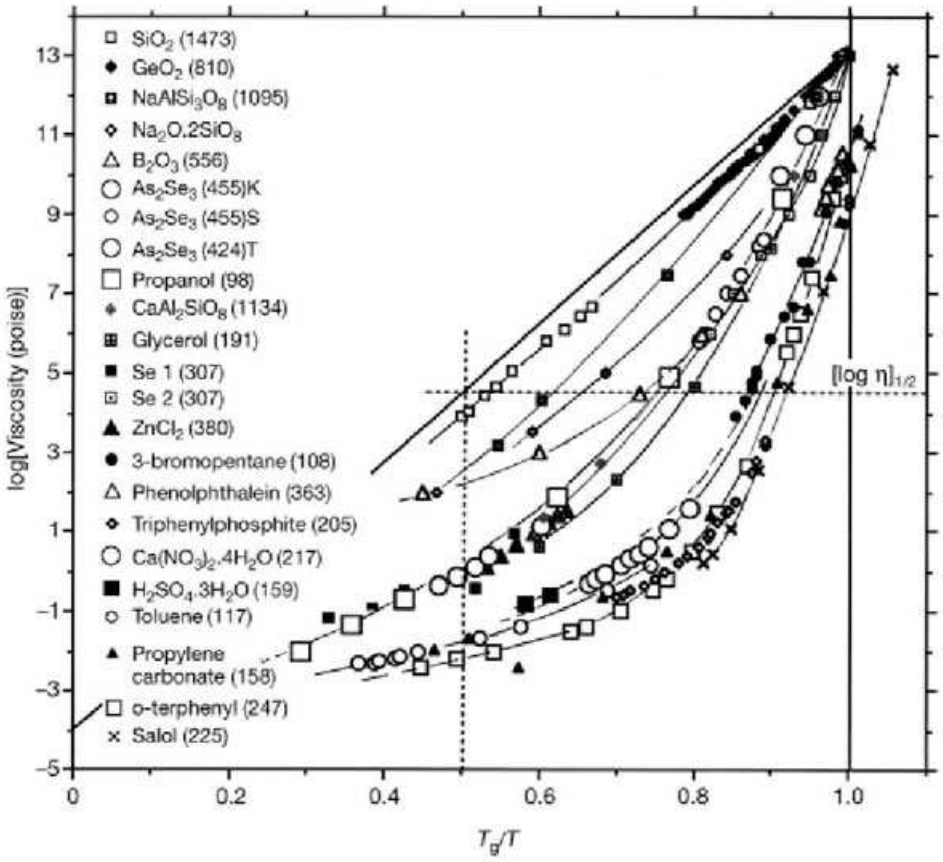

Figure 2.1: *Log of viscosity (y-axis) vs. T/T_g (x-axis) for different glass-forming liquids. Strong liquids, $\eta \sim \exp(A/T)$, straigth lines. Viscosity has a steeper increase near T_g for fragile liquids, $\eta \sim \exp(A/(T - T_{VF}))$.*

2.2 Mode coupling theory and p-spin

Mode coupling theory The Mode Coupling Theory (MCT) [14] is the best established theory describing the dynamical crossover observed in fragile systems. Fig.2.1 does show that, at a certain temperature, the viscosity curve bends (the same is true for relaxation time τ), marking a crossover from a slow to a much steeper increse in viscosity (relaxation time).
The signature of a qualitative change in the relaxational dynamics of the system approaching T_g comes from study of dynamical correlation function $C(t)$. This is generally defined in a liquid system as:

$$C(t_1, t_2) = \frac{1}{N} \sum_{k=1}^{N} \langle \varphi_k(t_1) \varphi_k(t_2) \rangle, \tag{2.3}$$

where $\varphi_k(t)$ is a generic quantity relative to particle k, observed at time t. Due to time translational invariance, the system is at equilibrium, this correlation function depends only on the difference of times, $t = t_2 - t_1$, and can be rewritten as:

$$C(t) = \frac{1}{N}\sum_{k=1}^{N}\langle\varphi_k(t)\varphi_k(0)\rangle, \tag{2.4}$$

In liquids, a typical choice for $\varphi_k(t)$ is the Fourier transform of the density fluctuations of a tagged particle k, $\delta\rho_k(\mathbf{q},t) = \exp[-i\mathbf{q}\cdot\mathbf{r}_k(t)]$, at fixed momentum $\mathbf{q}$. In this case, dynamic correlation function $C(t)$ coincides with incoherent intermediate scattering function $F_s(q,t)$ [15], which is normally measured in experiments. In systems other than liquids, $\varphi_k(t)$ may be any meaningful observable carrying a real space label (particle or spin). Correlation function $C(t)$ measures how quickly correlations within the system decay in time. In the high-temperature phase of a liquid, i.e. $T >> T_g$, $C(t)$ displays standard exponential decay:

$$C(t) = C_0\ \exp(-t/\tau)\ . \tag{2.5}$$

In this regime only one time scale, τ, is present in the system. If the temperature of the liquid is lowered to T_g, correlation function $C(t)$ develops a plateau (see fig.2.2), and two time scales can be identified. Roughly speaking, we can say that there is a fast process

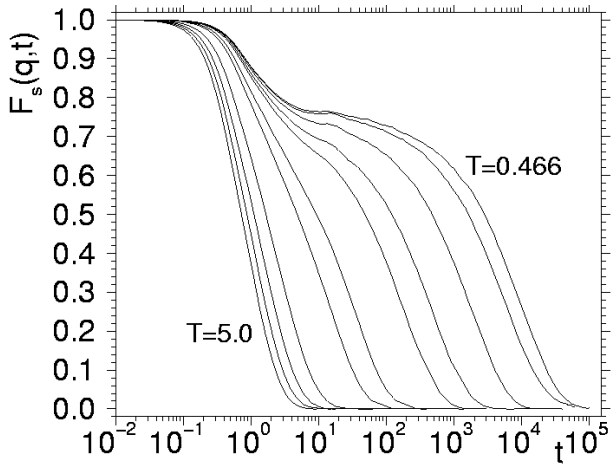

Figure 2.2: **Two steps relaxation** *The dynamic correlation function $C(t)$ in a Lennard-Jones system. In this case $C(t)$ is the incoherent intermediate scattering function $F_s(q,t)$, evaluated at the value of q where the static structure factor has the main peak. At high temperatures the decay is exponential, but when the temperature get close to T_g a plateau is formed and relaxation proceeds in two steps. Figure from [16].*

describing the relaxation of $C(t)$ to the plateau, and a slow process due to the decay of $C(t)$ from the plateau. Conventionally, these two processes are respectively called β (fast) and α (slow) relaxation.
The structure of $C(t)$ clearly indicates that there is a separation of time-scales: the lower the temperature the sharper the separation, and this is the qualitative landmark of glassiness.
The two-step relaxation of $C(t)$ described above can been obtained from MCT equations. These are equations for the time correlation of density fluctuation in a liquid derived by means of the Zwanzig-Mori projection formalism [17, 18]. The latter is a theoretical

scheme used to perform coarse graining of fast degrees of freedom in the dynamical equation describing a liquid system. This method allows us to write a set of self-consistent equations for $C(t)$, which, under some approximations [19], may be closed to the single equation:

$$\partial_\tau^2 C(t) + \Omega^2 C(t) + \nu \partial_\tau C(t) + \Omega^2 \int_0^\tau du F\left[C(\tau - u)\right] \partial_\tau C(t) = 0, \qquad C(0) = 1 \tag{2.6}$$

where Ω is a model-dependent frequency, and the precise form of kernel $F\left[C(\tau - u)\right]$, which is a function of $C(t)$, depends on the approximations used to close the set of MCT equations. The solution of eq.(2.6) depends on temperature. Accordingly there is a critical temperature, $T_c > T_g$, where the ergodicity is dynamically broken, i.e. the time correlation function does not decay to zero at infinite time $C(t = \infty) \neq 0$. Approaching T_c from above, $C(t)$ develops a plateau and two time-scales can be resolved, just as in real liquids. The height of the plateau is associated to non-ergodicity parameter f, and the regimes where $C(t)$ relaxes to the plateau and decay from it are well described by the following formulas:

$$C(t) = f + \left(\frac{t}{\tau_\beta}\right)^a \tag{2.7}$$

$$C(t) = f - \left(\frac{t}{\tau_\alpha}\right)^b \tag{2.8}$$

where τ_β and τ_α are the two time-scales over which $C(t)$ respectively relax to the plateau and decays from it. These time-scales actually correspond to β, fast, and α slow, as mentioned above. Although eq.(2.6) predicts the two-step relaxation observed in supercooled liquids, it cannot describe the supercooled liquid regime at all temperatures. According to MCT the length of the plateau at T_c becomes infinite, that is it diverges with a power law:

$$\tau_R \sim \tau_\alpha \sim \frac{1}{(T - T_c)^\gamma} \tag{2.9}$$

This is a spurious dynamic singularity, beacause glass-forming liquids are still able to relax within observation times at T_c, T_c being above T_g. Thus, the whole range of temperatures $T_g \leq T \leq T_c$ is not covered by mode coupling predictions.

An indication of what is happening in this temperature regime comes from the analogy between mode coupling theory and the dynamics of a particular class of spin glass models, p-*spin* models. A definition of the correlation function similar to that of eq.(2.4) can also be given for a spin system:

$$C(t_0, t_0 + t) = \frac{1}{N} \sum_{k=1}^{N} \langle \sigma_k(t_0) \sigma_k(t_0 + t) \rangle. \tag{2.10}$$

The dynamical equation for $C(t)$, calculated analitically within p-*spin* , is formally identical to that obtained within MCT [20, 21], i.e. eq. (2.6). It also provides the same predictions for $C(t)$, i.e. the existence of two-step relaxation and critical temperature T_c, at which the length of the plateau diverges, $C(t = \infty) \neq 0$. The common opinion is that, below T_c, the relaxation of the liquid goes through activated processes , which are not captured by the dynamical equation of MCT.

As these activated processes are the cornerstone of Random First Order theory, it is worthwile depicting a clearer scenario for the crossover at T_c. This can be done by studying what happens at T_c in p-*spin* models.

Topological crossover in p-*spin* . In p-*spin* models, the ergodicity breaking at T_c is related to a topological crossover in the energy landscape. The energy landscape of a system is of course always the same and does not depend on temperature. Nevertheless, depending on temperature, the system explores different regions of that landscape. For p-*spin* [22, 23] it has been shown that, approaching T_c, dynamical arrest occours beacause the system is trapped in local minima of the energy. p-*spin* is a model in which interactions have infinite range, the barriers between minima are also infinite, so that, as soon as the minima start to dominate the energy landscape, they can trap the system for an infinite time. Moreover, according to [22, 23], the dynamics above T_c is ruled by saddle points. Actually, at temperatures $T \geq T_c$, the system relaxes rolling down unstable directions of the stationary points of energy. It is the rarefaction of these unstable directions on approaching T_c which produces two-step relaxation and divergence of the plateau [22, 23]. Let us imagine a stationary point with only a few unstable directions, i.e., those typically visited by the system at temperatures slightly above T_c. The relaxation of $C(t)$ to the plateau (β relaxation) corresponds to the relaxation within the attraction basin of the stationary point, which has positive curvature along most directions. This process is fast. More time is needed by the system to find its way through one of the rare unstable directions, this is the time when $C(t)$ decays from the plateau (α relaxation). An ample description of this scenario is found in [24], together with many references on topological crossover in p-*spin* .

The crossover from a saddle-dominated to a minima-dominated energy landscape at T_c clarifies the role of activated events below T_c: in principle, they should be responsible for hopping between minima. In p-*spin* , this hopping is clearly impossible, due to the infinite barriers between minima: a dynamic singularity is found at T_c, just as mode coupling equations indicate.
Nevertheless, it is now clearer which feature of glass-forming liquids, which always have finite range interactions, can give insight on low-temperature dynamics. This feature is the structure of the potential energy landscape (PEL).

2.3 Topological crossover in supercooled liquids

Dynamical crossover and PEL. In this thesis, I present results on measuring the surface tension between the local amorphous excitations that arise within RFOT theory. My aim is to highlight some evidence that this surface tension is operatively well defined only when the potential energy landscape (PEL) of the system is dominated by minima. Hence, a brief overview of some previous results concerning the relationship between the slowing down of dynamics and the properties of PEL [2, 25, 26, 27, 28] must be made.
The idea of a link between the slowing down of dynamics and a topological crossover in the energy landscape dates back to Goldstein [2], according to whom, at sufficiently low temperatures, the PEL develops a huge number of local minima in which the system can easily be trapped for a long time. When the system enters this regime, a dramatic increase in relaxation time is observed.
At variance with p-*spin* models, mentioned above, the barriers between minima are always finite and the relaxation time, albeit long, is finite. The properties of the system at a given temperature are dictated by the basins sampled and their mutual accessibility [25], i.e., the height of the barriers separating the minima. Numerical evidence of the connection between the slowing down of dynamics in a glass-forming liquid and a crossover in the

energy landscape was noted for the first time by Sastry et al. [25]. They showed that the depth of PEL minima reached by quenching thermal configurations, i.e., following the steep descent path along the PEL surface, strongly depends on temperature T when T is below a certain threshold, $T \leq \hat{T}$. The above authors also found that the increase in relaxation time, measured in the same system, becomes faster than the simple Ahrrenius-like behaviour $\tau \sim \exp(A/T)$ precisely when T falls below threshold $\hat{T}$. From this, the authors concluded that the dynamical crossover is a signature of the underlying topological crossover in PEL.

Saddle-minima crossover The crossover to the low-temperature regime where dynamics is dominated by PEL minima is identified when two clearly separated time-scales can be resolved in the system [2, 26]: time scale τ_{intra} of *intra-basin* relaxation, which is the shorter and concerns vibrations around a minimum; and *inter-basin* relaxation time τ_{inter}, which is the time-scale of hopping between different basins.
We can state that τ_{intra} corresponds to time-scale τ_β of β relaxation, because both identify the time-scale of vibrations within a minimum. The same correspondence cannot be drawn between τ_{inter} and τ_α, as the former is defined as the time needed to jump a barrier, and the latter as the time needed to find an unstable direction.
Nevertheless, it is useful to think of critical temperature T_c, introduced when mentioning mode coupling and p-*spin* , as the temperature when the longest time-scale of the system passes from being τ_{inter}, defined below T_c, to being τ_α, defined above T_c. Above T_c, the longest time-scale is the time needed to find an unstable direction of a stationary point of PEL; below T_c, it is the time needed to hop from one minimum to another. The dynamics of the system can really be understood [26, 27] from the topology of the stationary points of PEL typically visited at a certain temperature.
Unfortunately, finding the saddle-minima crossover as a function of temperature is not as straighforward as we would like. The problem is that the mapping between equilibrium configurations and saddle points is not well defined [28]. The *saddle-minima* transition can only be defined properly as a function of the *energy* of stationary points of PEL.
Let us define $K(e)$ as the number of unstable directions of a stationary point with energy e. In order to find where the saddle-minima crossover is, we must consider the behaviour of the instability index:

$$\langle K(e)/N \rangle = \langle k(e) \rangle, \tag{2.11}$$

where the brackets $\langle\rangle$ indicate the average over a population of stationary points at the same energy, and N is the number of degrees of freedom of the system. Threshold energy e_{th} is defined as the energy where the instability index vanishes:

$$< k(e_{th}) >= 0. \tag{2.12}$$

As explained in [28], the vanishing of the instability index does not imply that unstable stationary points cannot be found below the threshold. It only means that, below e_{th}, saddles are subdominant with respect to minima: $\mathcal{N}_{saddles}/\mathcal{N}_{minima} \to 0$ in the thermodynamic limit. From the thermodynamic point of view, this means that, although unstable directions are present at energies below e_{th}, the system has an overwhelming probability of relaxing by hopping a barrier.

If we define the crossover as a function of temperature, then we must consider the energy of Inherent Structures instead of that of saddle points. We are forced to do this, because there is a well-defined map between equilibrium configurations and IS, whereas

this correspondence is lacking between equilibrium configurations and saddles. Given a configuration equilibrated at T, its energy is linked to that of the underlying Inherent Structure, i.e., minimum, by the relation:

$$e_{TH} = e_{IS} + \frac{3}{2} k_B T, \tag{2.13}$$

where e_{TH} is the energy of the equilibrium configuration and e_{IS} that of the inherent structure.

Thus, if we know the temperature, we also know the energy of the underlying minima. The threshold temperature can therefore be defined as that where the energy of the underlying minima is e_{th}. In [27], threshold temperature T_{th} was computed in this way, and was found to be equal to MCT temperature T_c computed for the same system.

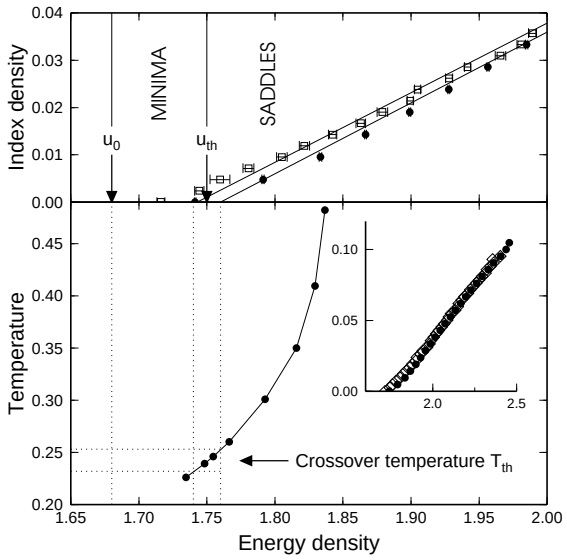

Figure 2.3: *Top: Average instability index density k vs. potential energy density u of the stationary points. Bottom: Temperature vs. equilibrium bare potential energy density, $u_b = u_{eq} - 3/2\ k_B T$. Figure is from [27].*

The subtlety in the identification of threshold temperature T_{th} is that, on one hand, we define e_{th} from the instability index of saddles; on the other, we rely on the correspondence between equilibrium configurations and minima to find T_{th} from our knowledge of e_{th}. The estimate of T_{th} must be always regarded with some circumspection. Thus, even if the MCT temperature is certainly closely related to the topological crossover, in our opinion it is safer to regard this crossover mainly as a function of the energy of stationary points.
I mention that the most recent paper on this subject [28] gave an updated value of e_{th} slightly larger than that obtained in [27].
Is it therefore possible that threshold temperature T_{th}, wherever we want to define it, may lie above the mode coupling one T_c ?
I will come back to this point when presenting numerical results on surface tension in the last chapter.

There is another piece of information contained in [27] which is of particular interest for the results I will discuss in this thesis. It is the direct measure of how barriers between IS increase as the energy of IS falls (see fig.2.4). These barriers are actually

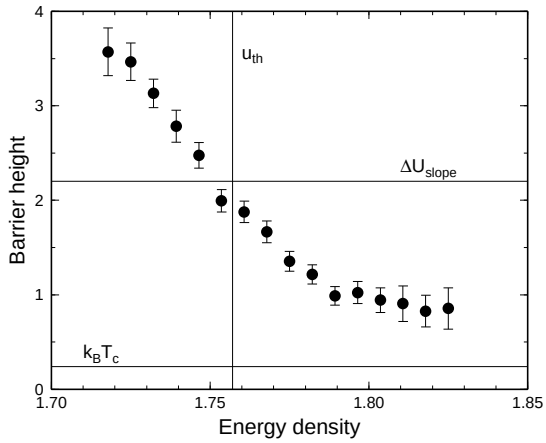

Figure 2.4: *Average potential energy barriers as a function of the potential energy density of the adjacent minimum. Figure is taken from [27].*

negligible compared with the sum of the thermal energy of all the particles within the system (fig.2.4). Nevertheless, as first pointed out by Goldstein [2], the rearrangement that allows the system to overcome a barrier concerns a finite amount of particles, so we may think that these barriers are still important. Leaving the landscape scenario with the feeling that *local* rearrangements of particles are required to overcome the barriers between minima seems to me the best way of introducing the Random First-Order Theory.
Indeed, as soon as we start to speak about *local rearrangements* , two compelling questions arise:
1) What is the typical length-scale of these rearrangements?
2) How does this length depend on temperature ?

2.4 Thermodynamic glass transition

Kauzmann entropy crisis. If we aim to cast the slowing down of supercooled liquids in a scenario with a thermodynamic singularity, the first step is to relate Vogel-Fulcher temperature T_{VF}, introduced in eq.(2.2), with Kauzmann temperature T_K. Kauzmann was the first to note [29] that a supercooled liquid has always a heat capacity, C_p, larger than that of the corresponding equilibrium crystalline phase. According to the formula

$$\Delta S(T) = \int_0^T dT \Delta C_p(T)/T, \tag{2.14}$$

where ΔS and ΔC_p are, respectively, the excess of entropy and heat capacity of the liquid phase with respect to the crystalline phase, the entropy of the supercooled liquid decreases faster than that of the crystal. This implies the existence of a temperature, called the Kauzmann temperature, where:

$$\Delta S(T_K) = 0. \tag{2.15}$$

The consequence is that, for $T < T_K$, the entropy of the supercooled liquid phase is less than the crystalline one. Because the entropy of the crystal vanishes linearly with temperature, the supercooled liquid then has negative entropy at zero T. This is in plain contradiction with the definition of entropy as the log of the number of available configurations, and does represent the well-known Kauzamann paradox. To solve this problem,

Kauzmann assumed that, for temperatures $T \leq T_K$ (see fig.2.5), the entropy of the supercooled liquid becomes equal to that of the crystal. It was the thermodynamic theory of Gibbs and Di Marzio [30] which first exploited the possibility of a second-order phase transition at T_K.
This *thermodynamic* transition cannot be observed experimentally because the extrapolated Kauzmann temperature is always below T_g. Nevertheless, we can deduce *how* the difference $S_c = S_{liq} - S_{solid}$ between the extrapolated entropy of supercooled liquid S_{liq} and the entropy of the crystal S_{solid} vanishes at T_K. From the definitions of heat capacity, $dS/dT = C_p$, and of the entropy difference S_c, we can write:

$$S_c(T) - S_c(T_K) = \int_{T_K}^{T} dT \frac{\Delta C_p}{T}, \tag{2.16}$$

where ΔC_p is the difference between the specific heats of the liquid and of the crystal. Assuming that ΔC_p is weakly dependent on temperature [13] and recalling that $S_c(T_K) = 0$, we can write:

$$S_c(T) = \Delta C_p \log\left(\frac{T}{T_K}\right), \tag{2.17}$$

which, in turn, expanding the logarithm for $T \sim T_K$, yields:

$$S_c = S_{liq} - S_{solid} \sim \Delta C_p \frac{T - T_K}{T_K} \tag{2.18}$$

Hence, as first approximation, the entropy difference S_c vanishes linearly at Kauzmann temperature T_K. The low-temperature dynamics of a supercooled liquid, as already mentioned, is characterized by two clearly separated time-scales: that of hopping between minima of potential energy, τ_{inter}, and that of vibrations within a single minimum, τ_{intra}. Similarly, the entropy of the supercooled liquid may be *approximately* written as the sum of two contributions, one *vibrational*, due to vibrations within a single minimum of PEL, and one *configurational*, due to the huge number of different minima which the system can visit: $S_{liq} = S_{conf} + S_{vibr}$. Because vibrational entropy is roughly equal to the entropy of the crystal, $S_{vibr} \sim S_{solid}$, it turns out that $S_c = S_{liq} - S_{solid}$ is configurational entropy. A plain definition of S_c, and more precisely of its intensive value Σ,

$$S_c(T) = N\Sigma(T), \tag{2.19}$$

can be given studying p-*spin* models.

Thermodynamics of p-*spin* . I have already mentioned how, for temperatures $T \leq T_c$, a p-*spin* model is dynamically trapped in an energy minimum. Nevertheless, this minimum has a negligible thermodynamic weight, and the thermodynamic properties of the system are not sensitive to the dynamical transition.
In turn, the existence of well-defined metastable states allows us to write the partition function of the system as the sum of many independent terms:

$$Z = \sum_{\alpha} Z_\alpha = \sum_{\alpha} e^{-N\beta f_\alpha} \tag{2.20}$$

where sum index α labels the different basins that can be sampled by the system at temperature T. The number of these basins is exponential with the size of the system, so

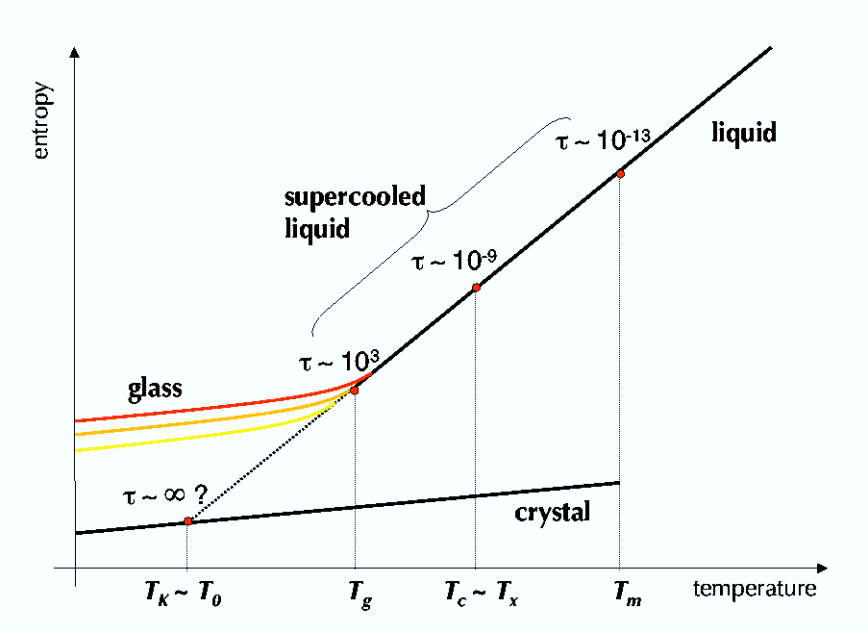

Figure 2.5: *Entropy of the supercooled liquid and of the crystal. The supercooled liquid freezes into an amorphous state (glass) at a temperature which depends on the cooling rate, but always lies above T_K. The glass has an entropy larger than the crystal, this excess entropy being the configurational entropy $S_c = S_{liq} - S_{solid}$.*

that the density of states $e^{N\Sigma(f)} = \sum_\alpha \delta(f - f_\alpha)$ can be introduced in eq.(2.20):

$$Z = \sum_\alpha e^{-N\beta f_\alpha} = \int df e^{N\Sigma(f) - N\beta f}. \tag{2.21}$$

The last integral in eq.(2.21) can be evaluated in the thermodynamic limit by the saddle point approximation. We can then write the Helmholtz free energy of the system as:

$$\Phi = -\frac{1}{N\beta} \log(Z) = f^* - T\Sigma(f^*), \tag{2.22}$$

where f^* is the value of f which minimizes $\beta f - \Sigma(f)$. f^* is the free energy due to vibrations within a single basin, and $T\Sigma(f^*)$ is the entropic contribution that counts the number of basins. In p-*spin* , there is a certain temperature T_0 below the dynamic transition, $T_0 < T_c$, where configurational entropy vanishes. At this temperature, there is a thermodynamic transition, where ergodicity is broken even at the thermodynamic level.

Once again p-*spin* represents the paradgmatic model for what happens in supercooled liquids. The thermodynamic transition placed at T_0 clarifies the meaning of the Kauzmann transition at T_K. At the transition temperature, T_0 in p-*spin* and T_K in supercooled liquids respectively, configurational entropy Σ vanishes. Moreover, in p-*spin* , we can *exactly* define Σ as the number of "amorphous states" sampled by the system when it is in the ergodic phase, which corresponds to the supercooled liquid phase.

2.4.1 Random First-Order Theory

The nucleation paradigm.

Compelling evidence that a thermodynamic phase transition exists in supercooled liquids at T_K is still lacking. Nevertheless, a theory that relates growing time-scales to growing

length-scales is needed.

The Random First-Order Transition theory (RFOT) was directly inspired by the phenomenology of p-*spin* models. This analogy was exploited in a series of papers of the 1980s by Kirkpatrick, Wolynes et al. [3, 31]. They elaborated a theory, RFOT, in which the increase of a characteristic lenght-scale ξ_{RFOT} in the supercooled liquid is due to a decrease of configurational entropy Σ. To understand the low-temperature dynamics of a supercooled liquid, we need a mechanism able to describe hopping between potential energy minima. According to RFOT, this mechanism is given by the same kind of *local cooperative rearrangements* described by Goldstein in 1969 and by the Adam-Gibbs theory [13]. What is new in the RFOT theory of [3] is the nature of the entropic force which drives these *cooperative* rearrangements and the existence of *surface tension* between different cooperative regions.
The main assumption of RFOT is that, at low temperature, not only does the system *as a whole* have an exponential number of states available, $\mathcal{N} \sim \exp(N\Sigma)$, but also each finite portion of linear size R has $\mathcal{N}(R) = \exp(\Sigma R^d)$ target states available. Each rearrangement of a size R region amounts to the entropic gain ΣR^d. But what is the typical length-scale of rearrangements at a given temperature?
At each temperature, the typical length-scale ξ_{RFOT} is given by the balance between free energy gain $T\Sigma R^d$ and *surface cost* ΥR^θ. Because the cooperative rearrangement happens independently of the position of other particles in the surroundings, there is generally an energy cost to be payed, due to the mismatch with boundaries: ΥR^θ . That is, a region of linear size R, in order to be rearranged, must overcome the free energy barrier:

$$\Delta F = \Upsilon R^\theta - T\Sigma R^d. \tag{2.23}$$

From this assumpion, directly inspired by the nucleation mechanism in first-order phase transition, the critical length-scale of the system follows from balancing of entropic gain $T\Sigma R^d$ and surface cost ΥR^θ:

$$\xi_{RFOT} = \left(\frac{\Upsilon}{T\Sigma}\right)^{\frac{1}{d-\theta}}. \tag{2.24}$$

This is the first time that surface tension is introduced in the context of supercooled liquids, and it also plays the very important role of determining the critical size of cooperative rearrangements. According to RFOT, the system is fragmented into a large number of regions of linear size ξ_{RFOT}. This is the origin of the name *mosaic*, which is commonly used to refer to RFOT theory. Each *patch* of the mosaic visits the phase space *independently* of all the others. Thus, according to RFOT, the mechanism employed by a supercooled liquid to visit the different minima of the energy landscape is to split in many finite portions, each of which independently visits a different minimum. It is then assumed that the leading time-scale in the system is the characteristic time of cooperative rearrangements over lenght-scale ξ_{RFOT}, which are activated events:

$$\tau = \tau_0 \exp(\Delta F(\xi_{RFOT})/T). \tag{2.25}$$

Hence, the growth of free energy barrier $\Delta F(\xi_{RFOT})$ causes the increase in relaxation time. In turn, free energy barrier $\Delta F(\xi_{RFOT})$ grows with increasing ξ_{RFOT}: this is the basic mechanism which links time—and length—scales in a supercooled liquid.
Near T_K, configurational entropy vanishes linearly, $\Sigma \sim T - T_K$. Moreover, according to [3], a renormalization group argument yields the surface tension exponent, $\theta = d/2$.

Inserting these two ingredients into eq.(2.24) scaling of ξ_{RFOT} near the Kauzmann temperature is obtained:

$$\xi_{RFOT} \sim \left(\frac{1}{T - T_K}\right)^{\frac{2}{d}}. \tag{2.26}$$

In turn, scaling of free energy barrier ΔF follows:

$$\Delta F \sim T\ \Sigma\ \xi^d_{RFOT} \sim (T - T_K)^{-1}, \tag{2.27}$$

By inserting this result into eq.(2.25) we have:

$$\tau \sim \exp\left(\frac{\Delta F}{T}\right) \sim \left(\frac{A}{T - T_K}\right), \tag{2.28}$$

which is the Voghel-Fulcher-Tamman law for relaxation time. This [3] was the first attempt after the Adam-Gibbs theory [13] to establish a quantitative link between the increases of lenght and time-scales in supercooled liquids.

2.4.2 Beyond the nucleation paradigm

The main point that is unclear about the nucleation paradigm introduced by Wolynes is the precise meaning of entropic driving force.
Why should the system increase its entropy by splitting into many regions which are arranged in some kind of amorphous order, independently from each other?
If the entropic gain for each region is $\Sigma\xi^d_{RFOT}$ and the number of regions is V/ξ^d_{RFOT}, then the total configurational entropy of the system, S_c, is independent of the number of regions:

$$S_c = \frac{V}{\xi^d_{RFOT}}\ \Sigma\ \xi^d_{RFOT} = V\Sigma. \tag{2.29}$$

The role of configurational entropy in producing a finite correlation length thus turns out to be still obscure. This point is clarified in the work of Biroli and Bouchaud [4], in which a theoretical framework is set up to characterize the length-scale of mosaic patches ξ_{RFOT} as the maximum length upon which a single metastable state is stable.
To explain how this happens a *gedanken experiment* is proposed in [4]. The whole system is immagined as frozen in a single amorphous state α. This is an equilibrium configuration at the working temperature, which can roughly be identified as a minimum of free energy. Then it is required to equilibrate all the particles in a cavity of linear size R, while all the others are frozen in their positions and act at the boundaries of the cavity as a pinning field. Lastly, what is the probability that particles inside the cavity remain in the same state α or are rearranged to a new state β ?
This construction can be formalized by writing the partition function of a constrained sphere of radius R, where the constraint is given by particles frozen in state α outside the cavity:

$$Z_\alpha(R) = \sum_{\beta\neq\alpha} e^{-\beta f_\beta R^d - \beta\Upsilon R^\theta} + e^{-\beta f_\alpha R^d}, \tag{2.30}$$

where β labels states different from α. For these states the additional free-energy cost ΥR^θ has been considered, which accounts for the mismatch at boundaries with state α. The availability of an exponential number of target states β allows us to introduce a density of states as in eq.(2.21),

$$Z_\alpha(R) = \int_0^\infty df e^{(\Sigma - \beta f)R^d - \beta\Upsilon R^\theta} + e^{-\beta f_\alpha R^d}. \tag{2.31}$$

The aim is to describe the system at temperatures close to the Kauzmann temperature, at which the size of the region which cooperatively rearranges is supposed to be large. This motivates the use of the saddle point approximation in evaluating the integral in the second term in eq.(2.31). With this approximation the partition function can be rewritten as:

$$Z_\alpha(R) = e^{R^d\Sigma - \beta f^* R^d - \beta\Upsilon R^\theta} + e^{-\beta f^* R^d}, \tag{2.32}$$

where f_α has been replaced by f^*, the equilibrium free energy at the working temperature. This can be done because, at a given temperature, all the metastable states have approximatively the same free energy.
The probabilities that particles stay, $p_{in}(R)$, or leave, $p_{out}(R)$, the state that matches boundary conditions are respectively:

$$\begin{aligned} p_{\alpha\alpha}(R) &= p_{in}(R) = \frac{e^{-\beta f^* R^d}}{Z_\alpha(R)} = \frac{1}{1 + e^{R^d\Sigma - \beta\Upsilon R^\theta}}, \\ p_{\alpha\beta}(R) &= p_{out}(R) = \frac{e^{R^d\Sigma - \beta f^* R^d - \beta\Upsilon R^\theta}}{Z_\alpha(R)} = \frac{1}{1 + e^{-(R^d\Sigma - \beta\Upsilon R^\theta)}} = 1 - p_{in}(R), \end{aligned} \tag{2.33}$$

which are, in turn, well approximated by step functions:

$$\begin{aligned} p_{in}(R) &= \frac{1}{1 + e^{R^d\Sigma - \beta\Upsilon R^\theta}} \sim \Theta(R^d\Sigma - \beta\Upsilon R^\theta), \\ p_{out}(R) &= \frac{1}{1 + e^{-(R^d\Sigma - \beta\Upsilon R^\theta)}} \sim 1 - \Theta(R^d\Sigma - \beta\Upsilon R^\theta). \end{aligned} \tag{2.34}$$

Therefore a critical length, $R = \xi_{RFOT}$, naturally arises, connected to the balancing of entropy gain $R^d\Sigma$ and surface cost $\beta\Upsilon R^\theta$, at which the probability $p_{\alpha\alpha}(R)$ to stay in the same state drops from 1 to 0, vice-versa is true for the probability to change state $p_{\alpha\beta}(R)$. The length-scale ξ_{RFOT} so defined is the maximal length up to which a single amorphous state α is stable.
Instead of referring to an "*entropic driving force*", we may simply state that the system changes state thanks to spontaneous thermal fluctuations. When $R < \xi_{RFOT}$, due to *surface tension*, it always ends up by visiting the same state ($p_{\alpha\alpha}(R) \sim 1$), the one which better matches the boundaries. For $R > \xi_{RFOT}$ the exponential number of target states is large enough for the equilibrated droplet to be found in most cases in a new state ($p_{\alpha\alpha}(R) \sim 0$), *despite* surface tension.
Size R of the rearranging region plays the same role of temperature in random-energy model (REM) [32], a paradigmatic model for disordered systems: R (like T in REM) is the parameter which tunes a discontinuous transition from ergodic (large R) to non-ergodic (small R) behaviour.
Within this scenario, the link between increasing length-scale ξ_{RFOT} and relaxation time τ of the system is an open issue. The free energy barrier to cooperative rearrangements is supposed to grow, because of the growing length-scale ξ_{RFOT}, by means of a simple power law scaling:

$$\Delta F \sim \xi_{RFOT}^{\psi}. \tag{2.35}$$

Nevertheless, no hypothesis is made on exponent ψ, which is in turn the key ingredient describing the increase in relaxation time:

$$\tau \sim \exp\left(\frac{\xi_{RFOT}^{\psi}}{T}\right). \tag{2.36}$$

	θ	ψ
RFOT + nucleation	$d/2$	$d/2$
RFOT alone	?	?

Table 2.1: *Predictions for exponents θ and ψ, either assuming or not the nucleation paradigm within RFOT.*

The absence of a precise assumption on the value of ψ is a remarkable difference with Wolynes scenario, in which the nucleation paradigm is assumed, and the exponent ψ is fixed by dimensional analysis of the free energy barrier. That is, assuming $\Delta F = \Upsilon R^\theta - T\Sigma R^d$, we have:

$$\begin{array}{rcl} \Delta F & \sim & \xi^\psi_{RFOT} \\ \Delta F & \sim & \xi^\theta_{RFOT} \end{array} \Longrightarrow \psi = \theta$$

Exponents which control relaxation between length and time. The following is a summary of the different predictions given within RFOT theory for free energy and surface tension exponents, respectively ψ and θ. We compare the point of view in which the nucleation paradigm is assumed and the more general theory of Biroli-Bouchaud [4]. According to both points of view, the following relations are true:

$$\begin{array}{rcl} \Delta F & \sim & \xi^\psi_{RFOT} \\ \xi_{RFOT} & \sim & \left(\frac{1}{T-T_K}\right)^{\frac{1}{d-\theta}} \Longrightarrow \tau \sim \exp\left[\left(\frac{A}{T-T_K}\right)^{\frac{\psi}{d-\theta}}\right] \\ \tau & \sim & \exp\left(\frac{\Delta F}{T}\right) \end{array} \tag{2.37}$$

Wolynes proposes a renormalized exponent for the interface cost [3], $\theta^* = d/2$, so that, if $\psi = \theta^*$, the VFT law is recovered. Biroli and Bouchaud claim that θ and ψ must be estimated independently, and only the inequality $\theta < \psi < d-1$ must be obeyed, according to [33]. The predictions for free energy barrier and surface tension exponents are summarized in Tab.(2.1). In this thesis, I present the numerical method used to give an estimate of both these exponents in a fragile liquid model.

2.4.3 Finite size effects: fluctuating surface tension

The *gedanken experiment* depicted above [4] is suitable to reproduce as a numerical experiment. The idea of measuring the probability that a droplet pinned by a frozen boundary stays/leaves the initial state after equilibration has been translated [6, 34] into the operative definition of a new kind of correlation function: the point to set correlation function. This is actually the overlap, $q_c(R)$, between the initial configuration of the liquid inside the pinned sphere and the one found after equilibration with frozen boundaries. Let us represent α as the amorphous state of the initial configuration. The liquid inside the droplet can either stay in the same state, with overlap $q_{\alpha\alpha} \sim 1$ between final and initial configurations inside that droplet, or change state, with a low overlap $q_{\alpha\beta} \sim 0$. The average value of the overlap measured in the innermost part of the sphere is (see [34] for problems arising in measuring the overlap over the *whole* sphere):

$$q_c(R) = p_{\alpha\alpha}(R) q_{\alpha\alpha} + p_{\alpha\beta}(R) q_{\alpha\beta}. \tag{2.38}$$

From eq.(2.32) one expects that the probability of staying in the same state $p_{\alpha\alpha}$ falls to zero roughly at the same R where the probability of changing state $p_{\alpha\beta}$ jumps to 1. Accordingly, $q_c(R)$ is expected to fall suddenly from 1 to 0 at a critical radius $R = \xi_{RFOT}$, that is when entropic gain compensates surface cost:

$$\Upsilon \xi_{RFOT}^{\theta} = T\Sigma \xi_{RFOT}^{d} \tag{2.39}$$

This is how the simplest version of RFOT predicts a sharp crossover of $q_c(R)$ at $R = \xi_{RFOT}$ [4]. The numerical results of [6] show that this is not in fact what happens: the crossover

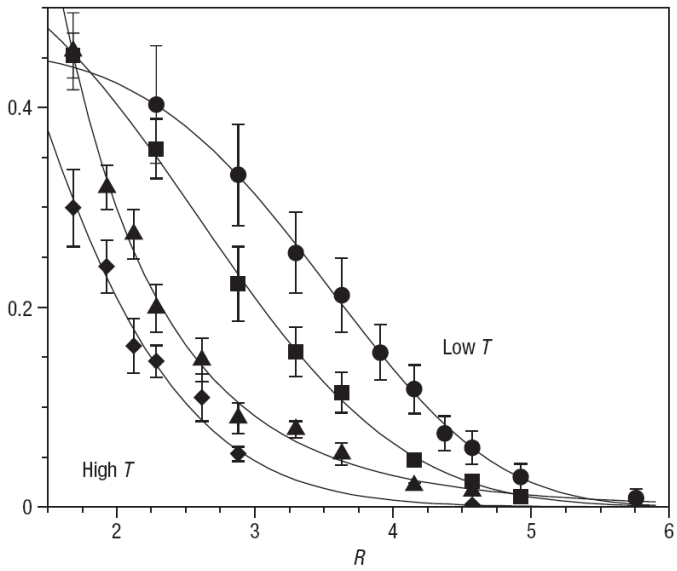

Figure 2.6: *Overlap at the centre of the mobile cavity $q_c(R)$ vs radius R of the cavity, for temperatures $T = 2.13T_c$ (diamonds), $T = 1.55T_c$ (triangles), $T = 1.09T_c$(squares), $T = 0.89T_c$ (circles), with T_c the mode coupling temperature. Lines are fits to eq. (2.45).*

is much smoother than expected. $q_c(R)$ does capture the existence of an increasing length-scale: fig.2.6 shows how the decay of $q_c(R)$ as a function of the size of the sphere becomes slower for decreasing temperatures. The decay of $q_c(R)$ defines a length-scale ξ_{RFOT}, which does increase at low temperatures [6]. Nevertheless, this decay is not as sharp as expected from the original theory (cfr. eqs. (2.34) and (2.38)). To account for their numerical results, the authors proposed a generalization of RFOT, based on the idea that effective interface tension, Υ, is in fact state-dependent [6]. Repeating the argument of [4] with this extra assumption, the probability that the liquid inside the cavity is found in a state different from the outside pinning (frozen) state is:

$$p_{in}(R) = \int d\Upsilon \, P(\Upsilon) \frac{1}{1 + e^{R^d\Sigma - \beta\Upsilon R^{\theta}}}, \tag{2.40}$$

where the possibility that Υ may depend on the states matching at the boundaries of the cavity is accounted by the distribution $P(\Upsilon)$, over which $p_{in}(R)$ must be averaged. The simple mosaic result of [4] is recovered by setting $P(\Upsilon) = \delta(\Upsilon - \Upsilon_0)$. Eq. (2.40) can be simplified further by noting that the approximation

$$(1 + e^{R^d\Sigma - \beta\Upsilon R^{\theta}})^{-1} \approx \Theta(\Upsilon - T\Sigma R^{d-\theta}), \tag{2.41}$$

holds even for quite small values of R (Θ is the step function). Hence:

$$p_{in}(R) = \int_{T\Sigma R^{d-\theta}}^{\infty} P(\Upsilon)\, d\Upsilon. \tag{2.42}$$

Assuming that in eq.(2.38) is $q_{\alpha\alpha} \sim 0$ and $q_{\alpha\beta} \sim 1$, it follows that the point-to-set correlation function $q_c(R)$ of the sphere has the same dependence on R as probability $p_{in}(R)$, thus:

$$q_c(R) \sim \int_{T\Sigma R^{d-\theta}}^{\infty} P(\Upsilon)\, d\Upsilon. \tag{2.43}$$

A probability distribution of surface tension with a finite width can explain the smooth decay of the overlap $q_c(R)$ with increasing R. In particular, assuming the following ν-parameter dependent distribution for Υ:

$$P(\Upsilon) = \frac{\nu}{\Upsilon_c} \left(\frac{\Upsilon}{\Upsilon_c}\right)^{\nu-1} \exp\left[-(\Upsilon/\Upsilon_c)^{\nu}\right] = -\frac{d}{d\Upsilon} \exp\left[-(\Upsilon/\Upsilon_c)^{\nu}\right], \tag{2.44}$$

the integral of eq.(2.43) yields:

$$q_c(R) \sim \exp\left[-(R/\xi_{RFOT})^{\nu(d-\theta)}\right] \sim \exp\left[-(R/\xi_{RFOT})^{\zeta}\right], \tag{2.45}$$

where the usual RFOT relation $\xi = (\Upsilon/T\Sigma)^{1/(d-\theta)}$ is assumed to eliminate Υ_c in favour of ξ_{RFOT}.
Within RFOT framework, the thermodynamic anomaly $\zeta = \nu(d-\theta)$ is directly related to the exponent ν describing the surface tension distribution. The narrower the surface tension distribution, the sharper the decrease of the point-to-set correlation function around ξ_{RFOT}. The data on the decay of $q_c(R)$ for increasing R found in [6] are well fitted by the compressed exponential of eq.(2.45), with ζ and ξ_{RFOT} as fit parameters: values of these exponents found by the authors are listed in tab.(2.2).
The increase of ξ_{RFOT} is remarkable, but maybe more remarkable is that of the exponent ζ: *this* is the landmark of the supercooled liquid phase. $q_c(R)$ measures how deeply inside the sphere penetrates the influence of frozen boundary conditions: its decay with R *must* be exponential in the liquid phase. A decay of $q_c(R)$ different from a simple exponential requires new theory. Whatever theory is welcome: nevertheless, authors of [6] showed that RFOT, with the extra assumption of a fluctuating surface tension, *does* work. Within RFOT the nonexpontiality of $q_c(R)$ depends directly on:
1) The existence of a surface tension between different metastable states,
2) The shape of the surface tension distribution.
Therefore at this step a further test of RFOT theory cries for a direct measure of surface tension. Last but not least, a positive measure of surface tension in the supercooled liquid phase is probably the most direct evidence that "many states" do exist.

2.5 Dynamic glass transition

2.5.1 Dynamical heterogeneities

RFOT is a thermodynamic theory in that it derives the typical length-scale ξ_{RFOT} of the system only from quantities which do not depend on time, i.e., configurational entropy and surface tension. Unfortunately, it is hard to detect a growing *static* length-scale

T/T_c	ζ	ξ_{RFOT}
2.13	1^*	0.617(40)
1.55	1^*	0.845(28)
1.09	2.79(52)	3.04(24)
0.89	4.00(60)	3.82(12)

Table 2.2: *Non-exponentiality degree ζ of the point-to-set correlation function $q_c(R)$ and correlation length ξ_{RFOT}, as obtained from data in [6].*

when dealing with supercooled liquids: it was accomplished for the first time only very recently [6]. Not only ξ_{RFOT} is difficult to measure, but even the idea of *amorphous* order, connected to the length-scale ξ_{RFOT}, is a challenging oxymoron.
The aim of this section is at introducing another kind of correlation length, whose physical meaning is perhaps more intuitive. This is the dynamic length-scale ξ_{DYN}: the characteristic size of dynamic cooperative effects. Let us leave apart, for the moment, everything about energy landscape, topological crossover, and activated processes: in this new framework dynamics becomes slower at lower temperatures *only* beacause larger and larger regions have to move simultaneously to allow for susbstantial motion of individual particles [7, 35, 36, 37, 38, 39, 40, 41, 42]. The characteristic size of these regions is defined as being ξ_{DYN}. This length is connected to the concept of *dynamical heterogeneities*.

A supercooled liquid is ergodic: provided that a large enough time is waited, all phase space is visited. The meaning of heterogeneous dynamics is that the tendency to decorrelate in time is inhomogeneusly displaced within the system. Particles with a higher degree of mobility tend to cluster, the same being true for immobile particles: that is, a particle cannot significatively decorrelate in time if the same does not happen for the sourrounding ones. This idea has been fully exploited by theories [7] developed to describe a particular class of theoretical models, i.e., kinetically constrained models (CKM)[8]. These models, particularly suited for numerical simulations, are aimed at reproducing the physics of supercooled liquids. In the contex of CKM the dynamics becomes correlated over increasing length-scales due to *local* constraints [8]. These constraints exploits the idea of *dynamical facilitation*, that is: a different degree of mobility is attached to particles within the system, only a fraction of them, which is conserved along the dynamics, has a good mobility. The rearrangement of all the other particles must be triggered by these *mobile defects*. A significative rearrangement can only take place when there is a percolation of *mobility defects* [7]. The lower is the number of defects the higher the time required for a rearrangement. The temperature of the system is tuned by changing the number of mobile defects. It comes out that the system is completely frozen only at $T = 0$, i.e. when the number of defects is zero. This is a rough description of how the dynamics of a supercooled liquid may be controlled by a zero temperature dynamical critical point [7]: no need of thermodynamic sigularities at finite temperature. Exactly because they place the singular point of dynamics at $T = 0$, these theories are suited to describe the behaviour of *strong* glass-forming liquids, which do not displays dynamical crossovers at finite temperature. That is why, later on, will be introduced another theory which describes the increase of dynamic cooperativity, i.e., the inhomogeneus mode-coupling theory (IMCT,[9, 43]). This theory, which places the singular point of dynamics at the mode coupling temperature T_c, is more suited to be compared with RFOT theory and with the behaviour of fragile glass-formers.

The length-scale ξ_{DYN} of cooperative rearrangements is more at hand with respect to ξ_{RFOT}: it can be measured by means of the four-point correlation function $g_4(\mathbf{r}, t)$, introduced for the first time in the context of mean-field p-*spin* glasses [37, 44]:

$$g_4(\mathbf{r}, t) = \langle \rho(\mathbf{r}, t)\rho(\mathbf{r}, 0)\rho(\mathbf{0}, t)\rho(\mathbf{0}, 0)\rangle - \langle \rho(\mathbf{r}, t)\rho(\mathbf{r}, 0)\rangle\langle \rho(\mathbf{0}, t)\rho(\mathbf{0}, 0)\rangle, \tag{2.46}$$

where $\rho(\mathbf{r}, t)$ represents density fluctuations at position $\mathbf{r}$ and time t. It is customary to

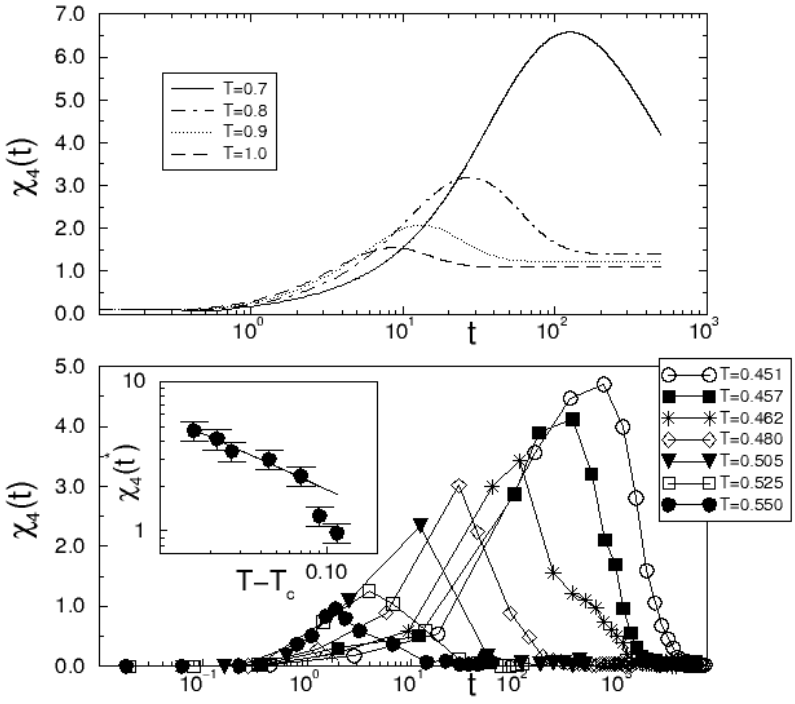

Figure 2.7: *Behaviour of the dynamical susceptivity $\chi_4(t)$ in a glass-forming liquid model (lower panel), and a p-spin model (upper panel). The peak of $\chi_4(t)$ increases, and shifts to larger times, as temperature T is lowered. Whereas in the glass-forming liquid model —ergodic— $\chi_4(t)$ vanishes at large times, in the p-spin , below T_c —non-ergodic phase, it decays to a finite value.*

introduce the overlap field $q(\mathbf{r}, t)$, which is a function of $\rho(\mathbf{r}, t)$ defined as:

$$q(\mathbf{r}, t) = \rho(\mathbf{r}, t)\rho(\mathbf{r}, 0). \tag{2.47}$$

This field measures at position $\mathbf{r}$ the propensity of the system to decorrelate over time t. The four point correlation function, in term of the overlap field, reads as:

$$g_4(\mathbf{r}, t) = \langle q(\mathbf{r}, t)q(\mathbf{0}, t)\rangle - \langle q(\mathbf{r}, t)\rangle\langle q(\mathbf{0}, t)\rangle. \tag{2.48}$$

The isotropic form $g_4(r, t)$ actually measures to what extent, on average, the displacement of a particle, over a time t, is correlated to the displacement of another particle placed at a distance r. This is clearly a measure of the average size of cooperative rearrangements. To explain why the attention was focused on the correlation function $g_4(r, t)$, let us recall the predictions of MCT theory, suitable to describe the physics of supercooled liquids at temperatures above T_c. This theory states that the dynamical correlation $C(t)$, at the

mode coupling temperature T_c, saturates at a finite value for infinite times (cfr. sec. 2.2). Therefore $C(t)$ can be regarded as the order parameter of the *dynamic* glass transition: it decays to zero in the ergodic phase and to a constant value in the non-ergodic phase, cfr. sec.(2.2). Clearly within this contex we are neglecting, for the moment, the activated processes intervening below T_c, which restore the ergodicy of the system. According to the definition of $C(t)$ given in sec. 2.2, we can write it also as:

$$C(t) = \frac{1}{V}\int_V d\mathbf{r}\langle\rho(\mathbf{r},t)\rho(\mathbf{r},0)\rangle, \tag{2.49}$$

which, assuming translational invariance, is equivalent to:

$$C(t) = \langle\rho(\mathbf{0},t)\rho(\mathbf{0},0)\rangle. \tag{2.50}$$

By comparing eq.(2.50) and eq.(2.47) it is clear that $C(t)$ and $\langle q(\mathbf{0},t)\rangle$ are the same object. In sec 2.2 it was described the analogy between MCT and p-*spin* spin-glass model, which is a mean-field model, i.e., it does not have any length-scale. The same is true for MCT, which describes the arrest of the dynamic as happening *homogeneusly* in the whole system. The first step in generalizing MCT, in order to introduce the characteristic length-scale ξ_{DYN} of cooperative dynamics, is take into account space fluctuations of the field $q(\mathbf{r},t)$. The function measuring the extent over which $q(\mathbf{r},t)$ fluctuations are correlated is precisely $g_4(\mathbf{r},t)$. Indeed, as the order parameter of the dynamic glass transition, i.e., $C(t) = \langle\rho(\mathbf{0},t)\rho(\mathbf{0},0)\rangle$, is already a two body object, $g_4(r,t)$ plays the same role as a standard two point correlation function: approaching the critical point, which is T_c in this contex, it describes the increasing extent of correlations. This is why researchers started to investigate the behaviour of $g_4(r,t)$.
Calculations within the scheme of MCT equations, but where also space fluctuations of the field $q(\mathbf{r},t)$ were taken into account, appeared in the literature with the name of Inhomogeneus Mode Coupling Theory (IMCT) [9, 43]. The goal of the Inhomogeneus Mode Couplig Theory (IMCT) has been to introduce within the framework of MCT equations the spatial length-scale ξ_{DYN}, i.e. the characteristic length-scale of $q(\mathbf{r},t)$ field fluctuations [9, 43]. At the temperature T_c where MCT predicts the ergodicity breaking, IMCT finds that the length-scale of $q(\mathbf{r},t)$ fluctuations —ξ_{DYN}— diverges. Both the predictions of MCT and IMCT are mean-field in nature, i.e., divergences of ξ_{DYN} and τ at T_c are an exact result only in $d > d_c = 6$ dimension: in real systems nonperturbative effects, i.e., activated processes, erease the singularity at T_c. Leaving apart the singular nature of IMCT at T_c, let us focus our attention on the behaviour at higher temperatures, at which the theory is still a good approximation. In this regime the liquid is ergodic: this means that at any finite distance r the correlation $g_4(r,t)$ decays to zero for sufficiently large times. This happens because, in defining $g_4(r,t)$, a reference configuration of the system was fixed. As long as the system is ergodic, the memory of any fixed intial condition is lost. The correlation $g_4(r,t)$ attains its maximum value at $r = \xi_{DYN}$ and $t = \tau$. Within the IMCT theory, the power law divergence of relaxation time at T_c (cfr eq.(2.9)) is connected to the increase of correlation length ξ_{DYN} by the dynamical exponent z:

$$\xi_{DYN} \sim \tau^{1/z}. \tag{2.51}$$

Not only cooperative rearrangements has a characteristic lengh-scale, ξ_{DYN}, but also a charachteristic time-scale, τ, the relaxation time of the system. In the vicinity of the critical point at T_c, albeit not divergent, ξ_{DYN} is expected to significatively increase even in

realistic glass-forming liquid models. Usually, when a certain observable has fluctuations correlated over increasing length-scales, there is susceptibility which is also increasing. Also, a susceptibility is often an observable more at hand compared with a correlation function. That is why the extent of dynamically correlations is often study by means of the dynamical susceptibility $\chi_4(r,t)$ [35, 36, 37, 38, 39, 40, 41, 42]:

$$\chi_4(t) = \beta \int d\mathbf{r} g_4(\mathbf{r},t). \tag{2.52}$$

Susceptibility $\chi_4(t)$ presents a typical non-monotonic time dependence with a peak centered at the liquid's relaxation time [7, 35, 36, 42]. At the maximum of $\chi_4(t)$ dynamically correlated regions (DCR) attains their maximum volume. As long as the dynamic becomes sluggish and correlated over an increasing lenght-scale the peak of $\chi_4(t)$ increase in size and shifts to larger times, see fig.2.7. As mentioned above, being mean-field in nature, the IMCT theory is approximated when applied to supercooled liquids. More precisely, when we extract ξ_{DYN} as the length-scale of the corralation function $g_4(r,t)$ *measured* in the system, it is found finite even at T_c, the same happening for the relaxation times τ.

From recent works [6, 11, 12, 45] we know that the mode coupling temperature T_c cannot be regarded *strictly* as an upper bound for the activated mechanisms of RFOT. There should be a range of temperatures, probabily narrow, around T_c where both amorphous static excitations, whose linear size is ξ_{RFOT}, and cooperative rearrangements extending on length-scale ξ_{DYN} are playing a role.

In the present work is proposed a method to measure *if* surface tension is present even between DCR. A positive result would say that an ingredient introduced within a thermodynamic theory of the glass transition (RFOT), i.e. *surface tension*, is common to both *static* and *dynamic* excitations.

Chapter 3

Interfaces in supercooled liquids: direct inspection

In this section is described the method we used to simulate the amorphous excitations of RFOT theory and study their energy cost. Within the multistate mosaic scenario, each state is equally amorphous. That is why, rather than attempting to detected the position of interfaces in equilibrium configurations, we propose a method to induce these interfaces in a well known and fixed position. The most important assumption made here is that the amorphous phases of a supercooled liquid, of which the mosaic patches are local realizations, can be well approximated by inherent structures, i.e., the minima of potential energy. The position of the interface induced between a pair of inherent structures is completely under control and allows us a detailed study of its energy cost. Some interesting results of this study will be also discussed.
The behaviour of surface tension between equilibrium configurations will be also studied. The interface between equilibrium configurations is induced with the same method employed for inherent structures, whereas, in this case, its relaxation under the effect of a finite temperature is studied.
Let us start, in what follows, from the description of the method used to induce an interface between a pair of inherent structures.

3.1 Surface tension beteween ordered phases

This section describes how surface tension can be measured at the interface between two equilibrium phases by defining a *Gibbs dividing surface* (GDS). Localization of the GDS is straightforward in systems in which the two phases are clearly distinguished by a different value of a macroscopic order parameter: for instance, the gas-liquid interface. I explain how this method is applied to define an interface between amorphous phases in a glass-forming liquid model. In this case, the different phases, being amorphous, lack a macroscopic order parameter allowing us to distinguish them. This is why, in a supercooled liquid, still being unable to distinguish each single phase, we can only ask if two portions of the system are in the same phase or not.

Gibbs dividing surface. In order to calculate the surface tension between metastable amorphus states, let us recall the definition of surface tension given by Tolman in [46]. This definition was applied to standard phase coexistence in ordered systems. Nevertheless, it turned out to be the best *operative* dealing with interfaces between amorphous phases. Let

us consider the equilibrium condition for a system composed of two fluid phases, α and β, which meet at a surface of discontinuity. The system, according to equilibrium conditions when interactions have a short range, is homogeneus in the interior of the two phases, while inhomogeneity occours in the region of finite thickness, where the transition from one phase to another takes place. This finite layer is called the *surface of tension* . To quantify the energy stored in the *surface of tension*, let us imagine the two phases divided by a geometric surface, the GDS, perfectly homogeneous precisely to this imaginary surface. Clearly, it must be placed within the inhomogeneus transition layer. According to this construction, the total energy of the system may be written as

$$E = E^{\mathrm{s}} + E^{\alpha} + E^{\beta}, \tag{3.1}$$

where E^{α} and E^{β} are the energies of the two phases, calculated as if they were perfectly homogeneous right to the geometric surface of separation. E^{s} is the additional term which gives the necessary correction, arising from the finite thickness of the inhomogeneous transition layer. The same kind of equation may be written for all extensive quantities characterizing the system, like entropy:

$$S = S^{\mathrm{s}} + S^{\alpha} + S^{\beta}, \tag{3.2}$$

and the masses of the two species:

$$m_1 = m_1^{\mathrm{s}} + m_1^{\alpha} + m_1^{\beta}, \tag{3.3}$$

$$m_2 = m_2^{\mathrm{s}} + m_2^{\alpha} + m_2^{\beta}. \tag{3.4}$$

Tolman's result, which is of central importance for us, is the following: the work needed to increase the area of the *surface of tension*, without changing either volumes v^{α} and v^{β} occupied by the two species or the mass of each one, can be written as:

$$dW = dE^{\mathrm{s}} = TdS^{\mathrm{s}} + \sigma ds, \tag{3.5}$$

where s is the area of the GDS. The integration of eq.(3.5) from $s = 0$ to finite value s yields:

$$E^{\mathrm{s}} = TS^{\mathrm{s}} + \sigma s, \tag{3.6}$$

If we neglect the entropic term, then *surface tension*, i.e., the energy per unit area stored in the inhomogeneus layer between the two phases, is:

$$\frac{E^{\mathrm{s}}}{s} = \frac{E - E^{\alpha} - E^{\beta}}{s} = \sigma. \tag{3.7}$$

This equation is suitable as the *operative* definition of the surface tension we wish to measure. If we know the total energy of the system, E, then we have only to choose the exact position of the GDS and calculate E^{α} and E^{β} consistently. Indeed, there are many choices for geometric GDSs embedded in the inhomogeneous layer. In principle, they can lead to different results for E^{s}. Nevertheless, different choices of the GDS, at least for the numerical study presented here, give only second order corrections to E^{s} which can be neglected.

3.2 Surface tension between inherent structures

Determination of the surface free energy between the amorphous excitations of a supercooled liquid is very challenging. This is, first, because the interfaces are hard to detect, and second, because their lifetime is necessarily finite. A supercooled liquid, according to RFOT theory, is fragmentated in many amorphous domains. No simple order parameter is available to distinguish such domains, nor the interface between them.
The strategy applied to overcome this problem is the following:

- Identify a pair of *different* homogeneus amorphous phases, let use retain the labels α and β. This can be done in a supercooled liquid: they are two uncorrelated equilibrium configurations or, equivalently the Inherent Structures onto which the equilibrium configurations can be mapped [2, 47]. We will see how, in the latter case, the definition of surface tension, although approximated, is less problematic.

- Build the GDS between α and β.

- Let the system carry out some rearrangements, in order to reach the optimal shape of the interface between α and β. Check that even after rearrangements, the initial position of the GDS is unchanged. This check is done by means of a suitable order parameter, e.g. the local overlap $q(\mathbf{x})$, introduced at this point.

- Calculate E^{s} according to eq.(3.7).

Before developing the above further let us address the three following points:
1) Describe the glass-forming liquid model studied;
2) Define the ensembles of inherent structures regarded as the different phases of the supercooled liquid;
3) Define how local overlap $q(\mathbf{x})$ is calculated in the liquid model.

3.2.1 Numerical set-up

Model. The system studied is a binary mixture of soft particles which is a fragile glass-former [48, 49, 50]. In this numerical system, the particles are of unit mass and belong to one of the two species $\gamma = 1, 2$, present in equal amounts and interacting via the potential:

$$\mathcal{V} = \sum_{i<j}^{N} V_{ij}(|\mathbf{r}_i - \mathbf{r}_j|) = \sum_{i<j}^{N} \left[\frac{\sigma_{\gamma(i)} + \sigma_{\gamma(j)}}{|\mathbf{r}_i - \mathbf{r}_j|} \right]^{12}. \tag{3.8}$$

Radii σ_γ are fixed by the conditions $\sigma_2/\sigma_1 = 1.2$, $(2\sigma_1)^3 + 2(\sigma_1 + \sigma_2)^3 + (2\sigma_2)^3 = 4l_0^3$, and l_0 is the unit of length. The density is $\rho = N/V = l_0^{-3}$, and the Boltzmann's constant is set to $k_B = 1$. A smooth long-range cut-off is imposed setting $v_{ij}(r) = B_{ij}(a - r)^3 + C_{ij}$ for $r > r_c = \sqrt{3}$ and $v_{ij}(r) = C_{ij}$ for $r > a$, where a, B_{ij}, and C_{ij} are fixed by requiring continuity up to the second derivative of $v_{ij}(r)$. The thermodynamic quantities of this system depend only on $\Gamma = \rho/T^{1/4}$, T being the temperature of the system. Density is set to $\rho = l_0^{-3} = 1$, so that the thermodynamic parameter Γ is $\Gamma = 1/T^{1/4}$. The presence of two kinds of particles in the system strongly inhibits crystallization and allows the deeply supercooled phase to be observed. An efficient MC algorithm [51] was used to thermalize configurations even below the mode coupling temperature T_c ($\Gamma_c = 1.45$) [50].
In this work we considered the thermalized configurations of a system with $N = 16384$

particles confined in a periodic box, of side $L = 25.4$ in our unit of length. The temperatures studied, corresponding to $\Gamma = 1.49, 1.47, 1.44, 1.42$ and 1.35, are two below, $T = 0.89T_c$ and $0.95T_c$, and three above, $1.03T_c, 1.09T_c$ and $1.33T_c$, the mode coupling temperature.
Inherent Structures were obtained by minimizing the equilibrium configurations with an LBFGS algorithm [52], a geometrical optimized algorithm. In some special cases, to be discussed later on, minimization of configurations had to be menaged with particles placed at arbitrary small distances (see sec.3.2.3). The geometric LBFGS algorithm updates particle positions in order to minimize the potential energy V of the system. When $V \sim 10^{12}$, the algorithm crashes or starts a sort of fuzzy dynamic, but does not converge. To manage these highly stressed configurations a standard Monte Carlo with temperature set to zero was used as a minimizer. It is not very efficient, but it does propose particle displacements of fixed maximum amplitude: thus it can handle configurations in which particles are arbitrarily near and subject to arbitrarily large forces.

IS ensembles. According to the partionioning of phase-space introduced by Stillinger and Weber [5], two configurations of the liquid are regarded as different states when they belong to different *basins* of the potential energy landscape (PES). At the bottom of each basin lies an Inherent Structure (IS). Thus, the use of IS to represent the different states of the liquid appeared as a doable approximation, clearly, the lower the temperature the better the approximation. As quoted in [25], quenches at varying temperatures lead to IS with different average energy. The lower the temperature, the lower the energy of the minima sampled, and thus the lower the energy obtained quenching equilibrium configurations to IS.
As will be shown, the use of IS allows us to sharply define interfaces in the supercooled liquid: the goal is that the position and energy cost of interfaces do not depend on time. This approximation, i.e. the use of IS, is of great help and allows detailed study of the interfaces. When considering equilibrium configurations at finite temperature, where excitations and thus interfaces are constantly forming and relaxing, it is much more difficult to study the properties of interfaces.
IS can be partitioned in ensembles according to temperature T of parent equilibrium configurations. Throughout these analyses, I often mention observables averaged over a set of IS and how these observables depend on temperature. This temperature is the one where the set of IS used to average was sampled. For instance, the energy cost $\langle \Delta E(T) \rangle$ indicates the average cost of an interface between IS sampled at T.

Overlap. The correct order parameter that measures how much the local amorphous order has changed from one configuration to another is local overlap $q(\mathbf{x})$. A suitable definition of this overlap, for the off-lattice system considered, is given according to a method similar to that used in [34]. First, the system is divided in cubic cells of side $l = 0.4$, small enough to have negligible probability of finding two particles within the same cell. Then, having two configurations σ and τ, we calculate the quantity

$$q_{\sigma\tau}(x, y, z) = n_\sigma(x, y, z) n_\tau(x, y, z) \ , \tag{3.9}$$

where $n_\sigma(x, y, z) = 1$ when the cell centred at x, y, z contains at least one particle, and $n_\sigma(x, y, z) = 0$ when the same cell is empty. To each cell we assign the weight:

$$w_{\sigma\tau}(x, y, z) = \frac{n_\sigma(x, y, z) + n_\tau(x, y, z)}{2} \ . \tag{3.10}$$

Global overlap $q_{\sigma\tau}$ between the two configurations σ and τ is given by

$$q_{\sigma\tau} = \frac{\sum_i q_{\sigma\tau}(x_i, y_i, z_i) w_{\sigma\tau}(x_i, y_i, z_i)}{\sum_i w_{\sigma\tau}(x_i, y_i, z_i)} \ . \tag{3.11}$$

where index i runs over all cells in the system.

3.2.2 Shape of interfaces

As mentioned, a suitable solution estimating the contact cost of two amorphous phases is to construct the interface between those phases. As a first step, in this study we approximate the amorphous phases of the supercooled liquid with Inherent Structures. Let us show how it is possible to build an interface between ISs.

Artificial droplets. I consider pairs of Inherent Structures, $\mathcal{C}_\alpha$ and $\mathcal{C}_\beta$, from independently thermalized configurations, i.e. Inherent Structures belonging to different basins of attraction, and create a mixed configuration from them: all particles within a sphere of radius R of $\mathcal{C}_\alpha$ are moved to a spherical cavity of the same shape and size in configuration $\mathcal{C}_\beta$; conversely, particles in the sphere of $\mathcal{C}_\beta$ are moved to the spherical cavity of $\mathcal{C}_\alpha$, as shown in fig. 3.1. In this way, two new configurations arise, $\mathcal{C}_{\alpha+\beta}$ and $\mathcal{C}_{\beta+\alpha}$.

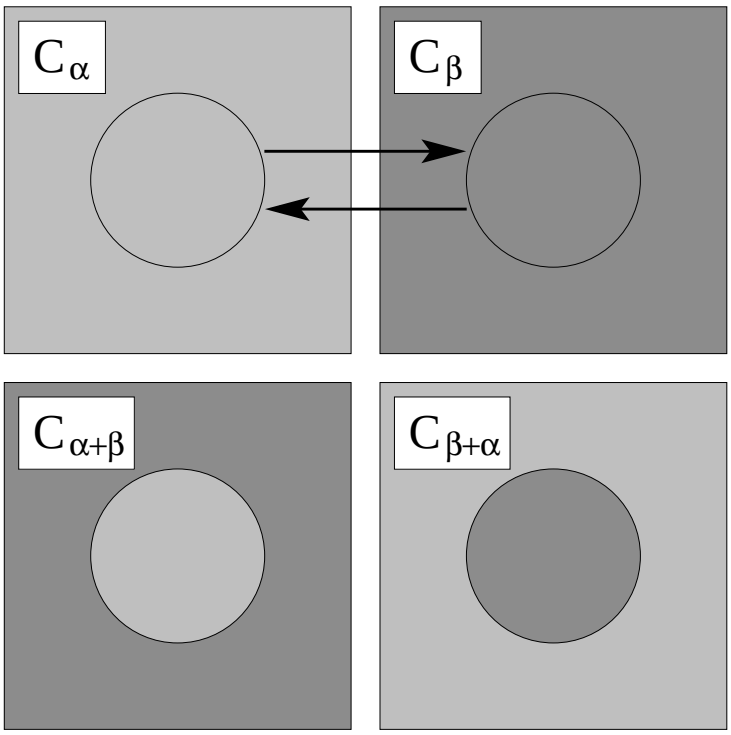

Figure 3.1: *Construction of the mixed configuration $\mathcal{C}_{\alpha+\beta}$ and $\mathcal{C}_{\beta+\alpha}$ using configurations $\mathcal{C}_\alpha$ and $\mathcal{C}_\beta$.*

Mass and species conservation The smooth geometric surface that bounds the cavity is regarded as the *Gibbs dividing surface* introduced in sec 3.1. Therefore, the spherical cavity in each pair of IS $\mathcal{C}_\alpha$ $\mathcal{C}_\beta$ must be choosen in order to conserve the total mass of each of the two species of particles in $\mathcal{C}_{\alpha+\beta}, \mathcal{C}_{\beta+\alpha}$. That is, the various steps are:

- Choose the radius of spherical cavity R. As density is $\rho = 1$, from R the number of particles N_s inside the cavity is known. Then choose the concentration of the two species inside the sphere, i.e. the numbers N_A and N_B, in order to have $N_A + N_B = N_s$ ($N_A = N_B$ when N even, $N_A = N_B + 1$ when N odd).

- Start a random walk of the centre of the spherical surface inside the simulation box.

- Stop when N_s particles with N_A and N_B of each type are found inside the surface and record the coordinate of the centre of sphere $(x_{sph}, y_{sph}, z_{sph})$.

- If $(x_{box}, y_{box}, z_{box})$ are the coordinates of the centre of the simulation box, shift the coordinates of all the particles by $(x_{sph} - x_{box}, y_{sph} - y_{box}, z_{sph} - z_{box})$, in order to have the spherical cavity centered in the simulation box.

- Relabel particles within the cavity of C_α as particles belonging to C_β and vice versa, i.e. exchange particles between the spherical cavity of the two configurations.

The hybrid minimum. In $\mathcal{C}_{\alpha+\beta}$ and $\mathcal{C}_{\beta+\alpha}$, unphysical stress is present at the boundary between the two phases. During the exchange process, near the boundary, particles within the cavity fall arbitrarily close to outsider particles. In order to relax the unphysical stress due to particles falling arbitrarily close, the mixed configurations $\mathcal{C}_{\alpha+\beta}, \mathcal{C}_{\beta+\alpha}$ are quenched to new hybrid minima $\mathcal{C}_{\alpha\beta}, \mathcal{C}_{\beta\alpha}$. For each mixed configuration $\mathcal{C}_{\alpha+\beta}$, due to the unphysical stress mentioned, the first part of the minimization is done with an MC algorithm with temperature set to zero, which acts as a minimizer. After 100 MC steps, when that stress is relaxed, the more efficient LBFGS geometric algorithm [52] completes the minimization. Within the hybrid minima $\mathcal{C}_{\alpha\beta}$ and $\mathcal{C}_{\beta\alpha}$ particles positions are close to those in parent minima α and β, far from the GDS, whereas close to it are different.
As it was not realistic to expect spontaneous excitations to be enclosed by an exactly spherical interface, the system had to be given a chance to optimize the shape of that interface.
The region where major displacements of particles took place in rearranging from $\mathcal{C}_{\alpha+\beta}$, $\mathcal{C}_{\beta+\alpha}$ to $\mathcal{C}_{\alpha\beta}$, $\mathcal{C}_{\beta\alpha}$ plays the role of the layer between different phases. Here, particle positions gradually switch from being typical of IS α to being typical of IS β.
A measure of the local overlap between mixed configuration $\mathcal{C}_{\alpha+\beta}$ and hybrid minimum $\mathcal{C}_{\alpha\beta}$ is of great help (fig.3.2). The spherical surface that exactly divides α from β in $\mathcal{C}_{\alpha+\beta}$ may be regarded as a good candidate for being the GDS in $\mathcal{C}_{\alpha\beta}$. Weather the choosen GDS is really placed within the layer between α and β in hybrid minimum $\mathcal{C}_{\alpha\beta}$ must be checked. Looking at the radial overlap profile of fig.3.2, we can say that this requirement is satisfied. The region where particles are more rearranged, with low overlap, encloses the position of the GDS.

Standard methods used to measure interface costs. The method employed to create a spherical excitation, in order to measure its energetic cost, may appear rather artificial. Nevertheless, to my knowledge, this is the first attempt to measure the cost of an interfaces within a supercooled liquid. There are indeed standard methods used to measure the cost of an interface, e.g. of linear size L, but they are suitable for the low-temperature non-ergodic phase, where the system is sensitive to boundary conditions. Let us consider a ferromagnetic system in a cubic periodic box of side L. Two ensembles

of configurations can be equilibrated, one with periodic and the other with antiperiodic boundary conditions along a given axis. The difference between the average energy measured in the two ensembles $\langle \Delta E(L) \rangle = \langle E_{antiper}(L) \rangle - \langle E_{per}(L) \rangle$ yields the cost of a flat interface of linear size L. A finite-size scaling (FSS) study of $\langle \Delta E(L) \rangle$ is the standard way of calculating exponent θ, which rules the scaling of the interface cost, $\langle \Delta E(L) \rangle \sim L^{\theta}$. FSS is indeed the most common way of calculating the stifness exponent in spin-glasses (see [53] and references therein). In [54, 55] the interface is induced in a spin-glass model by a method which is easily generalizable to off-lattice systems, for instance, liquids. Unfortunately, all these methods are only suitable for the non-ergodic phase. A supercooled liquid is in the ergodic phase and has no long-range order. In particular, according to RFOT theory, amorphous order has the typical *finite* length-scale $\xi_{RFOT}(T)$. A method similar to that of imposing periodic and antiperiodic boundary conditions [54], in our liquid model would lead to a null interface cost when $L > \xi_{RFOT}$. Therefore in this case the FFS study would fail.

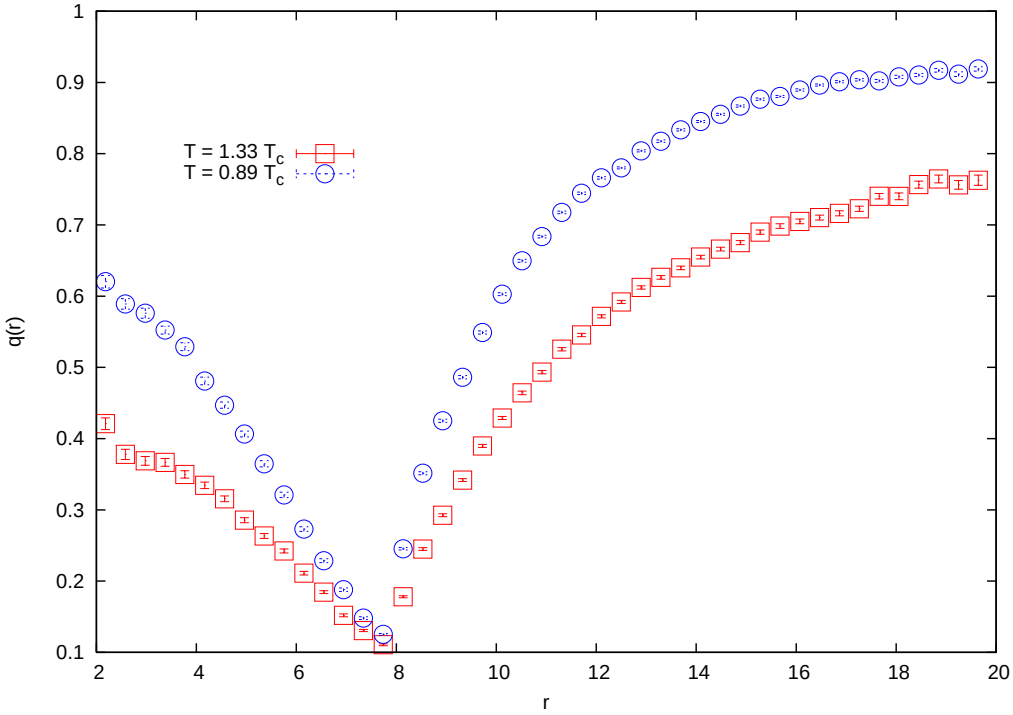

Figure 3.2: *Radial overlap* $\langle q(r) \rangle$ *averaged over the ensemble of hybrid minima enclosing a droplet of radius* $R = 8$ *. Blue circles, IS sampled at* $T = 0.89T_c$*; red squares, IS sampled at* $T = 1.33T_c$*.*

Gibbs Dividing Surface. It is assumed here that the position of the interface in $\mathcal{C}_{\alpha+\beta}$ is regarded as that of the GDS. This assuption was checked by controlling that the position of the interface in $\mathcal{C}_{\alpha+\beta}$ is where major rearrangements of particles took place passing from $\mathcal{C}_{\alpha+\beta}$ to $\mathcal{C}_{\alpha\beta}$. This can be seen from the radial overlap profile of fig.3.2. Here the local overlap $q(x, y, z)$ between each pair of $\mathcal{C}_{\alpha+\beta}$ and $\mathcal{C}_{\alpha\beta}$ was averaged over spherical shells concentrical with the spherical cavity. The lower the overlap value, the larger the displacement of particles in rearranging from $\mathcal{C}_{\alpha+\beta}$ to $\mathcal{C}_{\alpha\beta}$.

Far from the GDS, a high overlap value signals that particle positions closely resemble those of the original phases α and β. Far from the interface, the overlap is not 1. I quote

the scenario depicted by Goldstein [2] to show why the overlap is different from 1 far from the interface. According to Goldstein, small displacements of particles far from the interface can be ascribed to vibrations predictible within the theory of elasticity: *"The changes in atomic positions in the local region do not even approximately resemble displacements we might calculate from phenomenological elasticity, but at longer distances the atomic displacements, while of course not being identical with the macroscopical displacement vector, bear the same relation to it as they would if the displacement field were produced by a pure deformation of the body"*. The important point is that small displacements far from the interface are not related to optimization of the interface shape. This shape is clear in fig. 3.3, which represents particles rearrangements within a single *hybrid minimum*: the situation is clearly fuzzier than in the average behaviour to the average behaviour shown in fig. 3.2. In fig. 3.2 and even more clearly in fig. 3.3, the IS sampled at higher T appears as *softer*: it is easier to rearrange particle positions in order to optimize the shape of an interface. I show that this facilitation in rearranging particles at high T is directly related to the lower cost of the interface.

3.2.3 Energy cost of interfaces

Hybrid minimum $\mathcal{C}_{\alpha\beta}$ built in the previous section is closely related to what Goldstein [2] calls a *transition state*. The latter is intended as a configuration of the system which is near a minimum, but where a local rearrangement of particles has just taken place. This means that if a quench of this configuration is performed, *most* of the coordinates will have relatively small displacements. Thus, the *transition state* really differs from a minimum only around the local area where the cooperative rearrangement took place. It really looks like the definition of our hybrid minimum, $\mathcal{C}_{\alpha\beta}$, which differs from the parent inherent structures $\mathcal{C}_\alpha$ and $\mathcal{C}_\beta$ only in the neighbourhood of the interface.
Exact knowledge of parent configurations $\mathcal{C}_\alpha$ and $\mathcal{C}_\beta$ allows direct computation of energy cost of the interface. The potential energy of hybrid minimum $\mathcal{C}_{\alpha\beta}$ called here $E_{\alpha\beta}$, is the total energy of a system where coexistence of amorphous phases α and β takes place. At this stage, we can literelly follow Tolman's prescription [46]. The energy E_β^{out} of particles which are placed outside the GDS in $\mathcal{C}_\beta$, and the energy E_α^{in} of particles which are enclosed by the surface in $\mathcal{C}_\alpha$, are subtracted from $E_{\alpha\beta}$. Then, as the mass of the two species of particles is conserved inside/outside the spherical cavity, we can write:

$$E^{\mathrm{s}} = \Delta E(R) = E_{\alpha\beta} - E_\alpha^{in} - E_\beta^{out} \tag{3.12}$$

From now on, $\Delta E(R)$ will indicate the cost of a spherical interface of radius R. By construction, the number of particles of the two species is conserved on the two sides of the interface in $\mathcal{C}_{\alpha+\beta}$. Unlike within the rearrangements which take place passing from $\mathcal{C}_{\alpha+\beta}$ to $\mathcal{C}_{\alpha\beta}$, a few particles migrate through the GDS. Thus, in $\mathcal{C}_{\alpha+\beta}$, the density of the two kinds of particles of our binary mixture is not exactly conserved on the two sides of the GDS. Let us show that this change of density of the two phases separated by the GDS amounts to a correction of order $1/N$, N being the total number of particles, to $\Delta E(R)$.

Eq.(3.12) can be written as:

$$\Delta E(R) = N\epsilon_{\alpha\beta} - m\epsilon_\alpha - (N-m)\epsilon_\beta, \tag{3.13}$$

where m is the number of particles located within the spherical cavity in $\mathcal{C}_{\alpha+\beta}$. We can write the first-order correction to the energy of particles within the sphere due to a small

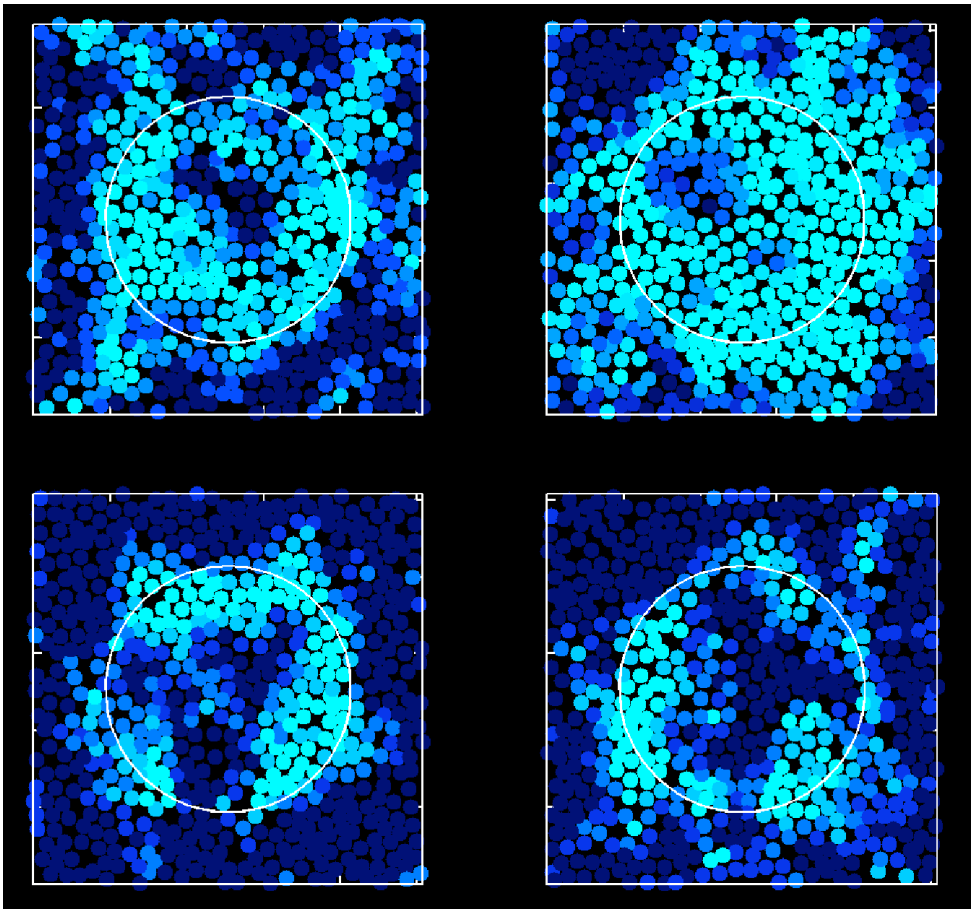

Figure 3.3: *Overlap, i.e. similarity, between the configuration right after the exchange of the spheres and the hybrid inherent structure after minimization. Only a thin slice located at half height of the 3-d system is shown. Colors code for the displacement of the particle after the artificial excitation was created (dark blue: small displacement, high overlap; light blue: large displacement, small overlap). Upper panel: two configurations at high temperature* $T = 1.33\,T_c$. *Lower panel: two configurations at low temperature* $T = 0.89\,T_c$. *The hybrid minimum clearly bears memory (high overlap, dark blue) of the parent IS far from the boundary of the sphere (white circle). On the other hand, particles move along the interface (low overlap, light blue).*

change in density inside/outside the cavity passing from $\mathcal{C}_{\alpha+\beta}$ to $\mathcal{C}_{\alpha\beta}$ as

$$\epsilon'_\alpha = \epsilon_\alpha + \epsilon_\alpha \frac{\Delta\varrho^\alpha}{\varrho^\alpha}, \tag{3.14}$$

where ϱ^α is the density of particles of phase α within the GDS in $\mathcal{C}_{\alpha+\beta}$ and $\Delta\varrho^\alpha$ is the error made in assuming that the same density is present in $\mathcal{C}_{\alpha\beta}$. If m' is the number of particles really enclosed by the GDS in $\mathcal{C}_{\alpha\beta}$, then the correct surface cost may be written as

$$\begin{aligned} \Delta E(R)' &= N\left(\epsilon_{\alpha\beta} - \frac{m}{N}\epsilon_\alpha - \frac{N-m}{N}\epsilon_\beta + \frac{m'-m}{N}(\epsilon_\beta - \epsilon_\alpha)\right), & (3.15)\\ &= \Delta E(R) + (m'-m)(\epsilon_\beta - \epsilon_\alpha) & (3.16) \end{aligned}$$

Generally $(m'-m)$, which is the number of the particles migrating across the surface, was checked to be at least one order of magnitude smaller than m. Hence, prefactor

$(m' - m)/N$ of last term on the right in eq.(3.16) is at least one order of magnitude smaller than the prefactor of the other terms. Moreover, as it is always true that $\epsilon_\alpha >> (\epsilon_\beta - \epsilon_\alpha)$ and $\epsilon_\beta >> (\epsilon_\beta - \epsilon_\alpha)$, having $\mathcal{C}_\alpha$ and $\mathcal{C}_\beta$ approximatively the same energy, and also $\epsilon_{\alpha\beta} >> (\epsilon_\beta - \epsilon_\alpha)$ we have:

$$\begin{aligned} \epsilon_{\alpha\beta} &>> \frac{m' - m}{N}(\epsilon_\beta - \epsilon_\alpha) \\ \frac{m}{N}\epsilon_\alpha &>> \frac{m' - m}{N}(\epsilon_\beta - \epsilon_\alpha) \\ \frac{N - m}{N}\epsilon_\beta &>> \frac{m' - m}{N}(\epsilon_\beta - \epsilon_\alpha). \end{aligned} \tag{3.17}$$

Therefore the last term in brackets in eq.(3.15) can be dropped and we can retain $\Delta E(R)' \sim \Delta E(R)$ with good approximation.

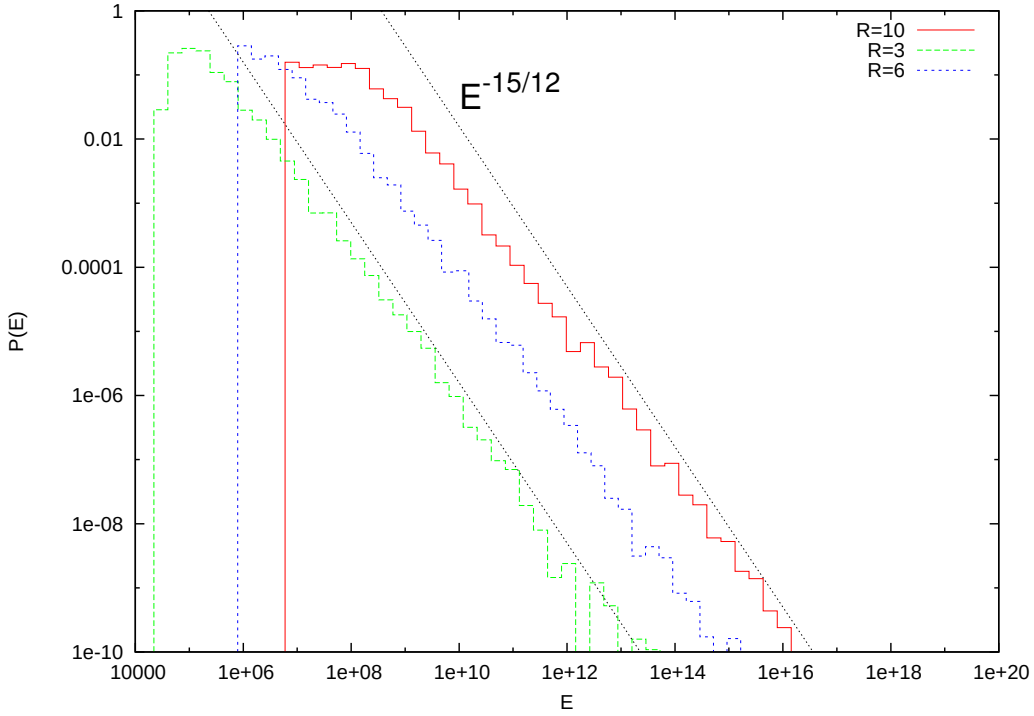

Figure 3.4: *Distributions of energies $E_{\alpha+\beta}(R)$, measured immediately after the exchange between different IS of the particles located within a spherical cavity. IS come from the ensemble at $T = 0.89T_c$. Distribution of $E_{\alpha+\beta}(R)$ are plotted for $R = 3, 5, 10$. Large E tails are compared with $E^{-15/12}$ to show that distributions are not normalizable. $E^{-15/12}$ is motivated in the text.*

Energy distribution controlled by random events. Configuration $\mathcal{C}_{\alpha+\beta}$ immediately after the switch is highly stressed, and is thus assumed to be uninteresting physically. Nevertheless, to check wheather pieces of information were being lost, the energy cost:

$$\Delta E_{\alpha+\beta}(R) = E_{\alpha+\beta} - E_\alpha^{in} - E_\beta^{out} \tag{3.18}$$

of the interface embedded in $\mathcal{C}_{\alpha+\beta}$, was measured immediately after the switch of particles in the spherical cavity. From a set of 25 IS sampled at $T = 0.89T_c$ an ensemble of 650

mixed configurations $\mathcal{C}_{\alpha+\beta}$ was build for each R, for some values of R. The scaling of $\langle \Delta E(R) \rangle$ with R was studied. The naive expectation was to find $\langle \Delta E(R) \rangle \sim R^2$. Instead $\langle \Delta E(R) \rangle$ was found not even to increase monotonically with R.
The origin of this unexpected result lies in the distribution of the total energy $E_{\alpha+\beta}(R)$ of the system immediately after the switch. Fig. 3.4 shows the histograms of the distribution of $E_{\alpha+\beta}(R)$ for three different values of R. These distributions have long tails, compatible with power law $E^{-15/12}$, so they are not even normalizable. This is why average values $\langle \Delta E(R) \rangle$ do not behave physically. From the data, E_α^{in} and E_β^{out} in eq.(3.18) are known to be on average one order of magnitude below the smallest value found for $E_{\alpha+\beta}$, that is, $E_\alpha^{in}, E_\beta^{out} \sim 10^3 \div 10^4$, whereas $\Delta E_{\alpha+\beta}(R) \geq 10^5$ in our energy unit. So the distributions of $E_{\alpha+\beta}(R)$ and $\Delta E_{\alpha+\beta}(R)$ are almost identical. The distribution of $E_{\alpha+\beta}(R)$ is non-physical, for the purpose of measuring a surface tension, because it is dominated by the random events of a pairs of particles falling arbitrarily near. The latter is truly an artifact of our procedure to create the interface. Power law $E^{-15/12}$ mentioned above comes from the following integral:

$$P(E) = \int_{\partial R} d\mathbf{x} d\mathbf{y} \delta(u(\mathbf{x}-\mathbf{y}) - E) \sim R^2 E^{-15/12}, \tag{3.19}$$

where ∂R is the domain of integration of variables $\mathbf{x}, \mathbf{y}$, i.e. a skin round the spherical surface of radius R, and $u(\mathbf{x}-\mathbf{y})$ is the interaction potential of our system ($u(r) \sim r^{-12}$). It was assumed that the total energy of the system is dominated by the single event of two particles falling at an arbitrary distance. By construction, the pair of particles that produce the energy spike must be found in the neighbourhood of the interface. This makes $P(E)$ proportional to R^2. Nevertheless, the large E tail makes $P(E)$ non-normalizable, which actually means that $\langle E \rangle$ depends on the number of configurations used to average.

Periodic boundary conditions. It can be seen that particle rearrangements to optimize the shape of a spherical interface are clearly asymmetric inside and outside the droplet (see figs. 3.2 and 3.3). Particle displacements are always larger inside the sphere. Inside the droplet, interference occours between the influence of the interfaces. This is not a problem when the interference is inside the droplet, as this effect may be expected as a matter of course even in spontaneous excitations.
Instead we must avoid different points on the spherical interface influencing each other across the periodic boundary conditions imposed on the simulation box.
To calculate the maximum size allowed for a spherical droplet inside a periodic box, in order to avoid any kind of "self-interaction", the cost of interfaces was studied by means of a different geometry.

Parisi-Kob geometry. Of course, in studying the cost of an interface, one can choose any kind of geometry. In the present work, spherical geometry was preferred, in order to have results comparable with [6], in which the same kind of geometry was studied. In this section, the cost of flat interfaces between inherent structures sampled at $T = 0.89 T_c$ is also studied. The purpose is to find the minimum distance allowed between a pair of interfaces in order to avoid interference. Ensembles of *hybrid minima* enclosing a pair of flat interfaces of size L^2 are studied by varying distance d between the interfaces. The interfaces were created exchanging all the particles which had a coordinate, for instance z, within a given interval $[z_{min}, z_{max}]$, between a couple of inherent structures $\mathcal{C}_\alpha$,$\mathcal{C}_\beta$. The distance between the two α/β interfaces is $d = z_{max} - z_{min}$. The average surface cost

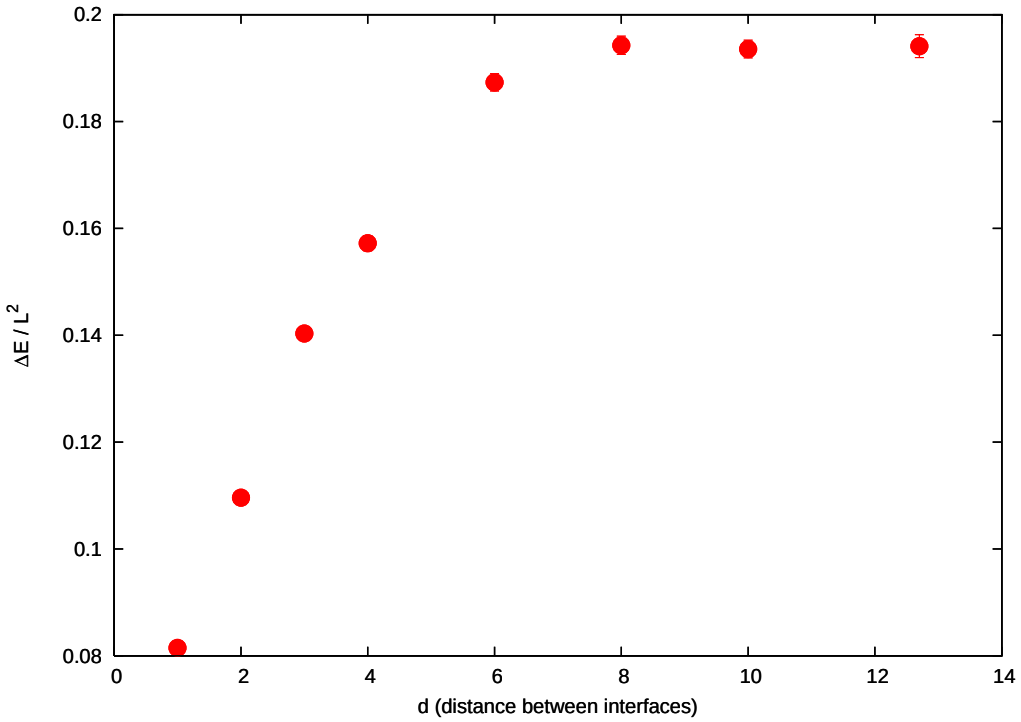

Figure 3.5: *Average surface cost* $\langle \Delta E(d) \rangle / L^2$ *of a flat interface between Inherent Structures as function of the distance* d *from another interface. Error bars are smaller than points. Inherent Structures are sampled at* $T = 0.89 T_c$.

ΔE was measured according to eq.(3.12), the only difference being in the definition of E_α^{in},E_β^{out}.
In this context, E_α^{in} is the energy of particles in $\mathcal{C}_\alpha$ with z within $[z_{min}, z_{max}]$, and E_β^{out} is the energy of particles in $\mathcal{C}_\beta$ with z outside the interval $[z_{min}, z_{max}]$. Distances ranging from $d = 1$ to $d = 12.7$, i.e. the maximum distance allowed by the periodic boundary conditions (box side is $L = 25.4$), were studied. It turns out that, for $d \leq 8$, particle rearrangements in the proximity of the two interfaces are strongly correlated. Fig. 3.5 shows surface cost $\langle \Delta E(d) \rangle$ as a function of distance d between the interfaces. As the size of the interfaces is constant for all d, variations in $\langle \Delta E(d) \rangle$ can only be due to a different mutual influence between the interfaces. Because $\langle \Delta E(d) \rangle$ saturates roughly at $d = 8$, this value is regarded as the smallest distance allowed to avoid unwanted interference effects between different interfaces. This result is useful for knowing the maximum size allowed for a droplet inside a periodic box. That is, the radius of the droplet cannot be larger than $R = 8.5$, otherwise its energy cost would suffer spurious effects from boundary conditions.

3.3 Study of surface tension

Υ as order parameter for metastable states. This section describes how the surface tension Υ between amorphous states of the supercooled liquid has been calculated. In order to obtain it the scaling with R of $\langle \Delta E(R) \rangle$, the energy cost of spherical interfaces, is studied in detail. Presenting results in the last chapter it will be shown that Υ displays an interesting dependence on temperature, $\Upsilon = \Upsilon(T)$, and is a good order parameter to characterize the regime where RFOT excitations are well defined.

3.3.1 Scaling with size

A first glance at amorphous surface tension. The average energy cost $\langle \Delta E(R) \rangle$ was calculate, according to the method introduced in section 3.2, for spherical droplets with radius ranging from $R = 1.5$, i.e., enclosing 14 particles, and 8.5, i.e., enclosing 2572 particles. The brackes $\langle\rangle$ indicate the average performed over ensembles of 150 hybrid minima (HM), each ensemble at a different temperature. Therefore the energy cost $\langle \Delta E(R) \rangle$ depends directly on droplet size and indirectly on temperature. The energy cost of differently sized droplets has been studied at temperatures $T = 0.89T_c, 0.95T_c, 1.03T_c, 1.09T_c$ and $1.33T_c$. The scaling of $\langle \Delta E(R) \rangle$ with R is reported for different temperatures in log-log scale in fig.3.6 and in linear scale in fig.3.7. The first remark is that this contact cost has a well-defined increase with growing radius R of the sphere (figs .3.7 and 3.6).

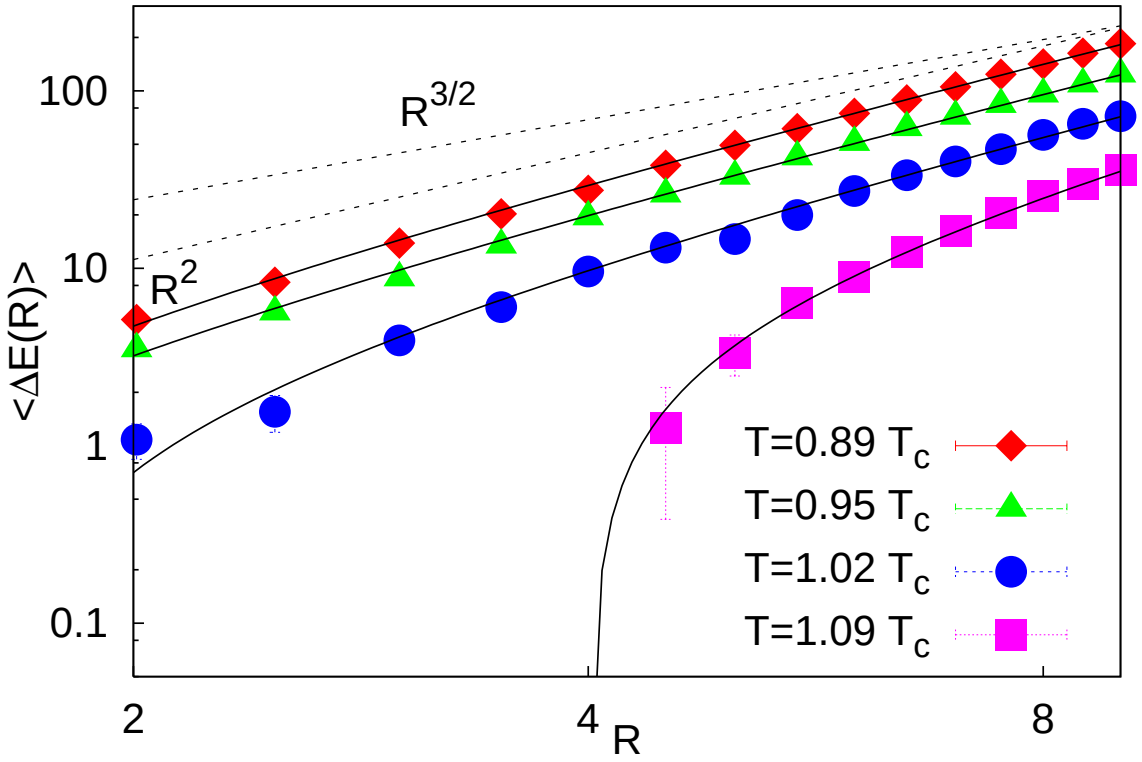

Figure 3.6: *ΔE vs. excitation radius R at various temperatures. Full lines: fits according to eq. 3.20, with $\theta = 2$ and $\omega = 1.2$. Dotted lines: power laws with exponents 2 and 3/2 for reference. Error bars are smaller than symbol size.*

Moreover, as is clear expecially from fig. 3.7, the higher the temperature, the slower the increase of energy cost of a droplet with size. The set of data at the highest temperature, $T = 1.33T_c$, is nearly flat (fig.3.7). Let us note that, at this temperature, the cost of an interface does not only appear independent of its linear size R, but is also negative. This does not make sense, if these data are to be explained by a single power law ΥR^θ. A correction of negative sign to leading behaviour ΥR^θ of surface tension must be considered, formally accounting for negative values of $\langle \Delta E(R) \rangle$. This point will be clarified later on. The temperature at which IS are sampled plays a very important role: if we fix size R of a droplet, its cost definitely increases as the temperature falls. The low-temperature ordering of the amorphous configurations implies higher cost of the contact between differently

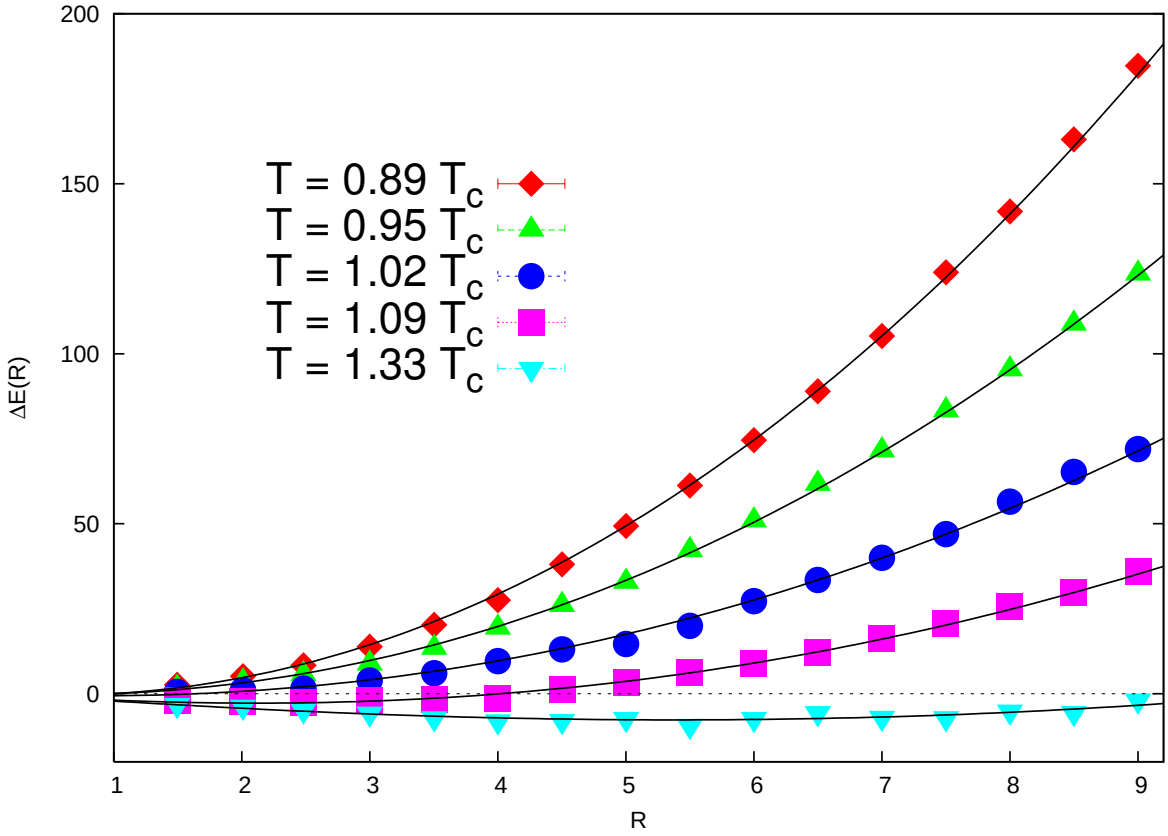

Figure 3.7: ΔE *vs. excitation radius* R *at various temperatures in linear scale. Full lines: fits according to eq. 3.20, with* $\theta = 2$ *and* $\omega = 1.2$*. Error bars are smaller than symbol size.*

ordered configurations.

Why a subleading correction term to ΥR^θ ? A simple power law ΥR^θ, expected for a surface energy cost, is enough to fit low-temperature data. This is not the case for higher temperatures, where a correction is needed to have a good description of the data, expecially for small droplets (in particular at $T = 1.33 T_c$ for all sizes).
What happens if we choose the easiest way to avoid the problem —that is, forgetting about data at higher temperature, i.e., $T > T_c$? After all, the RFOT scenario is presumed to describe the relaxation of a supercooled liquid below T_c. There are two good reasons for rejecting this choice and introducing a correction to leading order term ΥR^θ of surface cost:

1. The best fit of the data with a single power ΥR^θ, *even* at the lowest temperature, gives a value for θ greater than $d-1$. Let us recall that the minimization leading from $\mathcal{C}_{\alpha+\beta}$ —smooth interface— to $\mathcal{C}_{\alpha\beta}$ —optimized interface— is composed by 100 MC steps and the subsequent use of the LBFGS algorithm. With the standard method already outlined, the cost of the interface whitin configuration half-way through minimization, was measured immediately after the 100 MC steps at zero temperature. At this stage of minimization, it was found that the cost of the surface was simply proportional to the square of R. It does not make sense, for the following minimization, to lead to a steeper increase in contact energy.

2. A correction to the leading behaviour of the surface cost may simply be due to

curvature [56], and at the same time it is quite common for interfaces in disordered systems [57, 58, 59]. Therefore it is not something strange that we must avoid.

For these reasons, is proposed, at each temperature, a description of the data with a leading term and a correction:

$$\Delta E(R) = \Upsilon R^{\theta} - \delta R^{\omega}, \tag{3.20}$$

The points that will be addressed in the following are, in order:

- The estimate of exponent θ from data;
- General features of interfaces in disordered media;
- Considerations on the self-averaging nature of ΥR^{θ};
- How to fix the exponent of the subleading correction δR^{ω};
- Roughening interpretation of the correction δR^{ω};

Estimate of the exponent θ. As already pointed out, a single power is not enough to explain the scaling of the energety cost with droplet size. Nevertheless, the curves of fig. 3.6 exhibit a common trend for large values of R. It is from this "asymptotic" trend that the value of the leading term of surface tension exponent $\theta = 2$ can be fixed. A wetting argument by Wolynes [60, 61] suggests the value $\theta = 3/2$ for the exponent of power law ΥR^{θ}, whereas a spin model theory with finite range interaction of Franz [62] indicates a competing $\theta = 2$. Although a slower trend may emerge for larger R values, it is always hard to fix an exponent over only one decade, and the more conservative choice, $\theta = 2$, is compatible with our data. Now that θ is fixed, we need to find Υ , δ and ω. A simple fit of the numerical mean energy cost with three free parameters is marginal: very different values of Υ are in good agreement with the data, provided that suitable variations are made to δ and ω. A physical interpretation of correction term δR^{ω} is needed to fix exponent ω.

3.3.2 Effects of disorder

Examples of interfaces in disordered media. Looking at data $\langle \Delta E(R) \rangle$ vs. R in fig. 3.6, we can say, first of all, that the sign of the δR^{ω} correction must be negative. To go any further, we need some interpretative scheme for analysis of δR^{ω}.
A power law δR^{ω} correction to the pure quadratic surface cost is quite common in disordered systems. It appears, for example, in the Random Field Ising Model (RFIM) [57]. In homogeneous spin-up phase, the surface cost to nucleate a domain of down-spins can eventually be balanced by the energy gain due the coupling of spins with the random external field. This mechanism breaks the long-range order for $d < 2$ in RFIM [57]. Because the sum of $N \sim R^d$ external field values fluctuates, according to the Central Limit Theorem (CLT), as $N^{1/2} \sim R^{d/2}$, the whole mean energy variation $\langle \Delta E \rangle$ to nucleate a droplet is [57]:

$$\langle \Delta E \rangle = \sigma R^{d-1} - h R^{d/2}. \tag{3.21}$$

We may say that the fluctuation term plays the role of a correction to the surface cost. If the correction in eq.(3.20) was due to an analogous effect, in $d = 3$, exponent ω would

be $\omega = 3/2$.
A very different mechanism [58], defined in a wide class of systems, is the roughening mechanism. Ground state energy E of an elastic surface embedded in a random potential has the following scaling:

$$\langle E \rangle \sim AL^{d-1} - BL^{\chi} \tag{3.22}$$

where L is the linear size of the surface. Again, ground state energy has a finite size correction, although in this case the exponent is model-dependent.
Also in the Directed Polymer (DP) problem [59], ground state energy has a coorection to leading order:

$$E \sim e_0 L + e_1 L^{\theta_{DP}}, \tag{3.23}$$

where d is assumed $d = 1$.
A very important feature, common to all these examples, is the behaviour of energy fluctuations when the size of the interface is increased. In the RFIM case, according to CLT, the fluctuation of the surface term, σR^{d-1}, coming from an extensive sum of independent variables, is expected to grow like the surface itself. Thus, surface term σR^{d-1} is self-averaging. It is not the same for the correction term, since the variance of local external field h does not depend on R. Indeed, at large R, only the fluctuations of the correction term are left:

$$(\Delta E - \langle \Delta E \rangle)_{RMS} \sim R^{d/2} \tag{3.24}$$

where $(\dots)_{RMS} = \sqrt{\langle (\dots)^2 \rangle}$.
The ground state energy of a rough surface and of a directed polymer also has fluctuations around its mean value, depending only on the correction exponent, χ or θ_{DP}, respectively:

$$(E - \langle E \rangle)_{RMS} \sim L^{\chi} \tag{3.25}$$

and:

$$(E - \langle E \rangle)_{RMS} \sim L^{\theta_{DP}}. \tag{3.26}$$

Again, the fluctuation of the prefactor of the correction term in eqs. (3.25) and (3.26) must not depend on L.
Although a priori the physical origin of term δR^{ω} in our system, eq.(3.20), is still not clear, it is possible that, as in the previous examples, the fluctuations of its prefactor δ dominate over the fluctuations of surface energy density Υ. Surface energy Υ should be self-averaging, whereas prefactor δ may have fluctuations independent of R. Let us exploit this possibility.

Considerations on the self-averaging nature of ΥR^{θ} If the measured energy cost of spherical interfaces $\langle \Delta E(R) \rangle$ is a self-averaging quantity, according to Central Limit Theorem we should find:

$$\begin{aligned} \langle \Delta E(R)_{\alpha\beta} \rangle = \sum_{i}^{R^2} \langle \varepsilon_i \rangle \quad &\Rightarrow \quad \mathrm{Var}[\Delta E_{\alpha\beta}(R)] = \mathrm{Var}[\varepsilon] R^2 \\ &\Rightarrow \quad \mathrm{Var}[\frac{\Delta E_{\alpha\beta}}{R^2}] = \frac{\mathrm{Var}[\varepsilon]}{R^2}, \end{aligned} \tag{3.27}$$

where sum index i runs over unitary element of area, whose energy cost is ε_i, and $\mathrm{Var}(x) = \langle x^2 \rangle - \langle x \rangle^2$. Fig.3.8 shows that $\mathrm{Var}[\frac{\Delta E_{\alpha\beta}}{R^2}]$ for large values of R violates the predictions of the CLT. For each sample, the interface cost may be written as:

$$\Delta E_{\alpha\beta} = \Upsilon_{\alpha\beta} R^2 - \delta_{\alpha\beta} R^{\omega}. \tag{3.28}$$

Let us now assume that fluctuations of $\Upsilon_{\alpha\beta}$ are ruled by the CLT:

$$\begin{aligned} \mathrm{Var}[\frac{\Delta E_{\alpha\beta}}{R^2}] &= \mathrm{Var}[\Upsilon_{\alpha\beta}] + \frac{\mathrm{Var}[\delta_{\alpha\beta}]}{R^{4-2\omega}} \\ &= \frac{1}{R^2} + \frac{\mathrm{Var}[\delta_{\alpha\beta}]}{R^{4-2\omega}} \end{aligned} \tag{3.29}$$

The decrease in $\mathrm{Var}[\frac{\Delta E_{\alpha\beta}}{R^2}]$, from data in fig. 3.8, is compatible with scaling R^{-2} for small R values. Differently, it deviates from this behaviour at larger radii, where it is compatible with $1/R$. Assuming now that $\mathrm{Var}[\delta_{\alpha\beta}]$ does not increase with R, from eq.(3.29) and observation of data we have a lower bound on ω, i.e.:

$$4 - 2\omega < 2 \Rightarrow \omega > 1. \tag{3.30}$$

This observation, also considering that the quadradic term must dominate over δR^ω at large R, yields the inequalities:

$$1 < \omega < 2, \tag{3.31}$$

which fix an upper and a lower bound for ω values compatibles both with our data and with the hypothesis of a self-averaging surface term ΥR^θ.

How to fix the exponent of the subleading correction δR^ω. Under the previous assumptions, at large R, the deviation of $\Delta E_{\alpha\beta}$ from its mean value is entirely due to the fluctuation of prefactor $\delta_{\alpha\beta}$ of the correction term. Let us make explicit that at large R, $\Delta E_{\alpha\beta}$ fluctuations are dominated by $\delta_{\alpha\beta}$ fluctuations. We do this by replacing $\Upsilon_{\alpha\beta}$ with its average value $\langle \Upsilon_{\alpha\beta} \rangle = \Upsilon$ in eq.(3.28):

$$\Delta E_{\alpha\beta} = \Upsilon R^2 - \delta_{\alpha\beta} R^\omega. \tag{3.32}$$

As in the RFIM, in the roughening case and in the DP, here too we assume, as a working

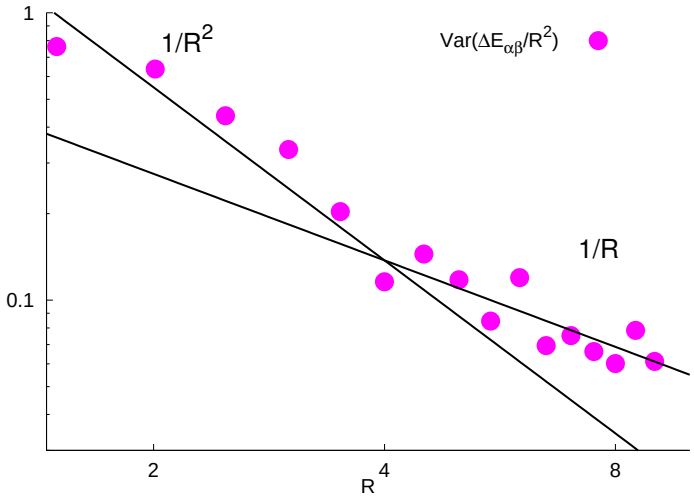

Figure 3.8: *Scaling of $Var[\Delta E_{\alpha\beta}/R^2]$ with R at $T = 0.89T_c$. Data are compatible with a scaling R^{-2} at small R and $R^{2\omega-4}$ at large R, according to formula eq.3.29. The exponent ω at $T = 0.89T_c$ is 3/2. Indeed the scaling of data at large R is compatible with $R^{2\omega-4} = R^{-1}$*

hypothesis, that the probability distribution of $\delta_{\alpha\beta}$ must not change with the droplet size. Indeed, if, from eq.(3.32), we have:

$$\delta_{\alpha\beta} = \frac{\Upsilon R^2 - \Delta E_{\alpha\beta}}{R^\omega}, \tag{3.33}$$

then we need to find a value of ω for which $\mathrm{Var}[\delta_{\alpha\beta}]$ does not change with R.
Let us consider a running value of ω. For each ω, it is possible to fit $\langle \Delta E_{\alpha\beta}(R) \rangle$ via eq.(3.20) and extract the resulting value, Υ, which in turn depends on the running value of ω: $\Upsilon = \Upsilon(\omega)$. At large R, because of the validity of eq.(3.32), we expect that all fluctuations are given by the correction term:

$$\mathrm{Var}(\Delta E_{\alpha\beta}(R)) = \mathrm{Var}(\delta_{\alpha\beta}(\omega)) R^{2\omega}. \tag{3.34}$$

This is true for each value of unknown exponent ω. At the same time, for an arbitrary value of ω, the fluctuations of $\delta_{\alpha\beta}(\omega)$ will generally depend on R. Only for one value, the one which we are looking for and which we call ω^*, we have:

$$\mathrm{Var}(\Delta E_{\alpha\beta}(R)) = \mathrm{Var}(\delta_{\alpha\beta}(\omega^*)) R^{2\omega^*} \tag{3.35}$$

with $\mathrm{Var}(\delta_{\alpha\beta}(\omega^*))$ not dependent on R. Because $\mathrm{Var}(\Delta E_{\alpha\beta}(R))$ is exactly the same quantity in eqs,(3.34) and (3.35), we can then write:

$$\mathrm{Var}(\delta_{\alpha\beta}(\omega)) = \mathrm{Var}(\delta_{\alpha\beta}(\omega^*)) R^{2(\omega^* - \omega)} \tag{3.36}$$

which, taking the logarithm, becomes:

$$\begin{aligned} \log(\mathrm{Var}(\delta_{\alpha\beta}(\omega))) &= \log(\mathrm{Var}(\delta_{\alpha\beta}(\omega^*))) + 2(\omega^* - \omega)\log(R) \\ &= \log(\mathrm{Var}(\delta_{\alpha\beta}(\omega^*))) + a(\omega)\log(R). \end{aligned} \tag{3.37}$$

A linear fit of $\log(\mathrm{Var}(\delta_{\alpha\beta}(\omega)))$ vs $\log(R)$ gives an angular coefficient $a(\omega) = 2(\omega^* - \omega)$ for each ω. Lastly, value ω^* is simply the ω which satisfies $a(\omega^*) = 0$.
Summarizing, a value of exponent ω was calculated for each ensemble of hybrid minima $\mathcal{C}_{\alpha\beta}$ at a given T, according to the following recipe:

1. Choose a value of ω and fit $\Delta E_{\alpha\beta}(R)$ vs R according to this value. Retain the fit parameter $\Upsilon(\omega)$.

2. Calculate for each value of R the distribution of $\delta(\omega, R)_{\alpha\beta}$ via eq.(3.33) using $\Upsilon(\omega)$. Calculate $\mathrm{Var}[\delta(\omega, R)_{\alpha\beta}]$ as a function of R.

3. Repeat points 2) and 3) until a set of ω is sampled.

4. For each value of ω, fit $\mathrm{Var}[\delta(\omega, R)_{\alpha\beta}]$ vs R, according to eq.(3.37), which yields coefficient $a(\omega)$.

5. From the linear fit of $a(\omega) = 2(\omega^* - \omega)$ find out value ω^* which makes fluctuation of $\delta_{\alpha\beta}$ independent of R.

Let us note that the validity of equations from eq.(3.32) to (3.37) relies upon two working hypotheses:

- $\mathrm{Var}[\Upsilon_{\alpha\beta}] << \mathrm{Var}[\delta_{\alpha\beta}]$;

- A value of ω exist, so that $\mathrm{Var}[\delta_{\alpha\beta}]$ does not depend on R.

T	ω
0.89 T_c	1.50(19)
0.95 T_c	1.60(18)
1.03 T_c	0.84(16)
1.09 T_c	1.36(28)
1.33 T_c	0.94(25)

Table 3.1: Values of ω as function of temperature.

If only one of these two hypotheses is wrong, eq.(3.37) also is wrong. In particular, if we try to compute $a(\omega)$ fitting data with eq.(3.37), there would be no reason to expect $a(\omega)$ to be a linear function of ω, let alone a linear function with coefficient -2 (cfr. eq.3.37). Indeed, the most striking evidence that the two former hypotheses are correct is the linear behaviour with coefficient -2 that we find for $a(\omega)$, shown in fig.(3.9) ($T = 0.89T_c$). The values of ω^* found at the various temperatures are listed in tab.3.1, in which values of ω^* are compatible within errors with the boundary $1 < \omega < 2$. Because $\omega^*(T)$ displays no definite trend with temperature, the average between varying temperatures may be viewed as the real value of ω in our model, that is:

$$\omega = 1.2 \pm 0.2. \tag{3.38}$$

The following section proposes a physical interpretation of correction term δR^ω, i.e. roughening of the interface.

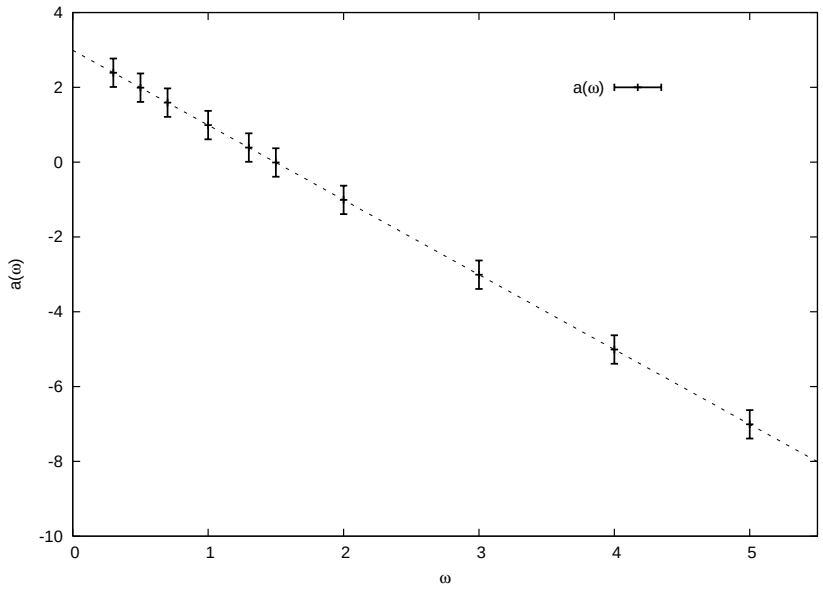

Figure 3.9: *Behaviour of $a(\omega)$ vs ω with $a(\omega)$ calculated fitting data on $\delta_{\alpha\beta}(\omega, R)$ via eq.3.37 ($T = 0.89T_c$). A linear fit of $a(\omega)$ vs ω has coefficient $b = -2$. This is in perfect agreement with the expectation $a(\omega) = 2(\omega^* - \omega)$ (see eq.3.37).*

Roughening interpretation of correction δR^ω. In disordered systems interfaces are typically rough. This phenomenon has been investigated in depth since studies on the directed polymer (DP) problem [63] and the Random Field or Random Bond Ising Model

(RBIM) [58, 64]. The roughening signature is the fact that the interface thickness w grows with linear size R of the interface itself:

$$w \sim R^{\gamma}, \tag{3.39}$$

where γ is the so-called roughening exponent. In the context of elastic manifolds in random media [65, 66], a precise relation exists between the energy cost of a rough interface and roughening exponent γ. The energy gained by roughening appears as a negative

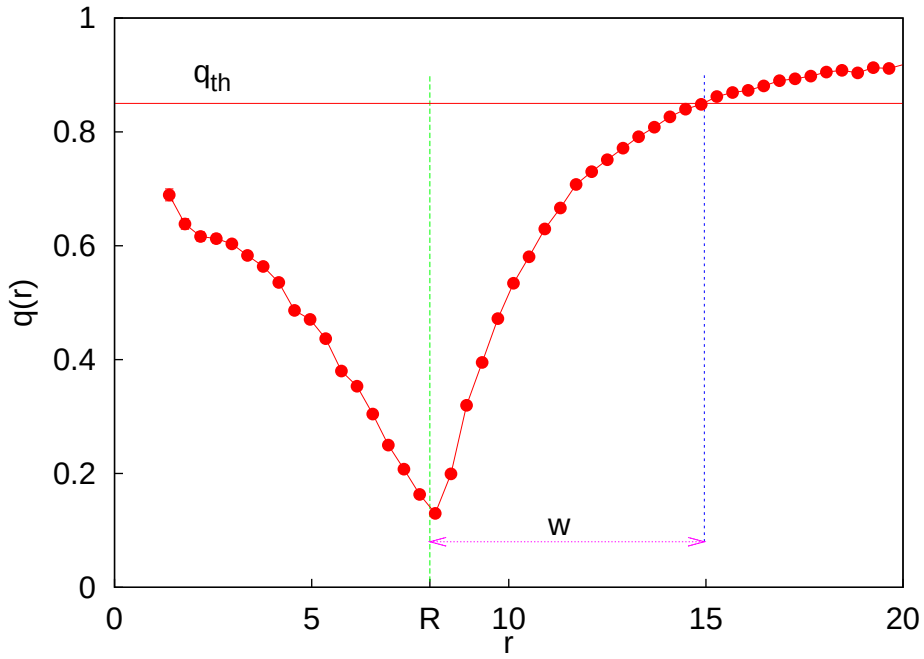

Figure 3.10: *Radial local overlap of a sphere of radius R=8. For the estimate of w we look only at the outer part of the interface. This side is not affected by finite size effects in small spheres.*

correction to the ground state energy of the manifold:

$$\Delta E = \Upsilon R^{d-1} - BR^{\omega}. \tag{3.40}$$

In this context, the exponent ω is model-dependent but, according to [65, 66], is linked to the roughening exponent γ by the following identity:

$$\omega = 2\gamma + d - 3 \qquad d = 3 \qquad \Longrightarrow \qquad \omega = 2\gamma. \tag{3.41}$$

Interface roughening seems to be an appealing interpretation of correction term δR^{ω} which emerges from our data. Exponent ω of our system was already calculated (see previous section). Now, in order to estimate γ, we must find how the thickness of our interface scales with its size (eq.(3.39)). To define thickness w of the interface, we consider the overlap between mixed configuration $\mathcal{C}_{\alpha+\beta}$ immediately after the switch and hybrid minimum $\mathcal{C}_{\alpha\beta}$. The overlap is small close to the interface, where particles have moved most, whereas it approaches one away from it. Hence, w is defined as the thickness of the region for which the local radial overlap of the excitation is smaller than an arbitrary

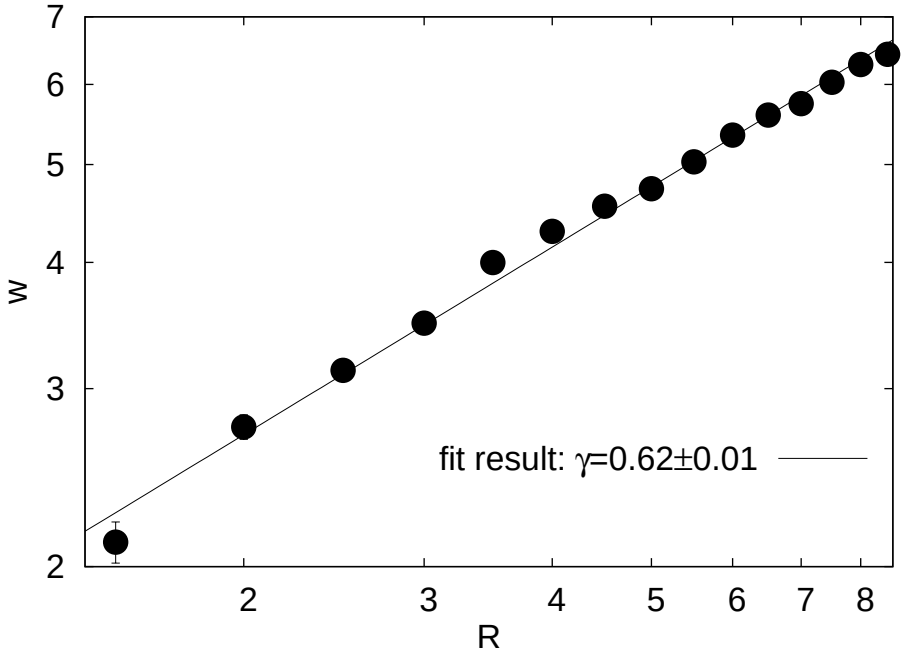

Figure 3.11: *Scaling of interface thickness w with size R of sphere. Data refer to interfaces between IS sampled at $T = 0.89T_c$.*

T	γ
0.89 T_c	0.62(01)
0.95 T_c	0.70(04)
1.03 T_c	0.71(03)
1.09 T_c	0.71(03)
1.33 T_c	0.90(04)

Table 3.2: Values of roughening exponent γ at various temperatures.

threshold value, q_{th} [1].
In fig. 3.10, the local overlap is plotted as a function of distance r from the centre of the sphere for a droplet of radius $R = 8$ at $T = 0.89T_c$. Inside the sphere the increase in the overlap away from the interface is clearly influenced by interference effects (see also sec. 3.2.2). It is thus convenient to define w from the behaviour of $q(r)$ outside the sphere (figure 3.10). Fig. 3.11 shows the scaling of interface thickness w with R for excitations at $T = 0.89T_c$. The roughening exponents found at different temperatures measuring the interface thickness with the method outlined above are listed in Tab. 3.2.

Comparing the set of γ values of Tab. 3.2 with exponent $\omega = 1.2 \pm 0.2$ of our model, we find that, for almost all temperatures (except $T = 1.33T_c$), equation $\omega = 2\gamma$ is fulfilled. Therefore, summarizing, we can state that the appearence of a correction to the leading behaviour ΥR^{θ} of the interface cost is probably due to roughening of the interface for the two following reasons:

[1] We must consider the possibility the measure of exponent γ may depend on the threshold q_{th}. At temperature $T = 0.89T_c$, q_{th} has been variated between 0.75 and 0.9, finding values of γ in the interval $[0.59, 0.63]$. Because with $q_{th} = 0.85$ it is measured $\gamma = 0.63 \pm 0.01$, the error amounts to 2% of γ value, whereas the variation of the exponent due to changing q_{th} amounts to 7% of γ value, hence it is larger. Nevertheless, provided that there is no trend in the variation of γ with q_{th}, we retain that the error on γ is understimated and are confident of the fact that γ does not depend on q_{th}.

- The correction term δR^{ω} behaves as is typical for corrections to the energy cost of interfaces in disordered media, i.e., it has fluctuations that violates the CLT (cfr. previous paragraph).

- The exponent ω fulfills the relation $\omega = 2\gamma$, with γ the roughening exponents.

A roughening exponent smaller than 1 implies that the ratio w/R between the width w and the linear size R of the surface decreases for larger spheres. Thus large excitations have *relatively* thin interfaces. This is clearly shown in figure 3.12, where two excitations with different radius ($R = 4$ vs. $R = 8$) are compared in a coordinate system where all lengths are rescaled by R, so that both rescaled spheres have virtual radius unity. The rescaling emphasizes the thick interface of the smaller excitation compared to the narrower interface of the larger excitation.

RBIM and Inherent Structures To understand why roughening occurs let us examine the Random Bond Ising Model (RBIM). This is an Ising spin model in which the nearest-neighbour bonds are random, albeit typically positive. In such a system, the position of a domain wall strongly depends on disorder, since weak bonds are more likely to be broken. On one hand, a smooth domain wall is preferable, as it would break the smallest number of bonds. On the other hand, some suitable deviation from smoothness may induce the breaking of weaker bonds and hence a lower energy cost. So a rough interface is the result of a complicated optimization problem: the cost of a large number of broken bonds is balanced by the gain due to the presence of very weak bonds among them. As a result, in a disordered system from the point of view of energy a rough interface may be favoured with respect to a smooth one.

What about Inherent Structures? When we create an excitation, a smooth interface between two different IS is placed in the system. All particles, except those close to the interface, are in equilibrium positions, as the IS are minima of potential energy. We can imagine that each interaction between a pair of particles plays the role of a bond. In regions where IS are more mechanically stable, bonds between particles are stronger, and vice versa. Around the spherical excitations that are created there will be regions which are more or less mechanically stable, i.e. their particles are linked by weaker or stronger bonds: hence, the analogy with the RBIM and probably the reason for rough interfaces between IS. This picture of IS assumes some heterogeneous mechanical stability closely resembling the inhomogeneous elastic response displayed by other glassy systems [67, 68].

3.3.3 Fluctuations

The energy cost of a surface between two IS is physically interesting, not only for its mean value but also for its distribution. The simplest version of RFOT theory [4] connects droplet formation with the competition between a volume term, proportional to complexity, and "surface" cost ΥR^{θ}, with a single value for surface tension parameter Υ. However it is resonable that the self-induced disorder in particle positions and presence of a large number of low temperature states may lead to different values of their contact cost. For these reasons in [6] a distribution for contact energy was introduced, to explain the smooth decay of the point-to-set correlation function $q_c(R)$ (cfr. sec.2.4.3), neither compatible with a simple one state scenario [34] nor with a sharp version of the RFOT theory with only one value of the surface tension [6]. It has already been pointed out that

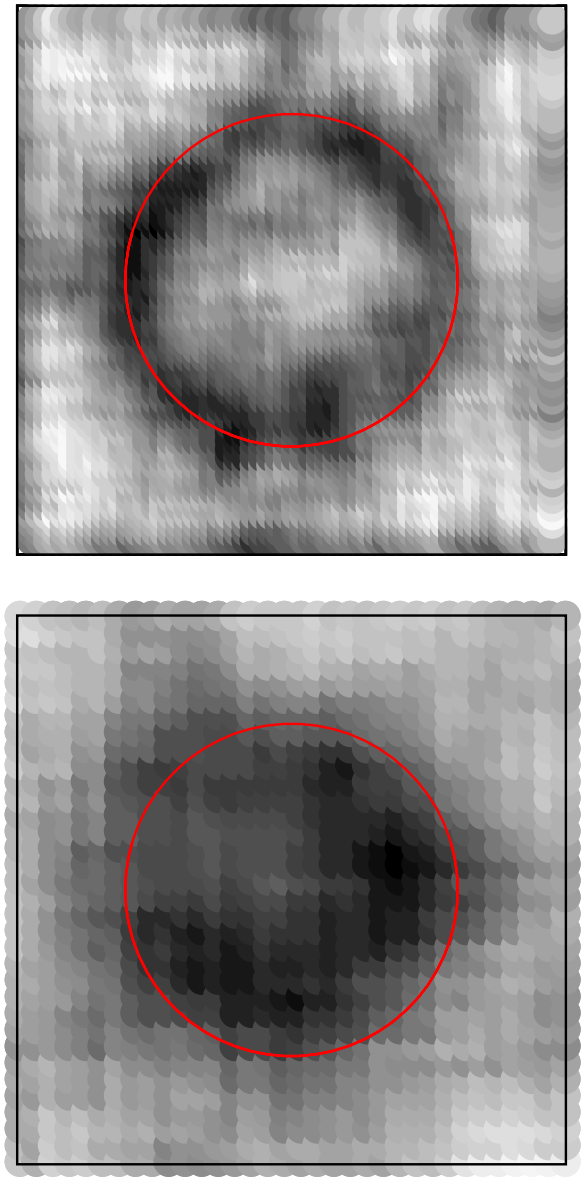

Figure 3.12: *Local overlap $q_{\alpha\beta}(x, y)$ between $\mathcal{C}^{IS}_{\alpha\beta}$ and $\mathcal{C}_{\alpha+\beta}$ for configurations with interface placed at $R = 8$ (top) and $R = 4$ (bottom); only a thin slice at half height of the system is shown. Plots are rescaled so that both spheres appear to be of the same size. Low overlap (dark grey) at interfaces indicates major rearrangements of particles; far from interfaces overlap with initial configurations is high (light grey). Clearly, larger sphere (top) has a relatively thinner, or smoother, interface.*

the dependence of contact costs between Inherent Structures is not a simple power law. Nevertheless, to be as consistent as possible with the description of [6], we may write:

$$\langle \Delta E_{\alpha\beta}(R) \rangle = \Upsilon R^2 - \delta R^{\omega} \tag{3.42}$$

as

$$\langle \Delta E_{\alpha\beta}(R) \rangle = y(R) R^2 \tag{3.43}$$

with

$$y(R) = \Upsilon - \delta/R^{2-\omega}. \tag{3.44}$$

The $y(R)$ thus defined is a *soft* surface tension, the mean value and distribution of which strongly depend on R. This is evident expecially at small R, where the contribution of the correction term to $y(R)$ is still important. From our numerical data, it is possible to obtain the above defined soft surface tension for each pair of IS:

$$y_{\alpha\beta}(R) = \Delta E_{\alpha\beta}(R)/R^2 \tag{3.45}$$

$$y_{\alpha\beta}(R) = \Upsilon_{\alpha\beta} - \delta_{\alpha\beta}/R^{2-\omega}. \tag{3.46}$$

We already know from subsection 3.3.2 that the variance of $y_{\alpha\beta}(R)$ values is ever-decreasing. At small R, because of the self-averageness of $\Upsilon_{\alpha\beta}$ in eq.(3.46). At large R, the fluctuations of $y_{\alpha\beta}(R)$ are dominated by the still large fluctuations of term $\delta_{\alpha\beta}$. Nevertheless, fluctuations of $\Delta E_{\alpha\beta}(R)/R^2 = y_{\alpha\beta}(R)$ at large R scale like $R^{2\omega-4}$ (see eq.(3.29)) with $\omega < 2$, are thus ever-decresing. Some of the distributions of the soft surface tension are shown in fig 3.13, for fixed temperature and increasing R, and in fig 3.14, for fixed R and different temperatures. Two main effects may be observed in the distribution of soft

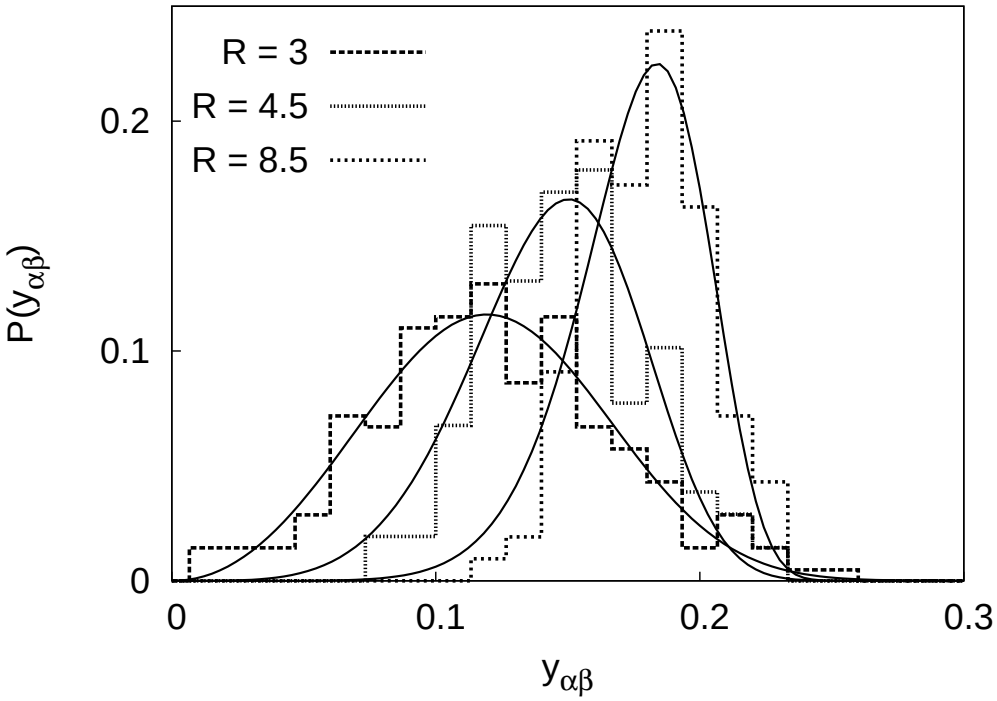

Figure 3.13: *"Soft" surface tension, $y_{\alpha\beta}(R) = \Delta E_{\alpha\beta}/R^2$, distributions of spherical interfaces between inherent structures: temperature is fixed, $T = 0.89T_c$, and various size of droplets are considered, $R = 3, 4.5, 8.5$. Distributions narrow with increasing R. Full lines: fits according to, $\Omega\ y^{\nu-1} \exp\left[-(y/y_c)^{\nu}\right]$: Ω, y_c, ν are fit parameters. ν increases with increasing R.*

surface tensions $y_{\alpha\beta}(R)$:

- At a fixed temperature, the distribution of surface tension $P\left[y_{\alpha\beta}(R)\right]$ narrows with increasing size R of the excitation. This observation, which has its quantitative

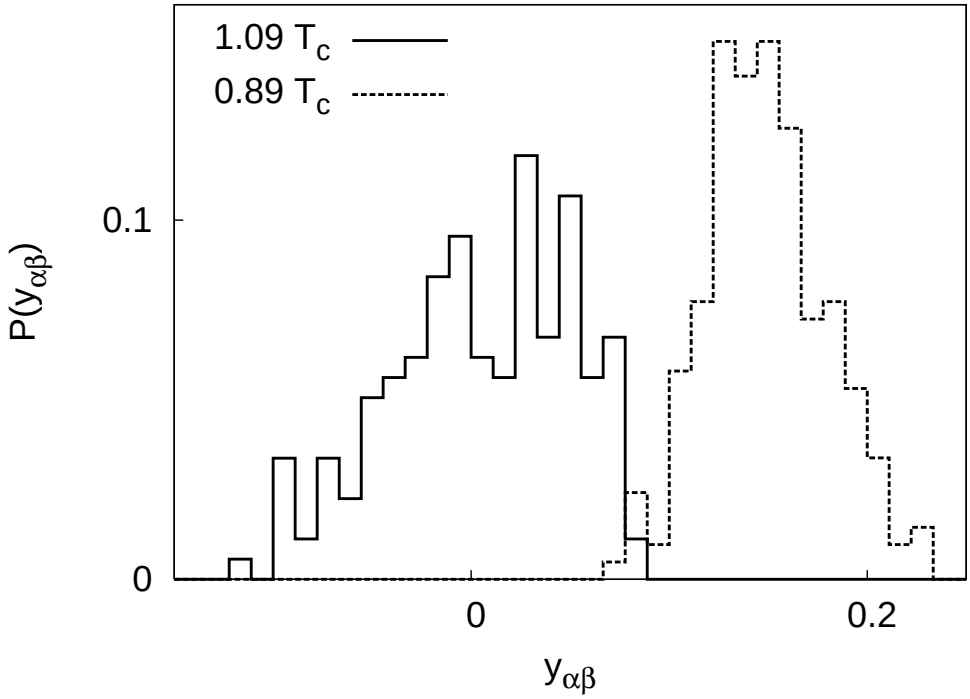

Figure 3.14: *"Soft" surface tension, $y_{\alpha\beta}(R) = \Delta E_{\alpha\beta}(R)/R^2$, distributions for spherical interfaces between inherent structures. Size $R = 4.5$ of droplets is fixed and two different temperatures are considered: one below, $T = 0.89T_c$, and one above, $T = 1.09T_c$, the mode coupling temperature.*

conterpart in the results on $\mathrm{Var}[y_{\alpha\beta}(R)]$, supports the hypothesis that fluctuating surface tension is a finite-size effect [6].

- At fixed size and increasing temperature, the distribution $P\left[y_{\alpha\beta}(R)\right]$ broadens and clusters around zero. The different states of the supercooled liquids, approximated in this study with inherent structures, slowly merge into each other, when temperature at which IS are sampled is raised above the mode coupling one, T_c, due to the vanishing of contact energy.

Numerical distributions $P\left[y_{\alpha\beta}(R)\right]$ measured at $T = 0.89T_c$, shown in fig.3.13, are well fitted with the functional form:

$$\Omega\ y^{\nu-1} \exp\left[-(y/y_c)^{\nu}\right], \tag{3.47}$$

proposed in [6], where Ω, y_c and ν are fit parameters. Let us note that the exponent ν, obtained fitting $P\left[y_{\alpha\beta}(R)\right]$ with eq.(3.47), increases with increasing R. Recall that, according to RFOT, by lowering the temperature ξ_{RFOT} increases. Although here T is fixed, we are studying the energy cost of increasing size excitations. To some extent it is like studying the behaviour of $P\left[y_{\alpha\beta}(\xi_{RFOT})\right]$ for increasing ξ_{RFOT}, hence for decreasing temperatures. The information we get from the increase of ν with increasing R is therefore that at lower temperatures the surface tension distribution of RFOT excitations narrows. Extrapolating, we may state that, according to our data, $P(y) \to \delta(y - y_c)$ when temperature is decreased. Recall how the behaviour of the point-to-set correlation function is related to $P(y)$, that is:

$$q_c(R) \sim \int_{T\Sigma R^{d-\theta}}^{\infty} dy P(y)(1 + e^{R^d\Sigma - \beta y R^{\theta}})^{-1}. \tag{3.48}$$

When $P(y) \to \delta(y - y_c)$ the above formula is well approximated by:

$$q_c(R) \sim \Theta(y_c - T\Sigma R^{d-\theta}), \tag{3.49}$$

that is, a sharp transition from non-ergodic to ergodic behaviour takes place at $R = (y_c/T\Sigma)^{d-\theta}$. We can conclude that the study of surface tension fluctuations may give indications that, at temperatures well below T_c, the sharp version of RFOT [4] can be recovered.

3.4 Surface tension between equilibrium configurations

In order to legitimate the Inherent Structures results, this section deals with how amorphous excitations relax at equilibrium. The main goal of approximating metastable states with IS has been the possibility to study time-independent observables. Nevertheless, it was also a limitation. Within the RFOT scenario, it is the *free energy* cost of an amorphous droplets which scales like:

$$\Upsilon R^{\theta}. \tag{3.50}$$

In the landscape-dominated regime, i.e., when equilibrium configurations are tipically found in the proximity of an energy minimum, it is assumed that free energy is well approximated by energy, hence the approximation of using IS. Using this approximation it was found that the surface cost of an excitation scaled like ΥR^2 (plus a correction). The first aim of this section is to put this result on a firmer basis. It is explained how the scaling ΥR^2 is not spoiled by a few steps of equilibrium dynamic. Moreover it is shown that the *hybrid minima* enclosing the interface between IS which were of central importance in the previous analysis, are closely related to amorphous excitation at finite temperature.

3.4.1 Time-dependent surface tension.

In this section the method used to build an interface between Inherent Structures is applied to equilibrium configurations. That is, pairs of configurations equilibrated at the same temperature $\mathcal{C}_{\alpha}^{th}$, $\mathcal{C}_{\beta}^{th}$ are considered and particles located within a spherical cavity of the same size are exchanged between them. At this stage, the procedure used to build the amorphous excitation is identical to that one described in sec. 3.2.2 for IS. The energy of the interface enclosed in $\mathcal{C}_{\alpha+\beta}^{th}$, $\mathcal{C}_{\beta+\alpha}^{th}$ is hereafter studied as a function of time. More precisely the configurations are relaxed by means of a standard Montecarlo algorithm. It should be stressed that the algorithm used at this stage is different from the one used to equilibrate configurations $\mathcal{C}_{\alpha}^{th}$, $\mathcal{C}_{\beta}^{th}$. This algorithm implements non-local moves [51] to achieve a fast equilibration, whereas the MC algorithm used in this section does not, in order to mimic the dynamics of the system. The smooth surface between α and β in $\mathcal{C}_{\beta+\alpha}^{th}$ is regarded as the GDS also in this context. Thus, the cost of the interface, which is now a time-dependent quantity, is calculated as:

$$\Delta E_{\alpha\beta}(R,t) = E_{\alpha\beta}(t) - E_{\alpha}^{th,in} - E_{\beta}^{th,out} \tag{3.51}$$

Here, the definition of $E_{\alpha}^{th,in}$, $E_{\beta}^{th,out}$ is identical to that given in sec. 3.2.3, with IS replaced by equilibrium configurations, and $E_{\alpha\beta}(t)$ is the energy of configuration $\mathcal{C}_{\alpha+\beta}^{th}$ after t, where

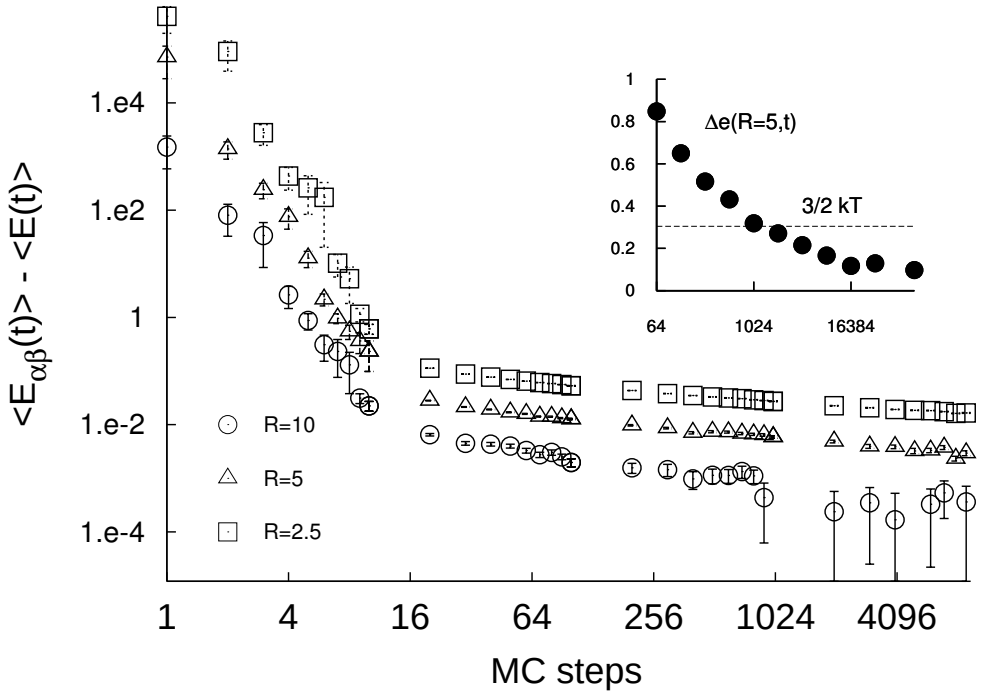

Figure 3.15: *Main:* $(\langle\epsilon_{\alpha\beta}(t)\rangle - \langle\epsilon\rangle)$ *vs* t*;* $\langle\epsilon_{\alpha\beta}(t)\rangle$ *is the average energy per particle along the relaxation of a spherical interface while* $\langle\epsilon\rangle$ *is the average energy per particle at equilibrium.* $\langle\epsilon_{\alpha\beta}(t)\rangle$ *is studied for spherical interfaces of radius* $R = 2.5, 5, 10$*. Inset: surface tension* $\langle\Delta E_{\alpha\beta}(t)\rangle/4\pi R^2$ *vs* t *for* $R = 5$ *compared to the thermal energy per particle. Data come from relaxational dynamics at* $T = 0.89T_c$

time t is measured in MC steps.
This time-dependent surface tension is expected to disappear completely at large times, because the system at the temperatures in question is deeply supercooled but still ergodic. The amorphous excitation of RFOT theory continue to form and relax, so that it is reasonable to expect that an interface placed in a precise position will be erased by these rearrangements.

Unphysical stress relaxation. As the case of Inherent Structures, the construction of a surface between two configurations leads to very high energy terms, due to accidental pairs of particles falling arbitrarily close (see sec. 3.2.3). However, only ~ 10 Montecarlo steps at the same temperature at which the initial configurations were equilibrated are enough to relax these unphysical energy contributions. The two stages in the relaxation of $E_{\alpha\beta}(t)$ are represented in fig. 3.15 for three different droplet size. After the initial transient, the excess energy per particle concentrated on the interface is of the order of thermal energy $3/2T$, as shown in the inset of fig. 3.15.

The relaxational dynamics of the interfaces has been studied at the temperatures $T = 0.89T_g, 1.02T_g, 1.09T_g, 1.33T_g$, with spherical interfaces of radius ranging from $R = 3$ to $R = 8$. The number of the initial equilibrium configurations $\mathcal{C}_\alpha^{th}$ is 9 for $T = 0.89T_g$, $1.02T_g$ and 12 for $T = 1.09T_g$, $T = 1.33T_g$. Thus ensembles of respectively 72 and 132 mixed configurations $\mathcal{C}_{\alpha+\beta}^{th}$ have been studied.

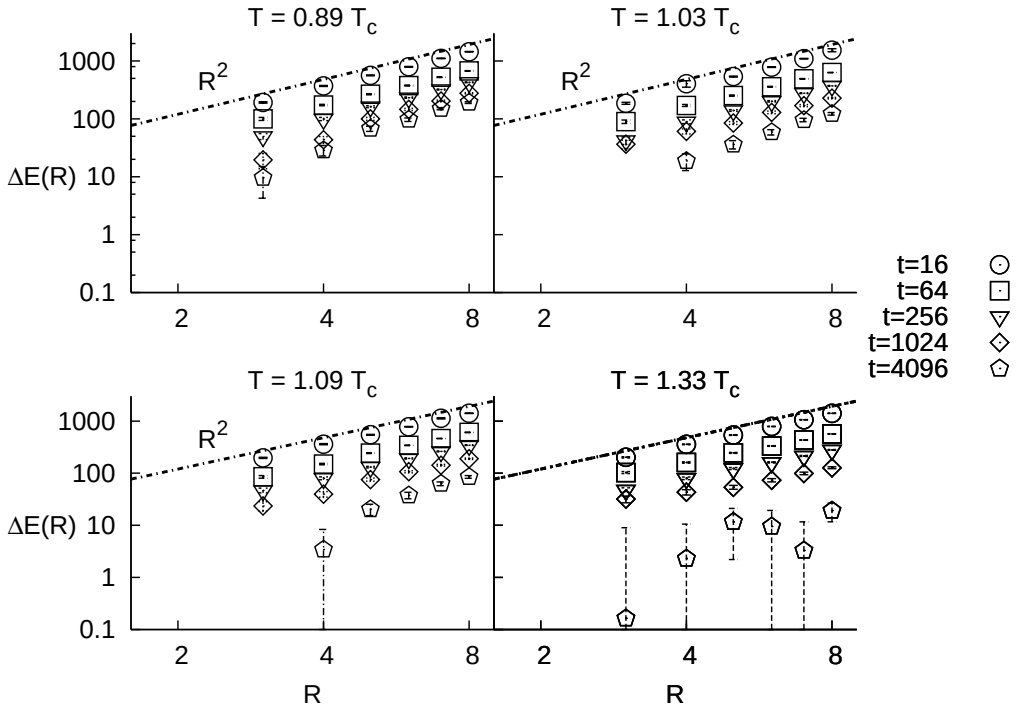

Figure 3.16: *Excess energy* $\langle \Delta E(R,t) \rangle$ *vs* R *measured at different times (different symbols) and different temperatures (different panels). Temperatures are* $T = 0.89T_g, 1.03T_g, 1.09T_g, 1.33T_g$. *Time* t *is measured in Monte Carlo steps.*

3.4.2 Quadratic scaling of interface energy

After the transient regime, in which the unphysical stress is relaxed, the trend appears of the average interface cost $\langle \Delta E(R,t) \rangle$ versus the size of spheres R, shown in fig. 3.16. The scaling of $\langle \Delta E(R,t) \rangle$ with R is shown for the various temperatures (different panels) at increasing times (different symbols). The log-log scale emphasizes that a simple power law with exponent 2 describes the growth of excess energy with droplet size. This clearly appears at times $t \leq 1000$, whereas at longer times, $t > 1000$, a small size correction appears. At large R values the quadratic scaling of $\langle \Delta E(R,t) \rangle$ with R is conserved for all times. This observation is the basis for the analysis carried out with Inherent Structures: even at finite temperature, at sufficiently large sizes, the power law ΥR^2 is found.

What about roughening ? At large times, scaling of the energy cost of interfaces exibits, at small sizes, a deviation from leading quadratic behaviour. Along the lines of sec. 3.3.1, we assume here a power law correction δR^{ω} to the leading quadratic cost. Exponent ω was fixed in order to make the variance of $\delta_{\alpha\beta}$ independent of R for large R values (see sec. 3.3.2). This study was carried out for the lowest temperature, $T = 0.89T_c$, after $t = 4096$ MC steps of relaxation of the interface. At this time a deviation from leading quadratic scaling is evident for small values of R. At $t = 4096$, roughening exponent γ was also calculated with the same method used in sec. 3.3.2. Exponents ω (much smaller than in the case of IS) and γ were compared, but their values did not fit the relation $\omega = 2\gamma$, which is fulfilled when roughening occurs.

We think that the analogy between the Random Bond Ising Models and IS described in sec. 3.3.2 fails when studying relaxation of interfaces at finite temperature. The analogy was based on the evidence that, in IS, almost all the particles are frozed in their

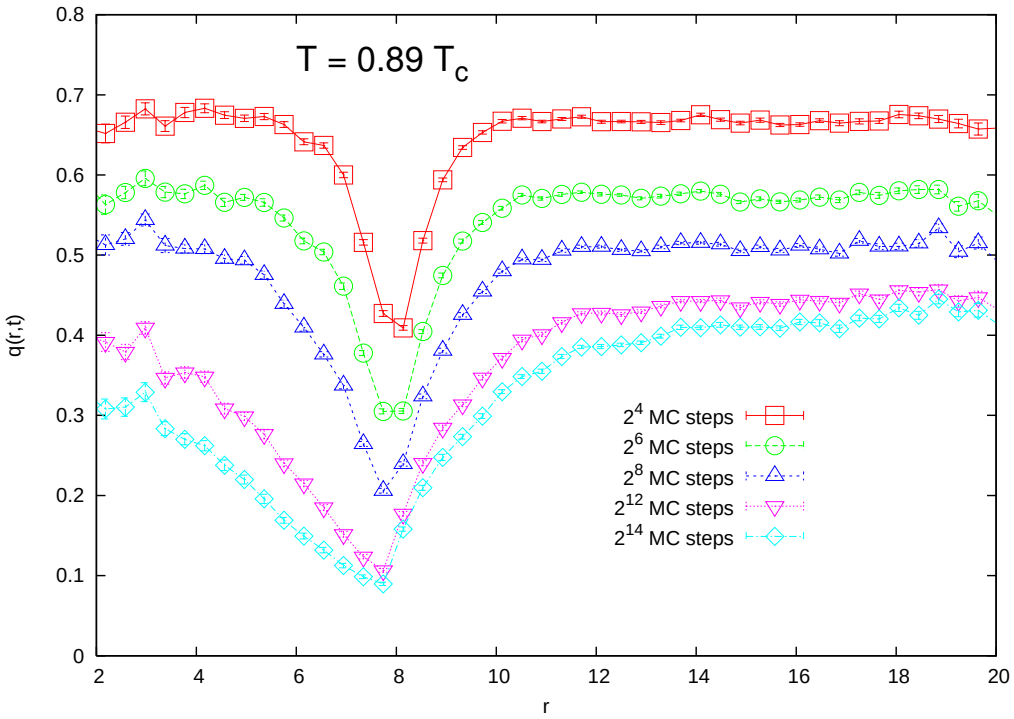

Figure 3.17: *Relaxation of a droplet at finite temperature* $T = 0.89T_c$. *Radial overlap* $\langle q(r)\rangle$ *averaged over 72 configurations at different times,* $t = 2^4, 2^6, 2^8, 2^{10}, 2^{12} MC steps$.

equilibrium positions, even when some of them have to change their positions in order to optimize the shape of an interface. In such a situation, it was reasonable to speak of an inhomogeneous displacement of mechanical stability around the interface. This inhomogeneity is responsible for roughening. The evidence that particles sufficiently far from the interface were —almost— frozen in their equilibrium position came from data on the local overlap, close to 1 far from the interface. Conversely along the relaxation of interfaces at finite temperatures even the overlap of regions far from interfaces decreases significantly, as can be seen in fig. 3.17. It no longer makes sense to speak of more or less mechanically stable regions enclosing the excitation. We are no longer dealing with minima of potential energy. Thus, the main mechanism responsible for roughening within IS seems to disappear. The most we can say, accepting that roughening plays a role even at finite temperatures, is that it appears to be neglibile or, perhaps, that we are unable to disentangle it from the effect of temperature.

Slowing down of $\Upsilon(t)$ For most of the time, the scaling of $\langle DE(R,t)\rangle$ with R is well fitted with a quadratic power. Thus, we calculated the time-dependet surface tension $\Upsilon(t)$ as a fit parameter from:

$$\langle DE(R,t)\rangle = \Upsilon(t)R^2. \tag{3.52}$$

Fig. 3.18 shows the behaviour of $\Upsilon(t)$ for $T = 0.89T_c, 1.02T_c, 1.09T_c$ and $1.33T_c$. Let us note that, the lower the temperature the more slowly surface tension relaxes. $\Upsilon(t)$ is an observable which keeps track of the slowing down of relaxation time of our glass-former. Nevertheless, scaling of $\Upsilon(t)$ does not show any qualitative change as temperature falls from above to below mode coupling temperature T_c.

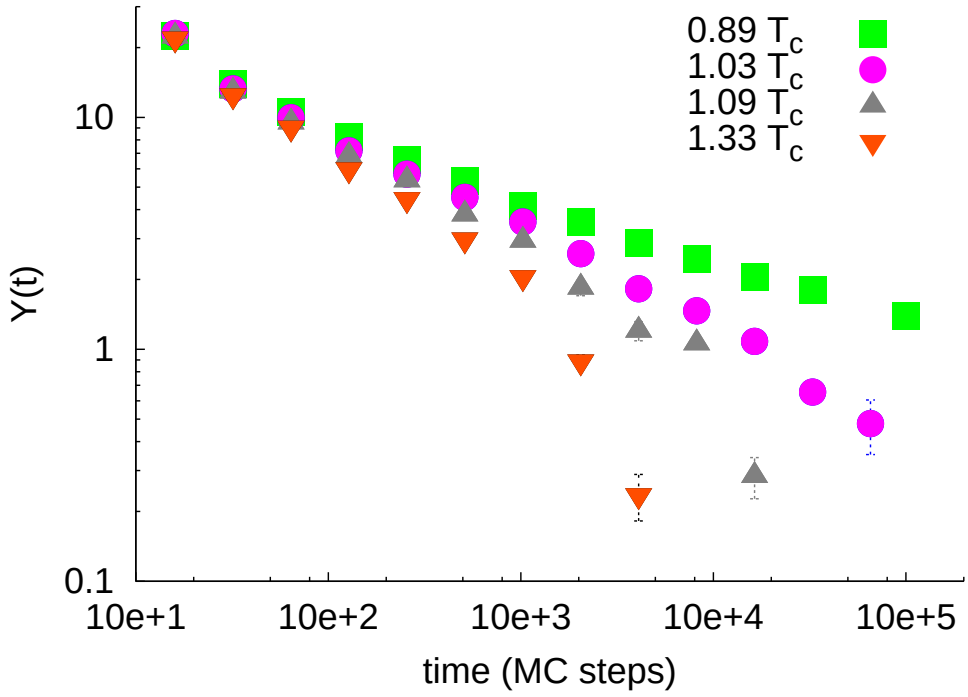

Figure 3.18: *Surface tension values obtained from equilibrium configurations at different times. At each time $Y(t)$ is obtained from a quadratic scaling ansatz $Y(t) = \langle \Delta E(R,t) \rangle / R^2$. Relaxation of $Y(t)$ is plotted for the following temperatures (left to right in the picture) $T = 1.33T_c, T = 1.09T_c, T = 1.03T_c, T = 0.9T_c$. Notice the slowing down of relaxation time for decreasing temperature.*

3.4.3 Hybrid minima and thermal droplets

We claim that the existence of surface tension on finite time-scales is not trivial. It signals that some metastable states with stressed regions can survive on such time-scales. They may be the instantons mentioned several times in the literature [3, 62, 61]. In this view, it would be interesting to find some evidence that *hybrid minima* are also related to the excitations at finite temperatures. In order to do this, we need a method to compare the surface tension measured between IS and the time-dependent tension measured at finite temperature. The problem is that, working with IS, we were measuring an interface cost ΔE independent of time. Now we must deal with a time dependent $\Delta E(t)$.
At what time should we compare $\Delta E(t)$ and ΔE of IS ? To tackle this problem, let us make use of the well-defined map between thermal configurations and Inherent Structures. Given the trajectory of a thermal droplet, i.e. the set of configurations:

$$\mathcal{C}_{\alpha\beta}(t_1), \ldots, \mathcal{C}_{\alpha\beta}(t_{max}) \tag{3.53}$$

saved along the relaxation of the interface, a trajectory of Inherent Structures

$$\mathcal{C}^{IS}_{\alpha\beta}(t_1), \ldots, \mathcal{C}^{IS}_{\alpha\beta}(t_{max}) \tag{3.54}$$

is obtained by quenching configurations $\mathcal{C}_{\alpha\beta}(t_i)$. Each quench is achieved with the geometric LBFGS algorithm [52]. The following energy cost has been calculated from the set of $\mathcal{C}^{IS}_{\alpha\beta}(t_i)$ inherent structures:

$$\Delta E^{IS}_{\alpha\beta}(R,t) = E^{IS}_{\alpha\beta}(t) - E^{in,IS}_{\alpha} - E^{out,IS}_{\beta}, \tag{3.55}$$

where $E^{IS}_{\alpha\beta}(t)$ is the total energy of $\mathcal{C}^{IS}_{\alpha\beta}(t)$ and $E^{in/out,IS}_{\alpha/\beta}$ are the energies of the IS obtained quenching the initial equilibrium configurations $\mathcal{C}^{th}_{\alpha}$ and $\mathcal{C}^{th}_{\beta}$. The labels *in/out* still signify particles *inside/outside* the spherical cavity.

Fig. 3.19 compares the behaviour of $\langle \Delta E^{IS}(R,t) \rangle$ and $\langle \Delta E(R,t) \rangle$ for linear sizes of

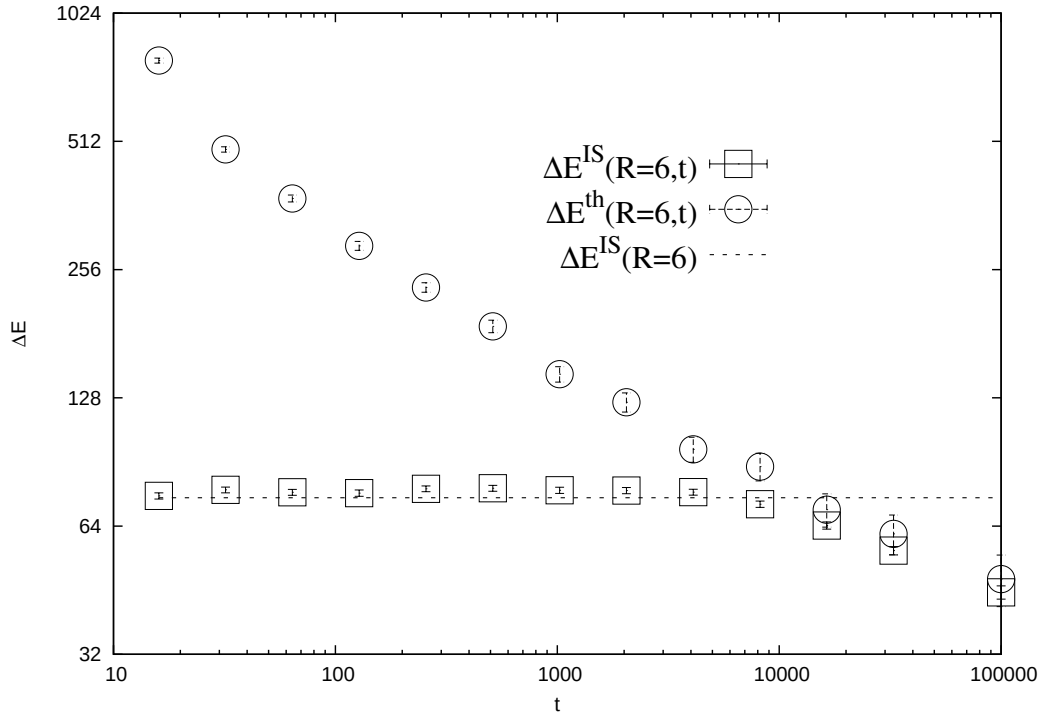

Figure 3.19: *$\langle \Delta E^{IS}(R,t) \rangle$ vs t (squares) plotted against $\langle \Delta E^{th}(R,t) \rangle$ vs t (circles): they are compared to $\langle \Delta E^{IS}(R) \rangle$ (straight line); $R = 6$ and $T = 0.89 T_c$. $\langle \Delta E^{th}(R,t) \rangle$ is the energy cost of an interface between equilibrium configurations after $n = t$ MC steps of relaxation; $\langle \Delta E^{IS}(R,t) \rangle$ is the energy cost of the interface enclosed in the IS obtained by quenching the above mentioned configurations; $\langle \Delta E^{IS}(R) \rangle$ is the energy cost of an interface between inherent structures, as measured in sec.3.2.*

droplets $R = 6, 8$. Up to a time $t^* \sim 10^4$ MC steps, a plateau is present in $\langle \Delta E^{IS}(R,t) \rangle$ whereas $\langle \Delta E(R,t) \rangle$ is ever-decreasing. When $t > t^*$ the two observables overlap.
Considering these data, we can try to answer the following question: are the *hybrid minima* —which enclose an interface between IS— somehow related to the excitations at finite temperature ?
The answer is yes: for a time interval t^* (length of the $\langle \Delta E^{IS}(R,t) \rangle$ plateau), the *hybrid minima* are the inherent structures onto which an equilibrium configuration enclosing an amorphous excitation can be mapped.
It should be noted that the *time-independent* energy cost $\langle \Delta E^{IS}(R) \rangle$, the one measured from IS in sec. 3.2, and the *time-dependent* $\langle \Delta E^{IS}(R,t) \rangle$, obtained along the relaxation of interfaces, *are equal* up to times $t \leq t^*$: this for a given radius (e.g. $R = 6, 8$) and a given temperature ($T = 0.89 T_c$). This is stressed in fig. 3.19, where $\langle \Delta E^{IS}(R,t) \rangle$ vs t is plotted for $R = 6$. All along the plateau $\langle \Delta E^{IS}(R,t) \rangle$ is equal to $\langle \Delta E^{IS}(R) \rangle$. This means that $\langle \Delta E^{IS}(R,t) \rangle$ not only is constant, but even comparable with the cost of interfaces obtained within the $T = 0$ analysis of IS. The situation is summarized in the following

flow-chart, which is true for times $t \leq t^*$:

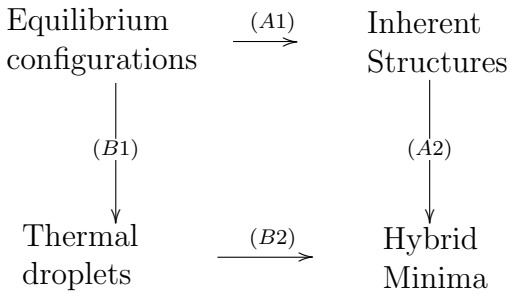

Actually, up to time t^*, we can reach *hybrid minima* enclosing an interface of the same cost following both paths in the flow-chart above, i.e. paths A and B summarized below:

A Consider a set of equilibrium configurations at T.
(A1) Obtain the corresponding IS with a quench.
(A2) Build hybrid minima from IS according to method in sec. 3.2.2, and measure average energy cost of enclosed interface.

B Consider a set of equilibrium configurations at T.
(B1) Build some amorphous excitations and let them relax at finite temperature.
(B2) Along relaxation, quench at various times, and measure energy cost of interface enclosed in IS obtained from these quenches.

We can conclude that, at least at our lowest working temperature, $T = 0.89T_c$, the *hybrid minima* enclosing an interface, studied in sec. 3.2, are the structures which underlie finite-temperature excitations, and not merely an artifact of the IS approximations.

Chapter 4

Interfaces in supercooled liquids: fixed overlap simulations

Motivations. This section introduces a method developed to face from another point of view the problem of measuring the surface tension in a supercooled liquid. When producing amorphous excitations, hopefully similar to that predicted by RFOT, by using either IS or thermal configurations, the basic strategy has been:

1. Identify *which* are the amorphous phases.

2. Build the interface between them and study it.

Clearly, the operative definition of amorphous phases was not arbitrary but, as far as possible, in agreement with a reliable definition of "phases" within a supercooled liquid [2, 5, 69], e.g. minima of the potential energy (or equilibrum configurations near minima). Once these phases were identified, the aim of the work presented in previous chapters was to reproduce *static* excitations, as close as possible to the kind described by random first-order theory [3, 4].
RFOT provides a neat relation between surface tension and correlation length. In the simplest case ($\theta = 2$), it is:

$$\xi_{RFOT}(T) = \frac{\Upsilon(T)}{T\Sigma(T)}. \tag{4.1}$$

This is perhaps the simplest relation imaginable between surface tension and correlation length. In the regime where $\Sigma(T)$ loosely depends on temperature, i.e., $\Sigma(T) \sim \Sigma$, $\xi_{RFOT}(T)$ is simply a linear function of $\Upsilon(T)$. In turn local excitations —the local realization of mean-field states— are well-defined, i.e., $\xi_{RFOT} \neq 0$, only when surface tension is different from zero. So far, so good.
Similarly, we could say that surface tension is present *only* when local excitations exist. Inverting the standard protocol, we could first identify the regime where amorphous excitations are present, and then look for surface tension in that regime. Following this strategy is not recommended, as a measure of ξ_{RFOT} is not very simple, as demonstrated in [34, 6].
Nevertheless, it is possible to retain, and perhaps also generalize, the main physical content of eq.(4.1):

- If there is *any* interesting correlation length in a supercooled liquid, then it should be related to the energy cost of the interfaces dislocated within the system.

Only recently numerical evidence has been shown indicating that the length-scale ξ_{RFOT} of RFOT amorphous excitations grows at low temperature [6] (cfr. sec. 2.4.3): much more effort has been devoted during the last decade to study of dynamical correlation length ξ_{DYN} [7, 35, 36, 37, 38, 39, 40, 41, 42], which measures the correlation between mobility of particles. It is still not clear which is the relation between ξ_{DYN} and ξ_{RFOT}, between *dynamic* and *static* cooperative regions. The purpose of the analysis introduced here is to find some evidence that surface tension, a key ingredient of RFOT, is present even between dynamically cooperative regions (DCR), in order to better understand the interplay between the two different correlation lengths.
As a first step in this direction, dynamical heterogeneities are studied here in a peculiar framework (fixed overlap), where they are presumed to behave differently according to weather the DCR are or are not separated by well-defined interfaces with surface tension.

From the first introductory chapter, we know that the mode coupling temperature T_c marks the border between activated dynamics —$T \leq T_c$ and leading length-scale ξ_{RFOT}— and non-activated dynamics —$T \geq T_c$ and leading length-scale ξ_{DYN}.

Inhomogeneous Mode Coupling Theory (IMCT) [9, 10] places the divergence of ξ_{DYN} at T_c, whereas according to RFOT ξ_{RFOT} is different from zero only below T_c. The temperature regimes dominated by the two length-scales are specular with respect to T_c. Nevertheless, on one hand, IMCT calculations are mean-field, i.e. the closer to T_c, the more approximated they are; on the other hand, there are both numerical and theoretical indications that ξ_{RFOT} may be finite even above T_c [6, 11, 12, 45]. It is therefore reasonable to expect that, at temperatures around T_c, both correlation lengths ξ_{RFOT} and ξ_{DYN} play a role. This is why we choose to investigate the surface tension between *dynamically correlated regions* (DCR), whose extent is measure by ξ_{DYN}, precisely at T_c.

The existence of interfaces between DCR is investigated in this section by means of a dynamical constraint on the overlap of a glass-forming liquid. We know from eq.(4.1) that $\xi_{RFOT} \sim \Upsilon$, so let us assume here that also:

$$\xi_{DYN} = g(\Upsilon), \tag{4.2}$$

where g is an unknown function which links dynamical correlation length ξ_{DYN} and surface tension Υ. We are therefore assuming that the existence of dynamically cooperative regions is connected to the existence of interfaces with a well defined surface tension. The correlation length ξ_{DYN} measures the extent of dynamical correlation at the relaxation time, $\xi_{DYN} = \xi(\tau)$, whereas the extent of the same correlations at infinite time vanishes, $\xi(t \to \infty) = 0$. We exploited the possibility that, if interfaces with a finite cost are present between DCR, $\xi(t)$ may display a different asymptotic behavior.

4.1 Constrained overlap

4.1.1 Definition of overlap

The model studied in this section is exactly the same glass-forming liquid model introduced in sec. 3.2.1, i.e. a binary mixture of soft-spheres, present in equal amount in the system. The only difference with the parameters introduced in sec. 3.2.1 is the size of the system, here composed by $N = 4096$ particles, with a simulation box side $L = 16$. A smaller system allowed to save computatational time in order to perform long dynamical runs. All dynamical observables discussed this section are averaged over an ensemble of 20 configurations, equilibrated independently at the mode coupling temperature, $T = T_c$

($\Gamma = 1.45$). Dynamical runs are performed by means of a Montecarlo algorithm with temperature fixed to $T = T_c$. Simulation at temperatures different from $T = T_c$ are discussed only in sec. 4.3.4.

Let us introduce a definition of the overlap between two configurations of a liquid slightly different from those of sec.3.2.1. As in sec.3.2.1, we define a scale l for spatial coarse-graining such that, partitioning the simulation box in cubic cells of side l, there is a negligible probability of finding more than one particle in each cell. Actually, the side of the cell is fixed to $l = 0.4$ (cfr. sec.3.2.1). Differently from sec.3.2.1, the definition of overlap given here neglects the possibility of double occupation of a single cell, but keeps track of the type of particles (we are working with a binary mixture). Let us call the reference configuration α and β any other configuration of the liquid that we want to compare with α. A value of overlap field $q_{\alpha\beta}(\mathbf{x}_i)$ is attached to each cell, $\mathbf{x}_i$ being the centre of the i-th cell, so that:

$$q_{\alpha\beta}(\mathbf{x}_i) = n_\alpha(\mathbf{x}_i) n_\beta(\mathbf{x}_i) \delta_{ab}, \tag{4.3}$$

where $n_\alpha(\mathbf{x}_i)$, $n_\beta(\mathbf{x}_i)$ are either 0 or 1, as the cell is empty or filled with at least one particle. The two indices a and b are either 1 or -1, depending on which type of particle is found in the cell, respectively in configurations α and β. Therefore, due to the kronecker delta δ_{ab}, local overlap $q_{\alpha\beta}(\mathbf{x}_i)$ is different from zero *only* when the cell is occupied by the same kind of particle in both α and β. The global overlap between configurations α and β is calculated as:

$$Q_{\alpha\beta} = \frac{1}{V} \sum_{i \in V} n_\alpha(\mathbf{x}_i) n_\beta(\mathbf{x}_i) \delta_{a_i b_i} = \frac{1}{V} \sum_{i \in V} q_{\alpha\beta}(\mathbf{x}_i) \tag{4.4}$$

where sum index i runs over all the cells and V is the volume of the simulation box. When the density of particles is set at $\rho = 1$, the definition of the overlap in eq.(4.4) fixes the self-overlap at on, $Q_{\alpha\alpha} = 1$. The overlap of system at time t along a dynamic run is usually measured with the intial configuration:

$$Q(t) = \frac{1}{V} \sum_{i \in V} n(\mathbf{x}_i, t) n(\mathbf{x}_i, 0) \delta_{a_i(t) a_i(0)} = \frac{1}{V} \sum_{i \in V} q(\mathbf{x}_i, t). \tag{4.5}$$

This sets the initial condition to $Q(0) = 1$.

4.1.2 Definition of constraint

In order to run a dynamic where the overlap with the initial configuration is fixed, we modified the acceptance ratio of a standard Monte Carlo algorithm. The standard Metropolis criterion was been modified in order to reject, with probability 1, all displacements that bring overlap $Q(t)$ below a certain threshold value $\hat{Q}$, which is an input parameter of the simulation:

$$\begin{aligned} p_{accept} &= \min\{1, \exp^{-\Delta E/T}\} \quad Q(t) > \hat{Q} \\ &= 0 \qquad\qquad\qquad\qquad\quad Q(t) \leq \hat{Q} \end{aligned} \tag{4.6}$$

A non-local efficient algorithm [51] has been modified in the same manner. This algorithm proposes the standard shift of particles but also a different kind of non-local move, summarized as follows:

1. A pair of particles is randomly choosen in the system.

2. Particle positions are exchanged.

3. Both particles are shifted after the exchange.

4. The whole move is accepted or rejected, according to the Metropolis criterion.

Within the above list of operations, $Q(t)$ is evaluated at step 4), and, in turn, the whole move is accepted or rejected in order to to have $Q(t) \geq \hat{Q}$. Clearly, the non-local algorithm is not used to simulate the dynamics, but rather to check the asymptotic behavior of time-dependent quantities, i.e. $\xi(t)$.

4.1.3 Effect of constraint

Fixing a lower threshold $\hat{Q}$ apparently lets the system explore the whole phase space with $Q(t) \geq \hat{Q}$. Nevertheless, since in the unconstrained system $Q(t)$ may only decrease with time, at times greater than t^* — this is the first time that $Q(t^*) \sim \hat{Q}$ — the system ends by getting stuck on the *hypersurface* defined by $Q(t) = \hat{Q}$. Fig.(4.1) shows the behavior of the total overlap, averaged over 20 initial conditions at $T = T_c$, both with free dynamics (black squares) and with constraint $\hat{Q} = 0.25$ (red circles). Along the constrained dynamics, the systems evolves freely until $Q(t) \sim \hat{Q}$. At times $t \geq t^*$, only small fluctuations of $Q(t)$ above the threshold take place, as can be seen from the inset of fig.4.1.

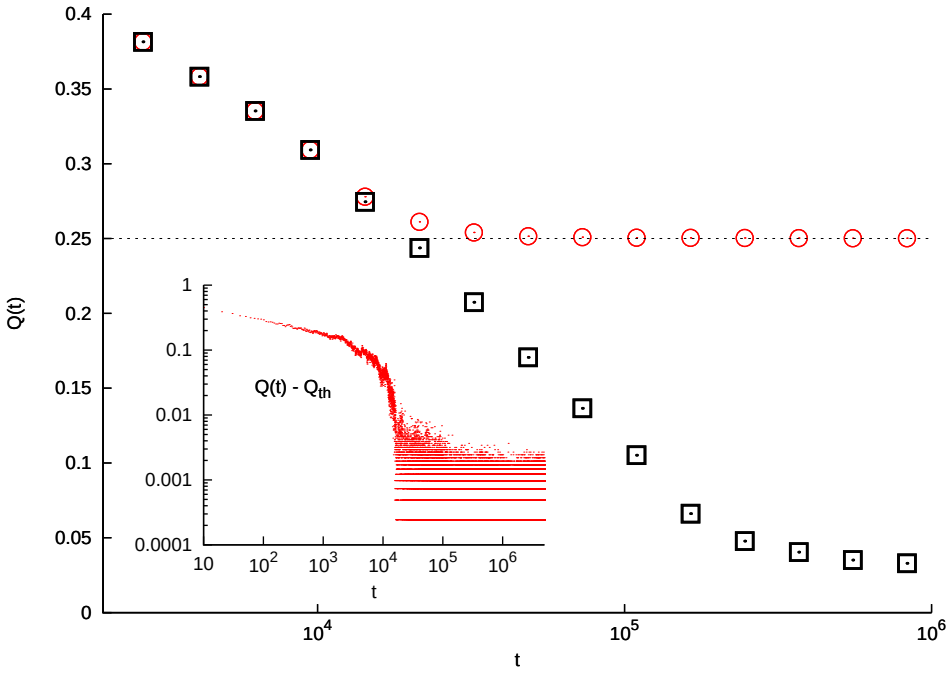

Figure 4.1: $\langle Q(t) \rangle$ *vs* t*, with free (red circles) and constrained,* $\hat{Q} = 0.25$*, (black squares) dynamics. Average is over 20 samples at* $T = T_c$*. Inset* $Q(t) - \hat{Q}$*, data from a single sample.*

4.2 Study of non-linear susceptibility $\chi_4(t)$

Non-linear susceptibility $\chi_4(t)$ is the observable most often considered in order to study dynamical heterogeneities in supercooled liquids [35, 36, 37, 38, 39, 40, 41, 42, 7]. This susceptibility represents a measure of the volume of dynamically correlated regions; it is defined as the integral of the four-point correlation function:

$$\chi_4(t) = \beta \int_V g_4(\mathbf{r}, t) d\mathbf{r}. \tag{4.7}$$

An increasing correlation length is in fact related to an increasing susceptibility, hence the interest of $\chi_4(t)$. Correlation function $g_4(\mathbf{r}, t)$ may be written in terms of the local overlap field:

$$g_4(\mathbf{r}, t) = \langle q(\mathbf{r}, t) q(\mathbf{r}, 0) \rangle - \langle q(\mathbf{r}, t) \rangle \langle q(\mathbf{r}, 0) \rangle. \tag{4.8}$$

From the definition of the total overlap

$$Q(t) = \frac{1}{V} \int d\mathbf{r} q(\mathbf{r}, t) \tag{4.9}$$

it follows that:

$$\chi_4(t) = \beta V \left[\langle Q(t)^2 \rangle - \langle Q(t) \rangle^2 \right], \tag{4.10}$$

i.e., the dynamical susceptibility is proportional to the mean square deviation of the time correlation $Q(t)$ of the system. Because a supercooled liquid is an ergodic system, at long times the memory of the inital configuration is lost: the average value of overlap $\langle Q(t) \rangle$, i.e., the correlation $C(t)$, decreases monotonically to zero (see fig.4.1). When the temperature is lowered, a supercooled liquid manifests a transient tendency to glassiness, i.e., the particle mobility becomes correlated on an increasing length-scale $\xi(t)$, which has its maximum at the relaxation time τ of the system, hence $\xi_{DYN} = \xi(\tau)$. This tendency is transient in that $\xi(t \to \infty) = 0$. Regarding glass transition as a dynamical critical point, in approaching this point, according to the theory of dynamics at criticality, the physics of the system must be invariant under a rescaling of time —and length— scales [70]. In this case, the correlation function $g_4(r, t)$ must obey the simple scaling:

$$g_4(r, t) = r^{2-d-\eta} \hat{g}_4(r/\xi, t/\tau), \tag{4.11}$$

where ξ and τ are the relevant length and time scales at a given temperature. Together with the above scaling assumption the integral in eq.(4.7) yields:

$$\chi_4(t) \sim \xi(t)^{2-\eta} \langle Q(t) \rangle^2. \tag{4.12}$$

As mentioned above, at long times the correlation vanishes due to ergodicity, $\langle Q(t) \rangle^2 \to 0$, and therefore also susceptibility vanishes. What about dynamic correlation length $\xi(t)$? In principle, it may be different from zero. Numerical results have shown that $\xi(t \to \infty) \to 0$ [71]. As when $\chi_4(t) = 0$, also $\xi(t)$ is zero, $\chi_4(t)$ may be regarded as a reliable indicator of the extent of dynamical correlations.

Equation (4.10) shows that non-linear susceptibility can easily be computed from the fluctuations of $Q(t)$, with no need to deal with $g_4(\mathbf{r}, t)$. Although $\chi_4(t)$ is a reliable measure of dynamical correlations in a standard situation, what about constrained dynamics? Is it still possible to measure the extent of dynamical correlations from the fluctuations of $Q(t)$ (eq.(4.10))? The behavior of $\chi_4(t)$ when the dynamic is constrained is shown in fig.4.2,

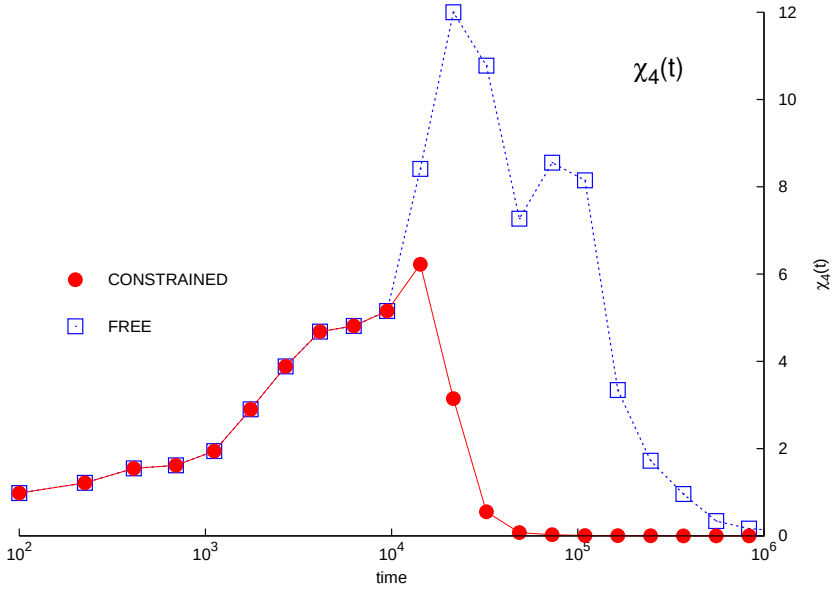

Figure 4.2: *Dynamical susceptivity $\chi_4(t)$ vs t, calculated at $T = T_c$ from the fluctuations of $Q(t)$ over an enesemble of 20 initial configurations. Free dynamics, squares: constrained dynamics,$\hat{Q} = 0.25$, circles. $\chi_4(t)$ along constrained dynamics drops to zero at t^* such that $Q(t^*) \sim \hat{Q}$, cfr fig.(4.1).*

where it is compared with the same quantity measured along free dynamic. With a free dynamic, $\chi_4(t)$ displays its well-known non-monotonic behavior. Instead the constrain on $Q(t)$ suppresses sample-to-sample fluctuations as soon as $Q(t) \sim \hat{Q}$, so that $\mathrm{Var}[Q(t)] = 0$ and $\chi_4(t) = 0$. When $Q(t) \sim \hat{Q}$, we have $\langle Q(t) \rangle^2 = \hat{Q}^2 > 0$. Therefore, from eq.(4.12) we can say that, as $\chi_4(t) = 0$ and $\langle Q(t) \rangle^2 > 0$, correlation length $\xi(t)$ must also be zero. It is not true.
The simplification that leads from eq.(4.7) to eq.(4.12) assumes that $g_4(r,t)$ is a positive definite function, which amounts to saying that $\chi_4(t)$ vanishes only when modulus $|g_4(r,t)|$ vanishes. This is equivalent to assuming the following relation:

$$\int d(r/\xi)\,(r/\xi)^{4-d-\eta}\,\hat{g}_4\,(r/\xi, t/\tau) \sim \langle Q(t) \rangle^2, \tag{4.13}$$

from which the scaling relation in eq.(4.12) follows. Nevertheless, susceptibility $\chi_4(t)$ may also vanish, because of the compensation of the positive and negative areas subtended by $g_4(r,t)$, in the special case where the function develops some nodes. Thus, even with a finite modulus $|g_4(r,t)| > 0$ (except for the nodes), we may have zero susceptibility. In this case:

$$\int d(r/\xi)\,(r/\xi)^{4-d-\eta}\,\hat{g}_4\,(r/\xi, t/\tau) \neq \langle Q(t) \rangle^2, \tag{4.14}$$

and, consequently the scaling of eq.(4.12) is wrong. A correlation function normally defined as positive may develop one or more nodes when a global conservation law is imposed on a system [72]. As shown in the following, this *is* the case of dynamics with constrained overlap.

4.3 Asymptotic $\xi(t)$ with constrained overlap

4.3.1 Four-point correlation function

With the coarse-graining of space in cubic cells of side l, our description of the liquid passed from a continuum to a discretum: overlap field $q(\mathbf{r}_i, t)$ is defined on the centers of the cubic cells, which in turn form a cubic lattice. The connected part of the isotropic four-point correlation function $g_4(r,t)$ is calculated as:

$$g_4(r,t) = \frac{\sum_{ij}\langle \delta q_i(t)\delta q_j(t)\rangle \delta(r - r_{ij})}{\sum_{ij}\langle q_i(0)q_j(0)\rangle \delta(r - r_{ij})}. \tag{4.15}$$

where sum indexes i,j label the cells of the box, r_{ij} is the distance between the centers of the i-th and j-th cells, and:

$$\begin{aligned} \delta q_i(t) &= q_i(t) - \langle Q(t)\rangle, \\ \delta q_j(t) &= q_j(t) - \langle Q(t)\rangle. \end{aligned} \tag{4.16}$$

The above definition matches with the initial condition:

$$\chi_4(t=0) = 0 = \int_V g_4(\mathbf{r}, t) d\mathbf{r}. \tag{4.17}$$

The correct discrete counterpart of the above (eq.4.17) integral is:

$$\begin{aligned} \chi_4(t) &= \sum_r \rho(r) g_4(r,t) \\ \chi_4(t) &= \sum_r \left(\sum_{ij} \langle q_i(0)q_j(0)\rangle \delta(r - r_{ij}) \right) g_4(r,t) \\ \chi_4(t) &= \frac{1}{N} \sum_r \sum_{ij} \langle \delta q_i(t)\delta q_j(t)\rangle \delta(r - r_{ij}) \\ \chi_4(t) &= \frac{1}{N} \sum_{ij} \langle \delta q_i(t)\delta q_j(t)\rangle \end{aligned} \tag{4.18}$$

from which it also follows that:

$$\chi_4(t) = \frac{1}{N} \sum_{ij} \langle \delta q_i(t)\delta q_j(t)\rangle = N\left[\langle Q(t)^2\rangle - \langle Q(t)\rangle^2\right]. \tag{4.19}$$

The time evolution of isotropic $g_4(r,t)$ is shown in figs.(4.3) and (4.5) for free dynamics and figs.(4.4) and (4.5) for dynamics with constrained overlap. The four-point correlation function $g_4(r,t)$, is closely related to the Van-Hove correlation function, $g(r)$, of the liquid [15], i.e.:

$$g_4(r, t=0) = g(r) - 1. \tag{4.20}$$

Therefore, $g_4(r,t)$ is not positively defined, but rather fluctuates around zero. Comparing figs.(4.3) and (4.4), it is clear that, along free dynamics, $g_4(r,t)$ fluctuations are more and more damped, while modulus $|g_4(r,t)|$ remains finite with $Q(t)$ constrained. That is, at large times, $g_4(r,t)$ splits into two parts, subtending respectively a negative and a positive area: clearly, the node placed between $r = 6$ and $r = 7$ (fig.4.4) has nothing to do with

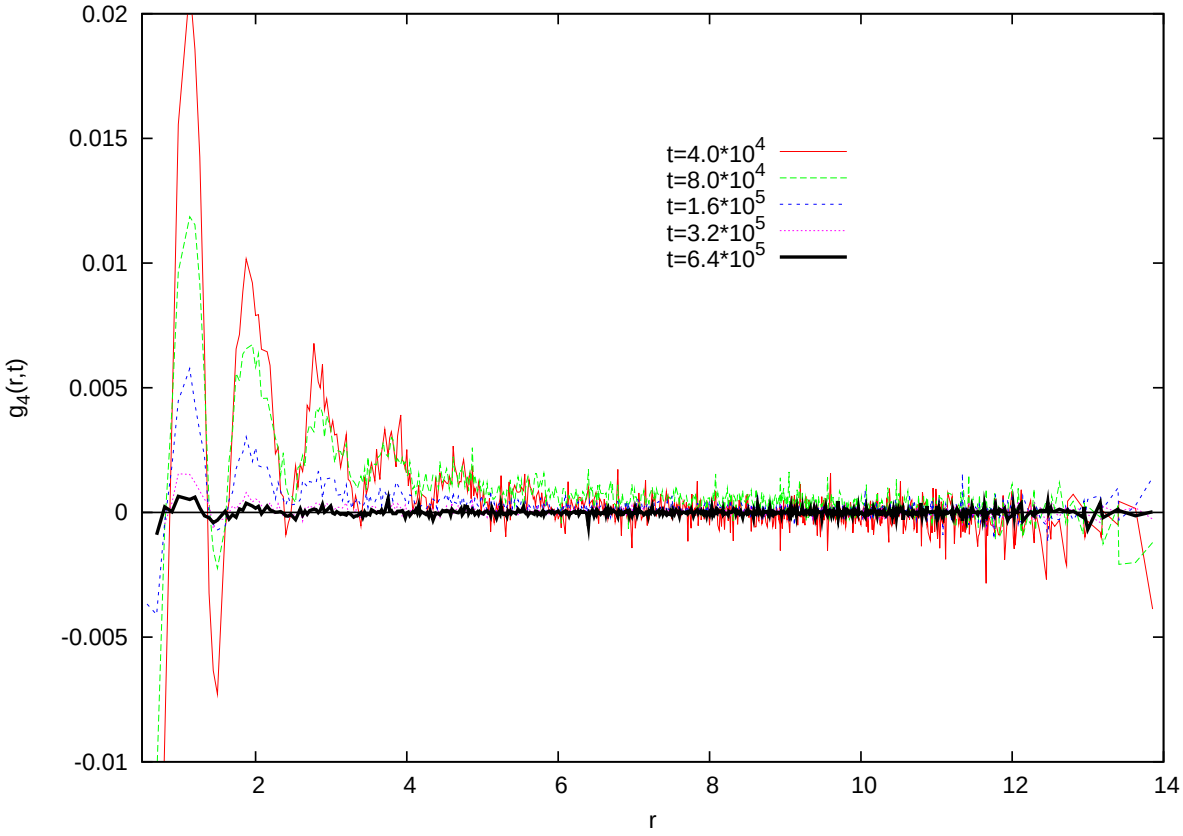

Figure 4.3: $g_4(r,t)$ *at different times, measured in MC steps, along free dynamics.*

the standard fluctuations of $g_4(r,t)$. As mentioned in [72], when describing the *conserved order parameter* (COP) dynamics of an Ising model, the connected correlation function of the system, although positive with free dynamics, may develop nodes when the order parameter is conserved. In particular, the position of the first node yields an estimate of the correlation length of the system [72]. In the present study, we are also dealing with COP dynamics, the overlap playing the role of the conserved order parameter. Therefore also the position of the node of $g_4(r,t)$ along our constrained dynamics may be regarded as an estimate of correlation length $\xi(t)$. The behavior of $g_4(r,t)$ along constrained dynamics shows that not only correlation length $\xi(t)$ does not vanish for large times, but also apparently saturates to a value $\xi \sim 6.5$. This datum was found in agreement with the analysis of dynamical structure factor $S_4(k,t)$ (see below).
Focusing on the behavior of the four-point correlation function and the related susceptibility, the difference between free and constrained dynamics may be summarized as:

$$\begin{aligned} \text{unconstrained dynamics} \quad &\Longrightarrow \quad \chi_4(t\to\infty) = 0 = \int g_4(r,t) \sim \int |g_4(r,t)| \\ \text{constrained dynamics} \quad &\Longrightarrow \quad \chi_4(t>t^*) = 0 = \int g_4(r,t) \neq \int |g_4(r,t)| > 0, \end{aligned} \tag{4.21}$$

where, as usual, t^* is the shortest time when $Q(t^*) \sim \hat{Q}$.
Let us now consider the representations of $g_4(r,t)$ with y axis in log scale. The envelope of the peaks is well fitted with a function $a(t)\exp\left[-(r/\xi(t))\right]$. With constrained dynamics, as can be seen from the straight lines in fig. 4.6, length scale $\xi(t)$ —the inverse slope of the lines— increases with time. Less clear is what happens with free dynamics: it is really

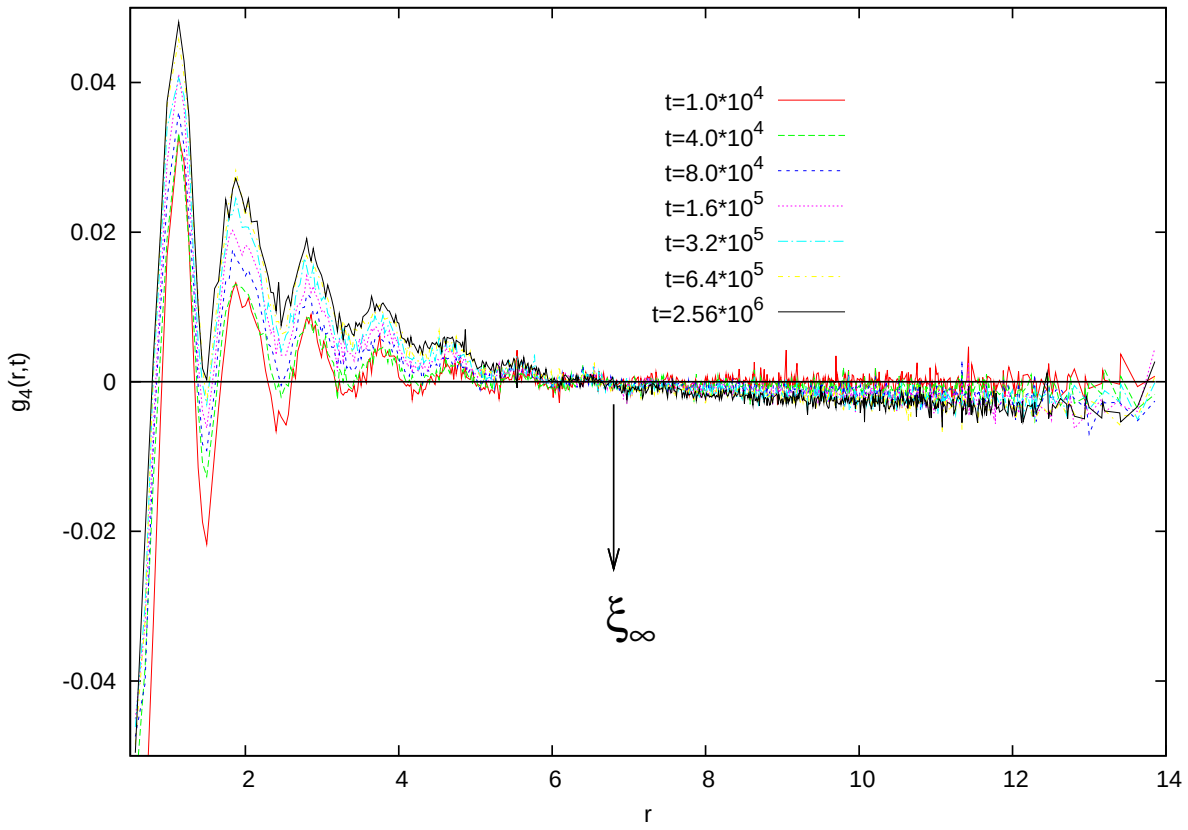

Figure 4.4: $g_4(r,t)$ *at different times, measured in MC steps, along constrained dynamics,* $\hat{Q} = 0.25$, $T = T_c$. *The node of the function, placed at* ξ_∞, *provides a measure of correlation length* $\xi(t)$ *at large times.*

difficult to disentangle the decrease of correlation length $\xi(t) \to 0$ from the damping of signal $a(t) \to 0$.
As already mentioned, the problem of the behaviour of $\xi(t)$ is still debated. In order to fix the framework, let us choose the more conservative interpretation of the data: $\xi(t \to \infty) \to 0$. A detailed study of the behavior of $\chi_4(t)$ and $g_4(r,t)$ in a glass-forming liquid may be found in [73, 71]. In particular, in [71] it is suggested that the behavior of $\xi(t)$ is better extrapolated from the low-momentum tail of the dynamic isotropic structure factor $S_4^c(k,t)$, rather than from the envelope of $g_4(r,t)$ peaks.

4.3.2 Dynamic structure factor

The dynamic structure factor of a liquid is usually defined as [15]:

$$S(\mathbf{k},t) = \frac{1}{N}\langle \rho(\mathbf{k},t)\rho(-\mathbf{k},t)\rangle, \tag{4.22}$$

where $\rho(\mathbf{k},t)$ is the Fourier transform of the density field. Similarly, we can define the four-point isotropic dynamic structure factor as:

$$S_4(\mathbf{k},t) = \frac{1}{N}\langle q(\mathbf{k},t)q(-\mathbf{k},t)\rangle, \tag{4.23}$$

where $q(\mathbf{k},t)$ is the Fourier transform of the overlap field:

$$q(\mathbf{k},t) = \sum_i \exp\left[i\mathbf{k}\cdot\mathbf{r}_i\right] q_i(t) \tag{4.24}$$

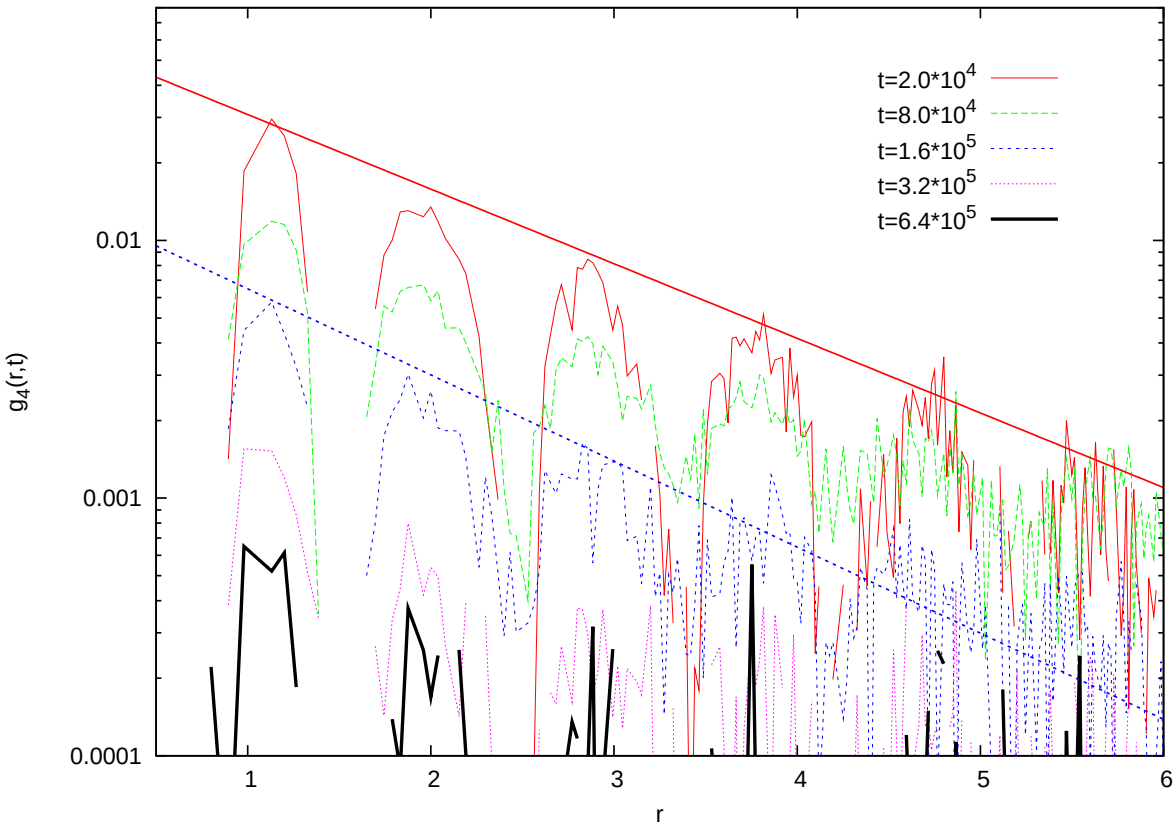

Figure 4.5: $g_4(r,t)$ *at different times, measured in MC steps, along free dynamics,* $T = T_c$*; y-axis in log scale. At fixed time, the exponential decay of* $g_4(r,t)$ *peaks with* r *is emphasized with straigh lines.*

and index i labels lattice sites, i.e., centers of cells. The *connected* $S_4^c(\mathbf{k},t)$ differs from $S_4(\mathbf{k},t)$ only by a delta function:

$$S_4^c(\mathbf{k},t) = \frac{1}{N} = \langle \delta q(\mathbf{k},t)\delta q(-\mathbf{k},t)\rangle = S_4(\mathbf{k},t) - \langle Q(t)\rangle \delta_{\mathbf{k},\mathbf{0}}, \tag{4.25}$$

where $\delta q(\mathbf{k},t)$ is:

$$\delta q(\mathbf{k},t) = \sum_i \exp\left[i\mathbf{k}\cdot\mathbf{r}_i\right]\left(q_i(t) - \langle Q(t)\rangle\right). \tag{4.26}$$

Therefore, except for $\mathbf{k} = 0$, $S_4^c(\mathbf{k},t) = S_4(\mathbf{k},t)$. We can show that connected dynamic structure factor $S_4^c(\mathbf{k},t)$ is the Fourier transform of $g_4(\mathbf{r},t)$, according to the definition of $g_4(\mathbf{r},t)$ given in eq.(4.15):

$$\begin{aligned}
S_4^c(\mathbf{k},t) &= \langle \delta q(\mathbf{k},t)\delta q(-\mathbf{k},t)\rangle = \\
&= \frac{1}{N}\sum_{ij}\exp\left[i\mathbf{k}(\mathbf{r}_i - \mathbf{r}_j)\right]\langle \delta q_i(t)\delta q_j(t)\rangle \\
&= \frac{1}{N}\sum_{\mathbf{r}}\exp\left[i\mathbf{k}\mathbf{r}\right]\sum_{ij}\langle \delta q_i(t)\delta q_j(t)\rangle\delta(\mathbf{r} - (\mathbf{r}_i - \mathbf{r}_j)) \\
&= \frac{1}{N}\sum_{\mathbf{r}}\exp\left[i\mathbf{k}\mathbf{r}\right]\left[\sum_{ij}\langle q_i(0)q_j(0)\rangle\delta(\mathbf{r} - \mathbf{r}_{ij})\right]\frac{\sum_{ij}\langle \delta q_i(t)\delta q_j(t)\rangle\delta(\mathbf{r} - \mathbf{r}_{ij})}{\sum_{ij}\langle q_i(0)q_j(0)\rangle\delta(\mathbf{r} - \mathbf{r}_{ij})} \\
&= \sum_{\mathbf{r}}\exp\left[i\mathbf{k}\mathbf{r}\right]\rho(\mathbf{r})g_4(\mathbf{r},t),
\end{aligned} \tag{4.27}$$

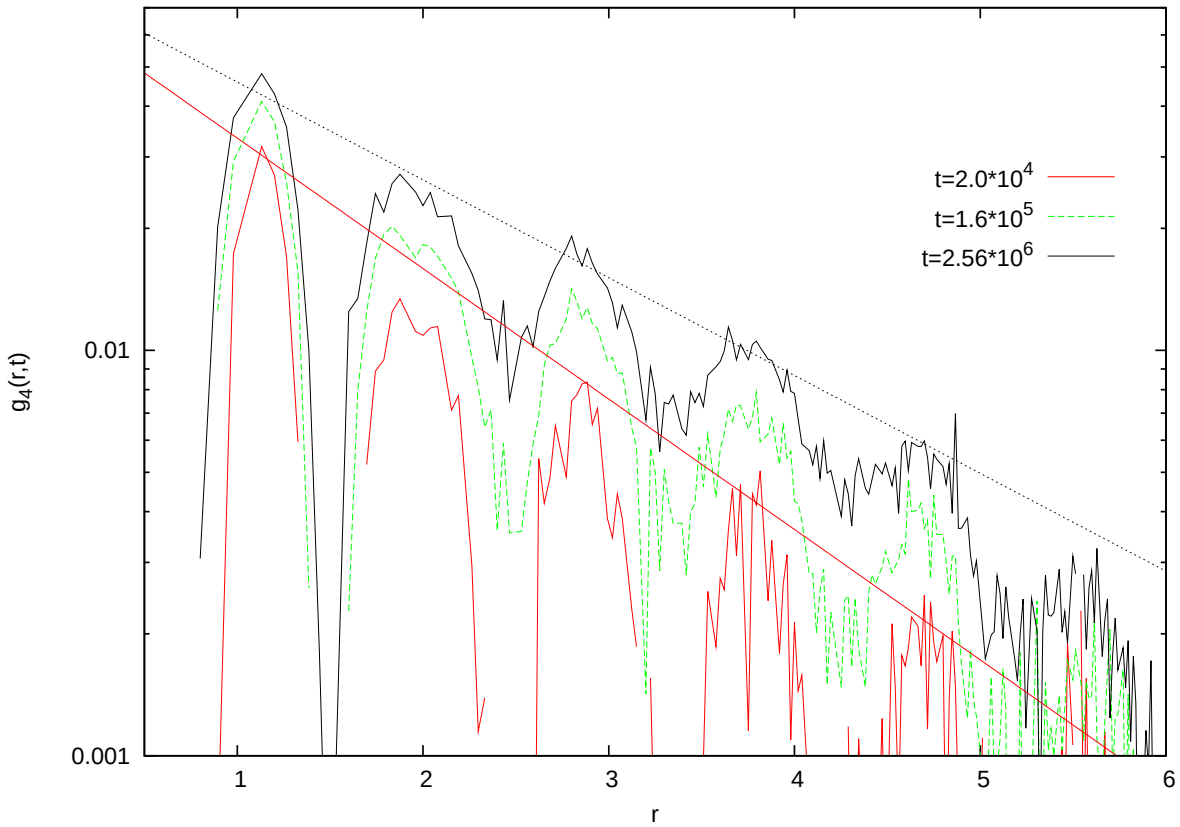

Figure 4.6: $g_4(r,t)$ *at different times, measured in MC steps, along constrained dynamics,* $\hat{Q} = 0.25$, $T = T_c$*; y-axis in log scale. At fixed time, the exponential decay of* $g_4(r,t)$ *peaks with* r *is emphasized with straigh lines.*

where $\rho(\mathbf{r}) = \sum_{ij}\langle q_i(0)q_j(0)\rangle\delta(\mathbf{r}-\mathbf{r}_{ij})$. Moreover, from the definition of eq.(4.27) it follows that:

$$\chi_4(t) = \frac{1}{\beta}S_4^c(k\to 0,t), \tag{4.28}$$

because:

$$\begin{aligned} S_4^c(k\to 0,t) &= \frac{1}{N}\sum_{\mathbf{r}}\rho(\mathbf{r})g_4(\mathbf{r},t) \\ &= \frac{1}{N}\sum_{\mathbf{r}}\sum_{ij}\langle\delta q_i(t)\delta q_j(t)\rangle\delta(\mathbf{r}-\mathbf{r}_{ij}) \\ &= \frac{1}{N}\sum_{ij}\langle\delta q_i(t)\delta q_j(t)\rangle = \chi_4(t). \end{aligned} \tag{4.29}$$

Dynamical correlation length $\xi(t)$ can be extracted from the low-k behavior of isotropic dynamical structure factor $S_4^c(k,t)$. According to the Ornstein-Zernike approximation [15], for small values of k we can write:

$$S_4^c(k,t) = \frac{S_4^c(0,t)}{1+\xi(t)^2k^2}, \tag{4.30}$$

so that $\xi(t)$ can be obtained as a fit parameter from the low-k tail of $S_4^c(k,t)$. Fig.(4.7) shows the behavior of $S_4^c(k,t)$ at different times along free (right panel) and constrained

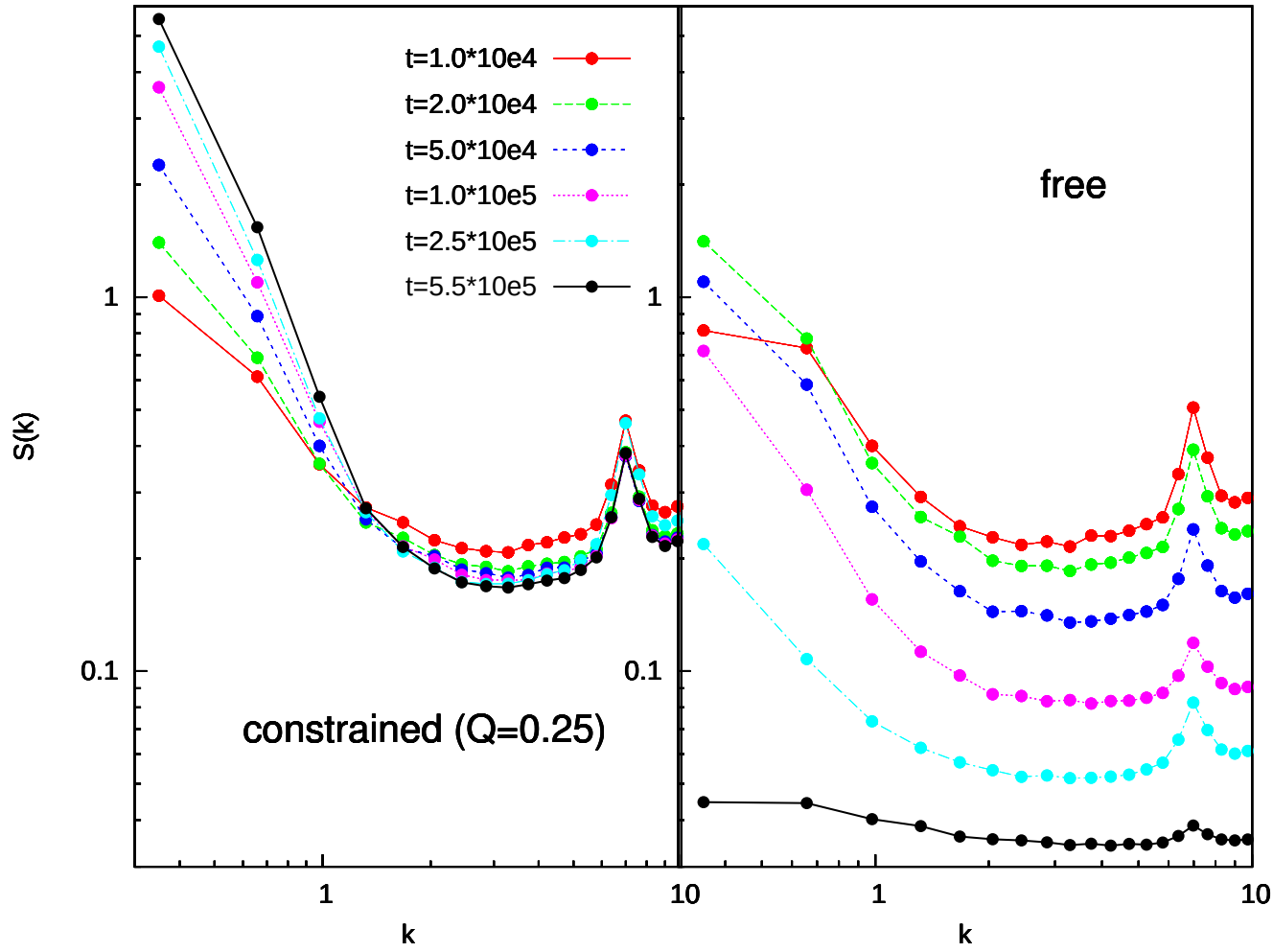

Figure 4.7: $S_4^c(k,t)$ *measured at different times along constrained (left panel) and free (right panel) dynamics,* $T = T_c$*; log-log scale.*

(left panel) dynamics; the values of free and constrained $\xi(t)$ are shown in fig.4.8. When the system is free, $\xi(t)$ decays to zero at large times, and with constrained dynamics size $\xi(t)$ of correlations keeps on increasing and saturates at a certain value. Studying both the position of the node in $g_4(r,t)$ and the low-k behavior of $S_4^c(k,t)$, we can state that this value is $6 < \xi(t \to \infty) < 7$.

Let us note that the damping of $S_4^c(k,t)$ observed in fig.(4.7), right panel, corresponds to the damping of $g_4(r,t)$ fluctuations observed in fig.(4.5). The extrapolation "by eye" to small k values of curves $S_4^c(k,t)$, in order to check that $S_4^c(0,t) \sim \chi_4(t)$, can only be done for the curves in the right panel of fig. 4.7 (free dynamics). More interesting is the behavior of $S_4^c(k,t)$ along constrained dynamics. Let us stress in particular the following points:

- We cannot expect $S_4^c(k \to 0,t) \sim \chi_4(t)$, because the conservation of $Q(t)$ represents a constraint on $\chi_4(t)$ and hence exactly on $S_4^c(0,t)$. Therefore, we cannot expect continuity from values of $S_4^c(k,t)$ at small k and $S_4^c(0,t)$.

- The values of $\xi(t)$, obtained as a fit parameter from eq.(4.30), are in agreement with the behavior of the low-k tail of $S_4^c(k,t)$. Fig.4.8 clearly shows that not only $\xi(t)$ no

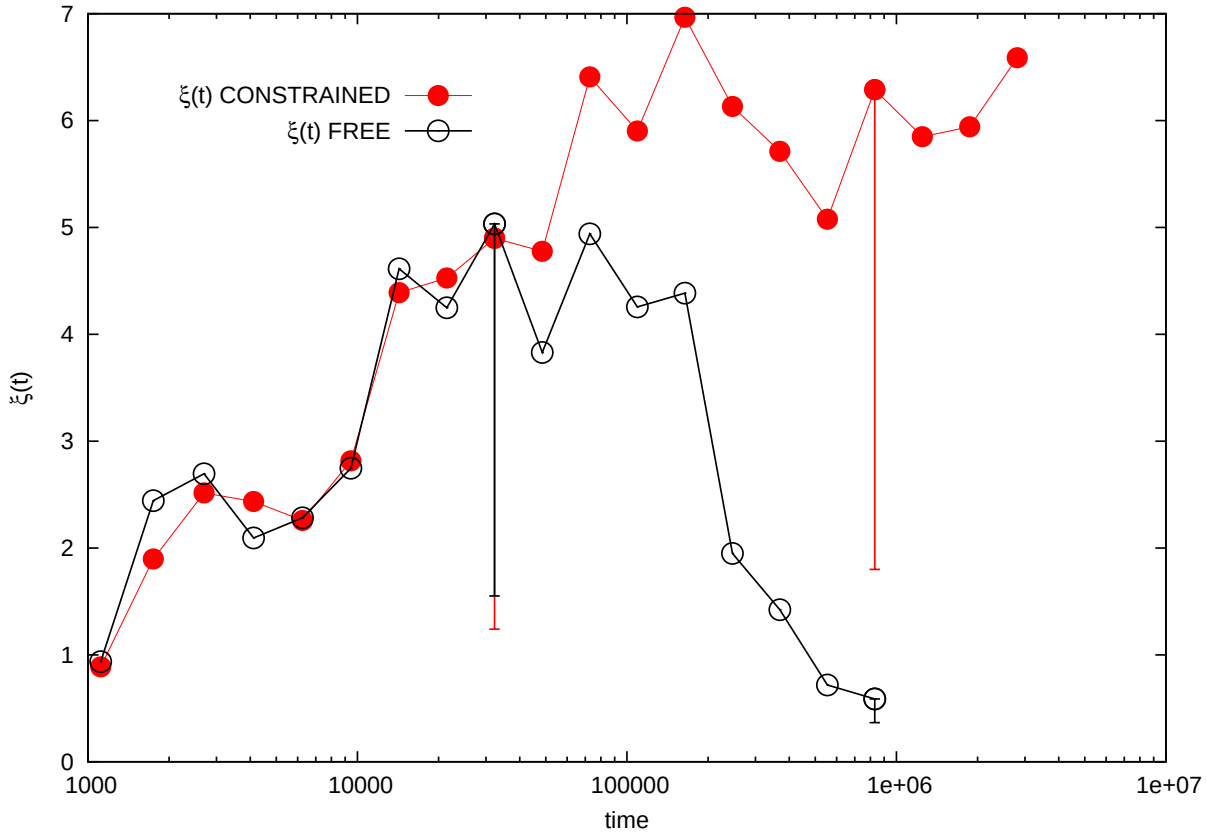

Figure 4.8: *$\xi(t)$ vs t for free (empty circles) and constrained (full circles) dynamics, $T = T_c$. Half error bars, which are very large, are reported in figure, only at the relaxation time $t = \tau$ —peak of unconstrained $\xi(t)$– and at a large time. Error bars have been evaluated by means of the bootstrap method. Their large size is the signature of the difficulty in estimating the exact value of $\xi(t)$ by fitting the low-k tail of the dynamic structure factor.*

longer decreases, but also that it keeps on increasing and levels off at a finite value.

Outlook. We claim that the leveling of $\xi(t)$ at a finite value signals that the system has attained a phase separation between high, $Q \sim 1$, and low, $Q \sim 0$, overlap. Further evidence supporting this assumption will be highlighted while summarizing results in sec. 5.4. In the following are presented some real-space snapshots of the $q(\mathbf{r}, t)$ field, in order to show that, with constrained dynamics, correlations over large length-scales persist over times beyond the relaxation time.

4.3.3 Visualizing phase separation.

Let us stress the different behavior of dynamical correlation length $\xi(t)$ along free and unconstrained dynamics. With free dynamics, $\xi(t)$ decays to zero at large times[1]; with constrained overlap, it keeps on increasing for times larger than the relaxation time and levels off at a finite value. Fig. 4.9 and 4.10 show snapshots of field $q(\mathbf{r}, t)$ at the relaxation

[1] $\xi(t)$ does not decrease *exactly* to zero but to $\xi(t = \infty) = 0.2$. This is because, according to the definition of sec. 4.1.1, the overlap between two configurations is *never* precisely 0. At any time, there is a finite probability of finding a particle of type A in a cell occupied by a particle of the same type at time $t = 0$. More precisely, this probability corresponds to the total number of type-A particles divided

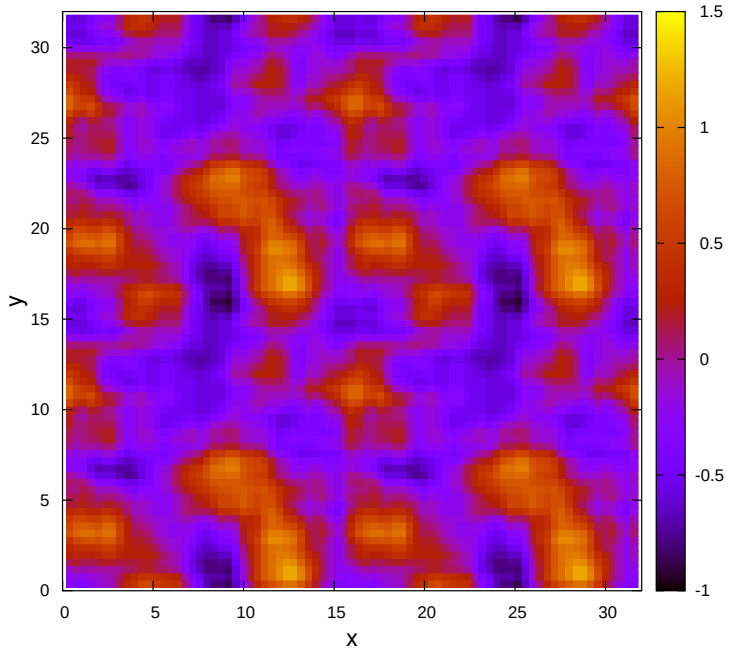

Figure 4.9: *Local fluctuations of the overlap field,* $\delta q(\mathbf{r},t)/Q(t) = (q(\mathbf{r},t) - Q(t))/Q(t)$. *The snapshot represents a slice of the system at fixed height, along free dynamics, at the relaxation time of the system,* $t = \tau$, *at the mode coupling temperature,* $T = T_c$.

time, i.e. $\tau \sim 4.0 \cdot 10^4$ MC steps for $T = T_c$, when large-scale fluctuations of the field are present both with free and constrained dynamics. Conversely, at times larger than the relaxation time, the constrained system still displays large-scale fluctuations of $q(\mathbf{r},t)$ (fig. 4.12); in the unconstrained system (fig.4.11) the length-scale of $q(\mathbf{r},t)$ correlations is significantly reduced. In the latter case, deviations from the average value of the overlap over the sample, $Q(t) = 1/V \sum_i q(\mathbf{r}_i,t)$, are isolated and due to the event of a single particle occupying a cell also filled at $t = 0$. Our interpretation is that, with constrained dynamics, the size of regions with the same value of order parameter Q increases until phase separation between high and low Q regions is attained. This should happen, in order to minimize the surface tension stored in the interfaces between regions with high and low value of the overlap. Study of the internal energy of the system along constrained

by the number of cells, i.e., $q(t = \infty) = 0.032$. From the definition of $g_r(r,t)$:

$$g_4(\mathbf{r},t) = \frac{\sum_{ij}\langle\delta(q_i(t) - \langle Q(t)\rangle)(q_j(t) - \langle Q(t)\rangle)\rangle\delta(r - r_{ij})}{\sum_{ij}\langle q_i(0)q_j(0)\rangle\delta(r - r_{ij})} \tag{4.31}$$

we know that, the larger the deviation of $q_i(t)$ from $\langle Q(t)\rangle$, the larger $|g_4(\mathbf{r},t)|$. Hence, correlation length $\xi(t)$ calculated from Fourier transform $S_4^c(k,t)$ measures the size of regions where the the value of $q(\mathbf{r},t)$ has larger fluctuations from the average $\langle Q(t)\rangle$. Then, when $Q(t) \sim 0.032$, $\xi(t)$ measures the size of regions with high overlap q. As mentioned above, it is possible to find a cell occupied at $t = 0$ filled with a particle of the same type at any time; hence, over a region of volume l^3, the overlap shows a pronounced fluctuation from the asymptotic value. It is the linear size, $l = 0.2$, of this region that is measured by $\xi(t = \infty)$ along unconstrained dynamics.

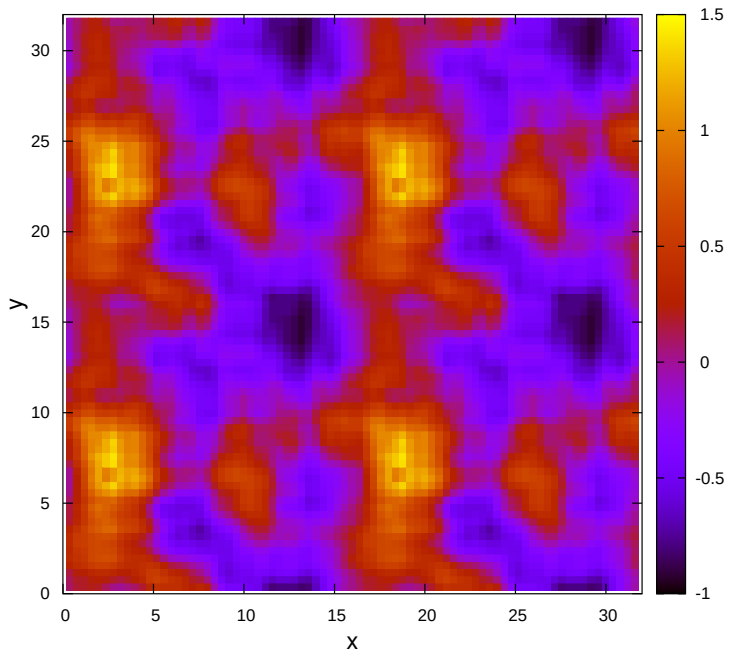

Figure 4.10: *Local fluctuations of the overlap field,* $\delta q(\mathbf{r},t)/Q(t) = (q(\mathbf{r},t) - Q(t))/Q(t)$. *The snapshot represents a slice of the system at fixed height, along constrained dynamics,* $\hat{Q} = 0.25$, *at the relaxation time of the system,* $t = \tau$, *at the mode coupling temperature,* $T = T_c$.

dynamics, which will be discussed in sec. 5.4, gives further support to this interpretation. The following discusses the effect of the overlap constraint at different temperatures, in order to show that the leveling of $\xi(t)$ at a finite value is not a trivial effect of the threshold, $\hat{Q}$, choosen for the overlap.

4.3.4 Constrained dynamics above T_c.

Monte Carlo simulations with the efficient algorithm of [51], which employs non-local moves, are not suitable to study the dynamics of the system. Nevertheless, this algorithm allows us to save computing time when we are only interested in the asymptotic value $\xi(t \to \infty) = \xi_\infty$. While the dynamics of the system has been studied in detail only at $T = T_c$, the asymptotic behavior of $\xi(t)$ has also been studied for other temperatures, i.e., $T = 2.13, 1.55$ and $1.15T_c$. At all these temperatures, the constrained dynamics was performed with the same threshold value, $\hat{Q} = 0.25$, for the overlap. The various values of ξ_∞ are listed in Tab.(4.1): clearly, ξ_∞ increases as the temperature falls. The finding of ξ_∞ values that actually depend on temperature, $\xi_\infty = \xi_\infty(T)$, is enough to rule out the possibility that the effect of the constraint on the dynamics is trivial.

The finding of a finite ξ_∞ when constraining the overlap —i.e. breaking the ergodicity of the system— may in principle be trivial. As observed for p-*spin* models and mode coupling theory, ergodicity breaking is always associated with finite correlations at infinite time,

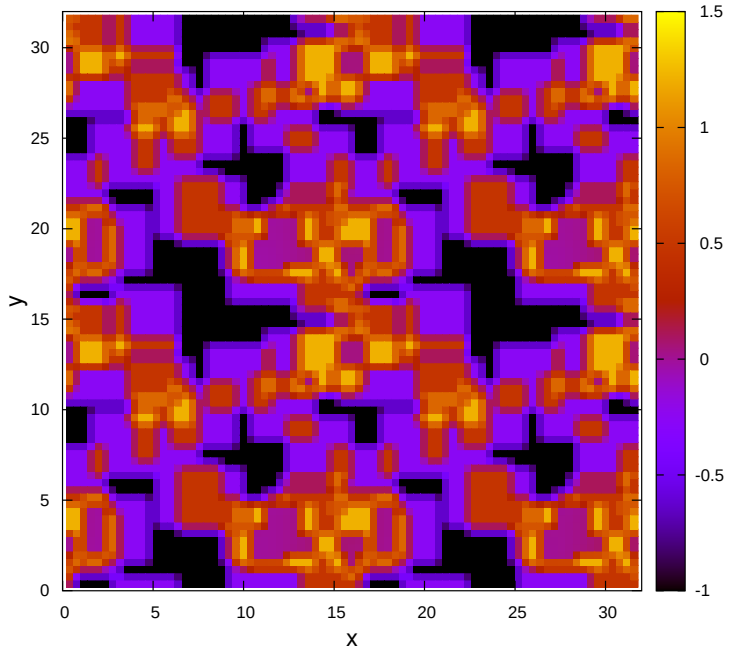

Figure 4.11: *Local fluctuations of the overlap field,* $\delta q(\mathbf{r},t)/Q(t) = (q(\mathbf{r},t) - Q(t))/Q(t)$. *The snapshot represents a slice of the system at fixed height, along free dynamics, at a time when overlap is significantively decreased,* $Q(t) \sim 0.05$ *(*$t = 6.4 \cdot 10^5$ *MC steps), at the mode coupling temperature,* $T = T_c$.

$Q(t = \infty) \neq 0$: therefore, $\xi(t = \infty) \neq 0$ can be expected. Following the same line of reasoning, we should also expect that for identical values of the correlation function at infinite time, i.e., $\langle Q(t = \infty) \rangle = \hat{Q}$, must be found the same value of $\xi(t = \infty)$, independently of temperature. The fact that ξ_∞ changes with temperature while imposing the same constraint, $\hat{Q} = 0.25$, is the main evidence that the phenomenon observed does not depend *trivially* on the induced breaking ergodicity.

T	ξ_∞
1.00 T_c	6.49(21)
1.15 T_c	4.12(19)
1.55 T_c	1.31(03)
2.13 T_c	0.75(03)

Table 4.1: *Asymptotic values of dynamical correlation length* $\xi_\infty = \xi(t \to \infty)$*; results are from simulations with MC non-local algorithm. Errors are evaluated from fluctuations of* $\xi(t)$ *since it attains a nearly costant value.*

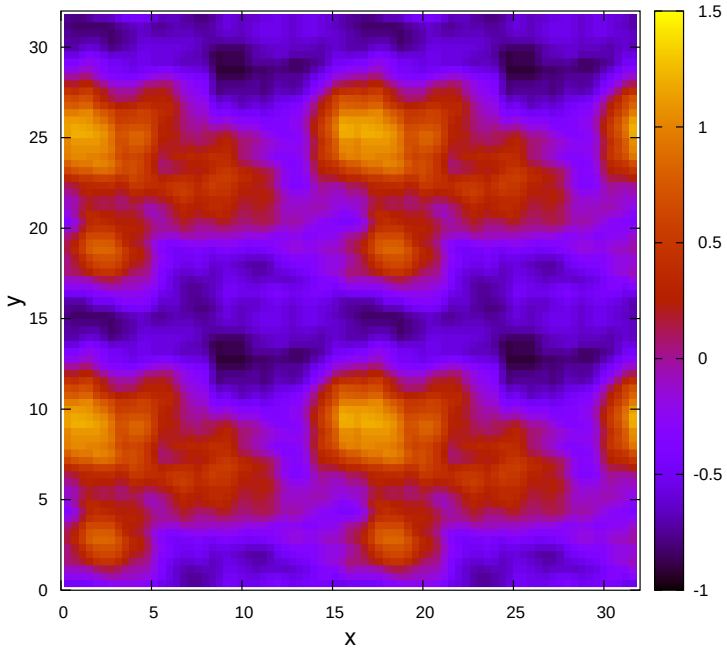

Figure 4.12: *Local fluctuations of the overlap field,* $\delta q(\mathbf{r},t)/Q(t) = (q(\mathbf{r},t) - Q(t))/Q(t)$. *The snapshot represents a slice of the system at fixed height, along constrained dynamics,* $\hat{Q} = 0.25$, *at a large time,* $t >> \tau$ ($t = 1.28 \cdot 10^6$ *MC steps), at the mode coupling temperature,* $T = T_c$.

Chapter 5

Surface tension, RFOT and dynamical heterogeneities

This section describes the most important results obtained facing the problem of surface tension in supercooled liquids with the two strategies outlined in previous chapters: first, selecting the amorphous phases of the supercooled liquid and artificially introducing the interfaces; second, performing a fixed overlap dynamic in order to test the hypothesis of a surface tension existing even between dynamically cooperative regions. In order, these results concern the following points:

Spinodal point for RFOT excitations. RFOT theory pictures a supercooled as a mosaic of amorphous domains, whose typical linear size ξ_{RFOT} is:

$$\xi_{RFOT} = \left(\frac{\Upsilon}{T\Sigma} \right)^{\frac{1}{d-\theta}} \tag{5.1}$$

The numerical calculation of Υ allows us to fix an upper limit of validity of the RFOT scenario. This limit turns out to be well-definied as a function of energy, not of temperature. Connections with the topological crossover scenario [2, 23, 27, 28] are outlined.

Surface tension fluctuations and RFOT. The increase in length-scale ξ_{RFOT} at low temperatures is traced in the behaviour of the point-to-set correlation function $q_c(R)$ [6]. The landmark of the liquid/supercooled-liquid crossover is the crossover to a low-temperature non-exponential decay of $q_c(R)$. The shape of the non-exponential decay is governed by the shape of surface tension distribution $P(\Upsilon)$. Below the MCT temperature $T < T_c$ we find a distribution, $P(\Upsilon)$, in *quantitative* agreement with previous results on $q_c(R)$ [6].

Time and length scale within RFOT. We introduce the measure of surface tension as a tool to study relaxation of amorphous excitations. As the formation and relaxation of excitations are closely related, we can study the scaling of the free energy barrier to nucleate an amorphous droplet:

$$\Delta F = \xi_{RFOT}^{\psi}, \tag{5.2}$$

in order to fix a value for the exponent ψ, which is left free in the RFOT formulation of [4].

Surface tension and dynamical heterogeneities: COP coarsening. We show further evidence supporting the phase separated scenario achieved with fixed overlap dynamics. That is, the behaviour of system energy is shown to be compatible with conserved orderd parameter (COP) coarsening, a phenomenon were surface tension plays a major role.

5.1 Spinodal point for RFOT excitations

The existence of many amorphous excitations is central to the mechanism of relaxation of RFOT. But, in order for such non-trivial excitations to exist, a non-zero surface tension is necessarily required. Moreover, the regime of validity of RFOT is bounded by a spinodal mechanism. While, at mean-field level, the spinodal transition corresponds to the point at which metastable states disappear[74], RFOT predicts that it is rather the surface tension Υ between finite-dimensional amorphous excitations which vanishes at temperatures higher than a spinodal value [31], loosely identified with the Mode Coupling temperature [14].
Having fixed exponents θ and ω in eq. (5.3), governing the increase in the energy cost of an amorphous droplet (sec. 3.3.1 and 3.3.2):

$$\langle \Delta E(R) \rangle = \Upsilon_\infty R^\theta - \delta R^\omega \tag{5.3}$$

$\Delta E(R)$ data can be fitted very well (fig. 3.7 sec. 3.3.1) to obtain asymptotic surface tension Υ_∞ as a function of temperature T (fig. 5.1, top). We find that Υ_∞ decreases with increasing T, and becomes quite small above T_c. This behaviour makes sense, indicating that amorphous excitations become softer as the temperature is raised. This is indeed what we expect physically as the system moves towards a spinodal point. Yet the decrease in surface tension is quite smooth, so that it is hard to define a spinodal temperature sharply. Since T_c roughly corresponds to the point at which activated processes become important for the relaxation of the system, we might expect that spinodal temperature and T_c would coincide [31]. However, our numerical data show that this is not really the case: although T_c is definitely within the range of temperatures where Υ_∞ becomes negligible, amorphous excitations with non-zero surface tension do exist even above T_c.
However, the onset of glassiness is *never* sharp in temperature. Nevertheless, regarding energy rather than temperature as a control parameter, a well-defined spinodal point clearly emerges: the Υ_∞ vs. $e_{\rm IS}(T)$ curve is nearly linear (fig. 5.2, left), and Υ_∞ vanishes at energy $e_{\rm th}$.
It is quite interesting to note that $e_{\rm th}$ is very close to *threshold* energy, i.e., the value below which minima start to dominate the energy landscape [27, 28]. More precisely, the threshold is defined as the point at which the instability index of saddles vanishes (fig. 5.2, right). Hence, the true spinodal point of amorphous excitations, fixing the upper limit of stability of the RFOT mechanism, is the very same energy $e_{\rm th}$ where a topological transition from saddle to minima takes place. This sharp transition in phase space, i.e. the vanishing of the saddle index from above and the surface tension from below, becomes a smooth crossover when studied as a function of temperature. Our results therefore indicate that energy, and not temperature, is the control parameter of dynamic glass transition, and that $e_{\rm th}$ truly marks the onset of glassiness: below the threshold energy, unstable saddles give way to stable minima and a non-zero surface tension develops, making it possible to sustain local amorphous excitations, whose relaxation is responsible for the sharp increase in relaxation time.

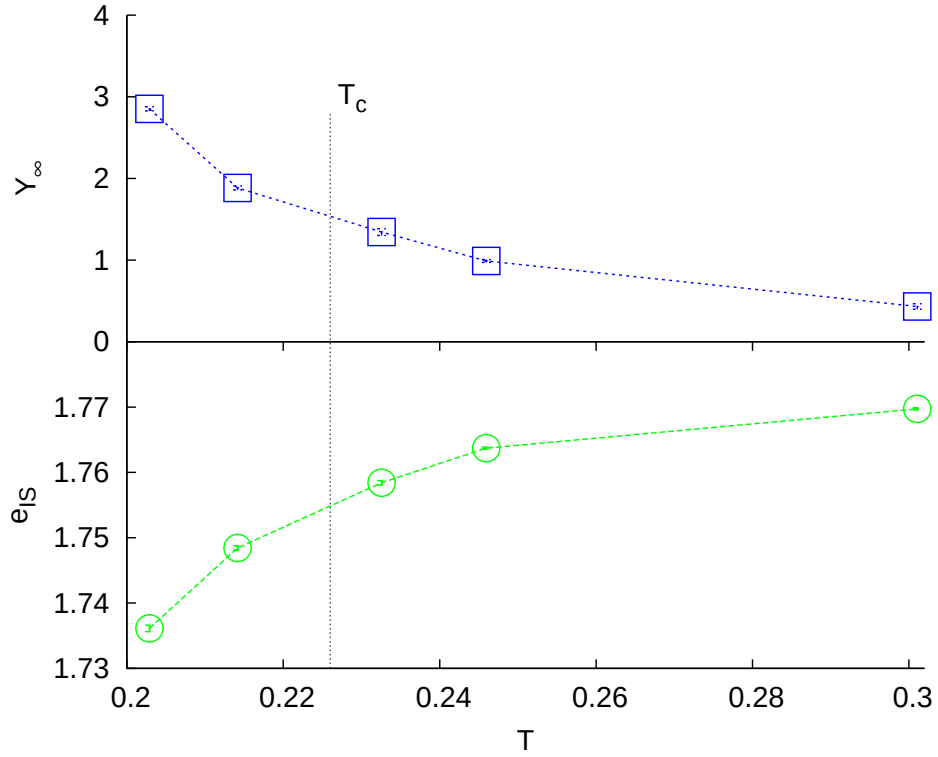

Figure 5.1: *Upper panel: Y_∞ as a function of the quenching temperature of the inherent structures. The vertical dotted line marks the mode coupling temperature. The surface tension decreases on increasing T, although too smoothly to indicate a sharp spinodal temperature. Lower panel: inherent structure energy as a function of the quenching temperature.*

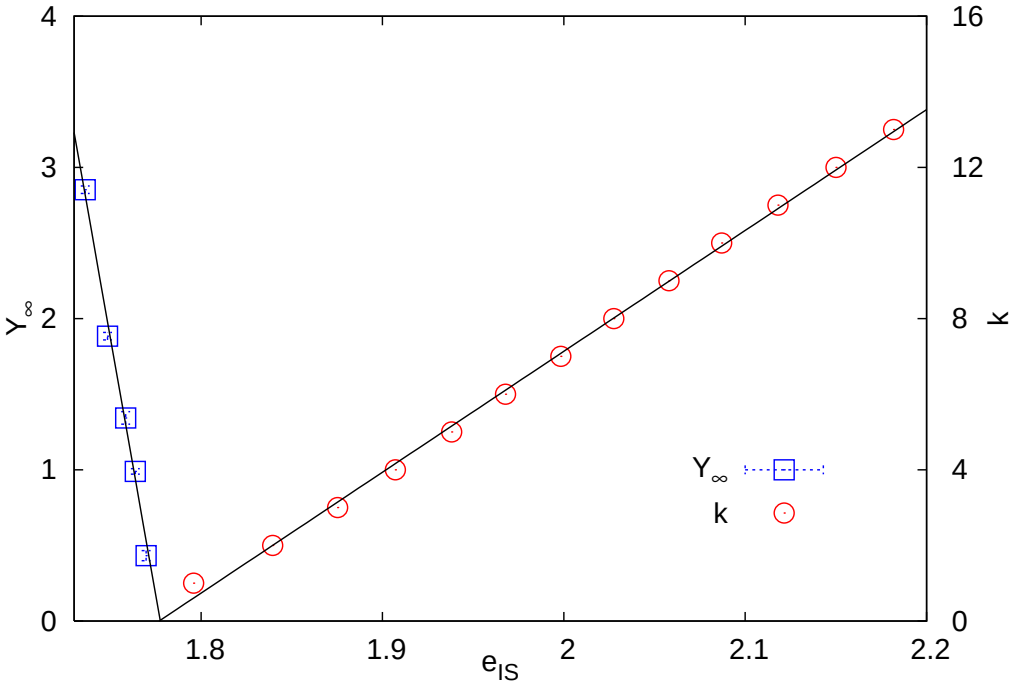

Figure 5.2: *Left: Y_∞ (squares) vs. IS energy. Right: intensive saddle instability index k (circles) vs. IS energy (data from ref. [28]). Lines are linear fits. Both the surface tension and the instability index seem to vanish at a similar energy, the threshold e_{th}, which is therefore the spinodal point.*

Linear decrease of $\Upsilon(T)$. Let us recall here the behaviour of barriers between adjacient minima, found in [27] and mentioned in sec.2.3 (fig.2.4) speaking about the connection between the topological crossover and the mode coupling temperature. It is interesting to note that both the height of barriers shown in fig. 2.4 and *surface tension* (fig.5.2), are linear functions of the energy of the IS. This suggests a link between the two phenomena. Not only the crossover from saddles to minima is related to the appearance of finite surface tension. Furthermore the way surface tension increases, when lowering the energy below e_{th}, is qualitatively similar to the increase of barriers between adjacient minima. Therefore the existence of RFOT excitations, i.e. local realization of mean-field metastable states, appears to be, studying the behaviour of surface tension, intimately connected with the topology of Potential Energy Landscape.

Spinodal point and Mode Coupling Theory. According to our data (fig.5.1) activated events start to play a role even above T_c. How can we recover an agremeent with [27], in which the authors produced evidence that threshold temperature T_{th} corresponds to mode coupling temperature T_c?
Should we really expect saddle-minima threshold temperature T_{th} and mode coupling temperature T_c to be the same? A strong point made in [27] is that, as soon as activated mechanisms are required for relaxation —RFOT escitations enter the game— they are very inefficient, hence the abrupt increase in relaxation times. Conversely our data on surface tension indicate that, when they appear, activated events are very efficient, because of very small surface tension. This means that at the threshold the time-scales for barrier hopping and for finding unstable directions can hardly be distinguished. We do agree with the strong point that, at T_c, the activation mechanism is inefficient: we only claim that T_{th} lies slightly above T_c and that, at T_{th}, activation and relaxation along unstable directions are still competitive. This scenario is quite interesting. RFOT excitations turn out to be well-defined also above T_c, although there activation is not the dominant relaxational mechanism. At temperatures above T_c, the slowing down of glass-forming liquids is well described in the context of dynamical heterogeneities, where the dynamical length-scale ξ_{DYN} is studied. The existence of a temperature range, that is, from our data, $T_c \leq T \leq T_{th}$, where both dynamical and thermodynamical excitations are well defined, seems interesting in order to investigate the relation between the two different length-scales ξ_{RFOT} and ξ_{DYN}. Numerical evidence of a temperature interval in which ξ_{RFOT} and ξ_{DYN} are both finite can be found in [12] and is also supported theoretically in [11].

5.2 Surface tension fluctuations and RFOT

In [6], the signature of mosaic-like anomalous behaviour is traced in the overlap with a reference configuration of an equilibrated sphere in the presence of a frozen boundary. A fit of this overlap, $q(R;T)$, *vs* the radius of the sphere defines the non-trivial exponent of a compressed exponential, low temperature anomaly ζ. In this context, it is suggested that the width of the surface tension distribution governs the extent of such an anomaly (cfr sec.2.4.3), due to the following connection between $q(R;T)$ and $P(\Upsilon;T)$:

$$q(R;T) - q_0 = (q_1 - q_0) \int_{T\Sigma R^{d-2}}^{\infty} d\Upsilon' P(\Upsilon';T) \tag{5.4}$$

where q_1 and q_0 stand for the self-overlap and the mutual-overlap of the low temperature mosaic states.
Distribution of tensions between RFOT states were numerically obtained (cfr. sec. 3.3.3), but comparison of our results with those for $q(R;T)$ in [6] needs some attention. First, we measured the contact cost of each pair of inherent structures arbitrarily chosen. Instead, the spontaneous formation of a nucleus in the cavity with a frozen boundary only happens if the final configuration is convenient from the energy viewpoint. To take into account only such configurations, we must restrict analysis to a subset of contact energy values $\Delta E^{IS}_{\alpha\beta}$. Consider all the hybrid minima $\mathcal{C}_{\alpha\beta}$, in which the parent IS β of particles outside the spherical cavity is fixed, while the state α inside the cavity can change. Among these let us retain only the hybrid minimum with the lowest value of energy $E^{IS}_{\alpha\beta}$:

$$E^{IS}_{\alpha^*\beta} = \min_{\alpha}\{E^{IS}_{\alpha\beta}\}. \tag{5.5}$$

Thus, only the subset of contact energy $\Delta E^{IS}_{\alpha^*\beta}$ is such that the final energy is the lowest for fixed external configuration β, i.e.:

$$\Delta E^{IS}_{\alpha^*\beta} = E^{IS}_{\alpha^*\beta} - E^{IN}_{\alpha^*} - E^{OUT}_{\beta}, \tag{5.6}$$

which represents the surface energy typical of a droplet which grows spontaneously in the numerical experiment studied in [6].
From

$$y(R) = \frac{\Delta E^{IS}_{\alpha^*\beta}}{R^2}, \tag{5.7}$$

we again find distribution $\mathcal{P}(y;R,T)$ for each temperature T and each radius R. When the surface tension distribution was introduced in [6] no dependence of $P(y,T)$ on the size of the excitation was accounted for. Differently, as described in sec.3.3.3 (cfr. fig. 3.13) the distributions we find strongly depend on the size of the excitation:

$$P(y,T) \Longrightarrow P(y,R,T) \tag{5.8}$$

We have a collection of $P(y;R,T)$ for each temperature T, instead of the single distribution $P(\Upsilon;T)$ suggested in [6]. This is because we artificially construct droplets of arbitrary size. However, we think that the probability distribution playing the main role in free droplet formation is, at each temperature, the probability distribution at critical size, $P(y;R_c(T),T)$. Only around R_c, according to RFOT, does the most frequent droplet formation occour. Recovering $q(R;T)$ using our distribution, $P(y;R_c(T),T)$, in eq.(5.4), needs the not clearly known value of complexity Σ of our system. Due to the lack of this parameter, it is worth defininig a new function, $\hat{q}(y;T)$, linked to $q(R;T)$ via a simple change of variable:

$$\hat{q}(y;T) = \int_y^{\infty} P(y';R_c(T),T)dy'. \tag{5.9}$$

Indeed, if distribution $P(y';R_c(T),T)$ has the same shape as distribution $P(\Upsilon';T)$, as suggested in (5.4), it follows that:

$$q(R;T) = (q_1 - q_0)\hat{q}(T\Sigma R^{d-2};T). \tag{5.10}$$

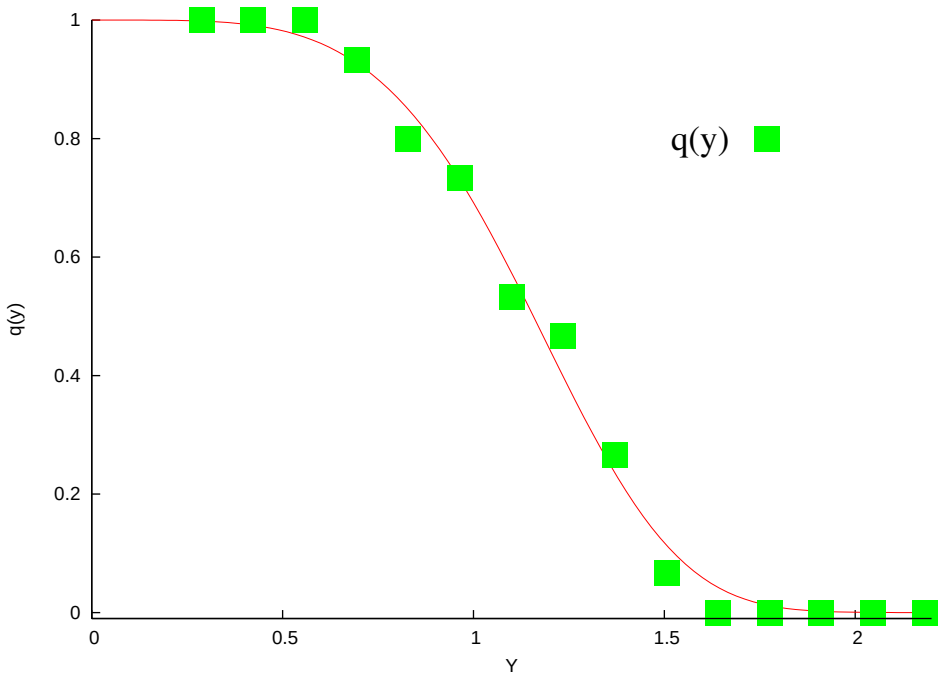

Figure 5.3: $q(y)$ *vs* y*, with* $q(y) = \int_y^\infty P(y'; R_c(T), T)dy'$ *,* $T = 0.89T_c$ *and* $R_c(T) = 3.8$*. Fit is* $\exp\left[-(y/y_c)^\zeta\right]$*, with* y_c *and* ζ *fit parameters,* $\zeta = 4.4 \pm 0.3$*. Remarkable agreement is found with* $\zeta = 4.0 \pm 0.6$*, non-exponentiality degree of* $q_c(R, T)$ *[6] at* $T = 0.89T_c$*.*

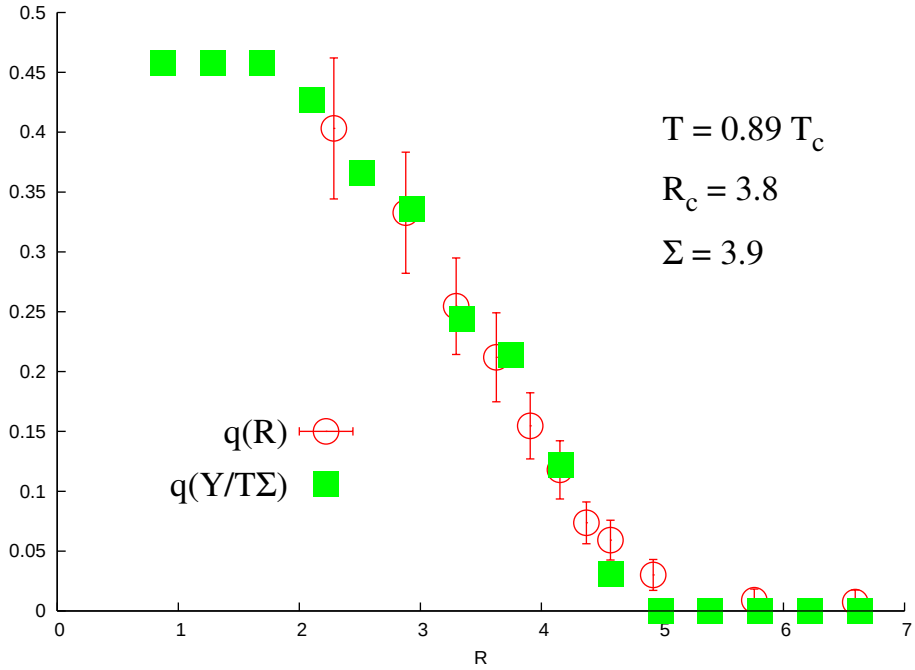

Figure 5.4: $(q_1 - q_0)q(y/T\Sigma)$ *vs* $y/T\Sigma$ *(squares) is plotted against* $q_c(R, T)$ *vs* R *([6],dots), with:* $\Sigma = 0.39$*,* $T = 0.89T_c$*.* $q(y/T\Sigma)$ *is* $q(y) = \int_y^\infty P(y'; R_c(T), T)dy'$ *with x-axis rescaled by* $T\Sigma$*. Value* $\Sigma = 0.39$ *of complexity leads to a remarkable collapse of the two curves.*

The feature showing the anomaly with respect to simple exponential decay of the point-to-set correlation function, is exponent $\zeta \neq 1$ of the best fitting function for $q(R; T)$:

$$q(R; T) = \Omega \exp(-(R/R_c(T))^\zeta). \tag{5.11}$$

From (5.10), it follows that, for $\hat{q}(y;T)$ we have:

$$\hat{q}(y;T) = \exp(-(y/y_c(T))^{\zeta}) \tag{5.12}$$

where $y_c = T\Sigma R_c^{d-2}$, while the parameter was only Ω giving an estimate of $q_1 - q_0$. Without any assumption regarding the value of complexity Σ, a fit as shown in eq.(5.12), with $y_c(T)$ and ζ as fit parameters, gives the value of the anomaly deriving from the distribution of the surface tension.
The result for the exponent ζ at $T = 0.89T_c$ is

$$\zeta = 4.4 \pm 0.3, \tag{5.13}$$

which is a value comparable with the anomaly obtained from the fit of $q(R;T)$ in [6]:

$$\zeta = 4.0 \pm 0.6. \tag{5.14}$$

Instead, direct comparison of $q(R;T)$ in [6] with $\hat{q}(y;T)$ can lead to an extimate of complexity. From eq.(5.10) an x-axis rescaling in $\hat{q}(y;T)$ by a factor $T\Sigma$ should make it collapse on $q(R;T)$. In particular, after rescaling the y-axis by constant prefactor $q_1 - q_0$, a variation of factor $T\Sigma$ is achieved, yielding the best collapse of the two curves. Fig. 5.4 shows the collapse of $\hat{q}(y;T = 0.89T_c)$ onto $q(R;T = 0.89T_c)$ obtained with $\Sigma = 0.39$. Unfortunately, extimates of Σ with which to compare this result are not abundant in the literature; the only reference value calculated for the same soft-sphere binary-mixture system is $\Sigma \sim 0.7$ in [75].

The numerical data of the energy cost of a surface between two inherent structures are perfectly sufficient to justify, in the RFOT theory scheme, the compressed exponentiality in the overlap found in [6] at $T = 0.89T_c$: at this temperature, we have quantitative evidence that the mosaic mechanism is effectively at work [45]. At higher temperatures, the correspondence between the results in [6] and ours is not as good as at $T = 0.89T_c$. Indeed, while at $T = 1.09T_c$, in [6], a compressed exponential for the overlap is still found, at the same temperature we find a distribution $P(y; R_c(T = 1.09T_c))$ which displays a large fraction of negative energy costs (cfr. fig. 3.14 in sec. 3.3.3) and has also a mean value smaller than zero. The presence of a large number of negative surface tensions and a negative mean value in the high-temperature cases is due to the disorder correction term δR^{ω}, not previously considered. As mentioned, bove T_c the surface tension Υ_{∞} between amoprhous states is very small [45], therefore in eq.(5.3) quadratic term $\Upsilon_{\infty} R^{\theta}$ is dominated by roughening correction δR^{ω}. The functional form introduced in [6] for $P(y)$ obviously does not account for negative valuse of y, therefore is not possible to compare our $P(y, R_c(T = 1.09T_c), T)$ with data at $T = 1.09T_c$ found in [6].

5.3 Time and length scales within RFOT

Starting from its first formulation in [3], the main challenge for the RFOT theory was to establish a functional relation between the increase in cooperative length ξ_{RFOT} and the increase in relaxational time τ of a supercooled liquid. As noted in sec. 2.4.2, in order to do this we need to know exponents θ and ψ appearing in:

$$\tau \sim \exp\left[\left(\frac{A}{T - T_K}\right)^{\frac{\psi}{d-\theta}}\right]. \tag{5.15}$$

In sec. 3.3.1 and 3.4.2 it was shown how the value of θ can be fixed to $\theta = 2$ in the glass-forming liquid model studied here. This section describes how to estimate exponent ψ from the relaxation of amorphous droplets at finite temperature.
The relaxation in deeply supercooled liquids proceeds through the activated rearrangement of clusters of correlated particles. As a result, the relaxation time increases exponentially with the size of these regions (eq. (2.36)). In this framework it is expected that the time-scales involved in the formation and relaxation of cooperative regions are in fact the same: each excitation relaxes through the cooperative rearrangement of new excitations. This means that we can follow the process of relaxation of an artificially produced excitation, rather than detect the spontaneous formation of it. This is the main working hypothesis we need to obtain ψ from data.

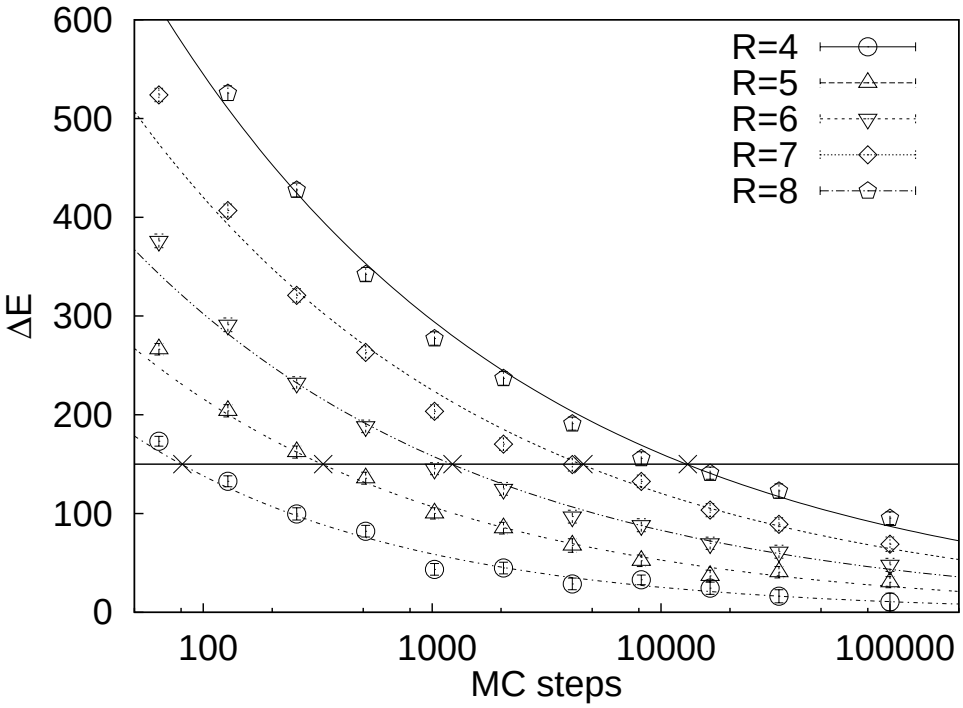

Figure 5.5: $\langle \Delta E(R,t) \rangle$ *vs. t for R ranging from* 4 *to* 8*, left to right. Points are experimental data, curves are power law* $\langle \Delta E(t,R) \rangle \sim t^{-\gamma(R)}$ *fits. The fits are used to give an estimate of* $\tau^*(R)$*, as shown in figure. The values of* γ *are within the range* $0.2 < \gamma(R) < 0.4$.

Actually, according to the method introduced in sec.3.4.1 to simulate amorphus excitations at finite temperature, we studied how average excess energy $\langle \Delta E(t,R) \rangle$ of different sized excitations relaxes with time. In particular we studied how at $T = 0.89 T_c$, that is the temperature at which mosaic mechanism is certainly at work, the rate of relaxation of the excitations changes with their size R. These data are shown in fig. 5.5: larger spheres relax over larger time scales. By simply fixing a threshold value ΔE^* for $\langle \Delta E(t,R) \rangle$ and measuring the time needed to have $\langle \Delta E(t,R) \rangle < \Delta E^*$, yields an estimate of time τ needed to relax an excitation of size R. The same procedure was performed at different sizes R of the sphere, thus obtaining a function, $\tau(R)$. According to:

$$\tau \sim \exp\left(R^{\psi}/T\right), \tag{5.16}$$

$T \log(\tau)$ must scale as R^{ψ}. The log-log plot of fig. 5.6 is reported shows $T \log(\tau)$ *vs.* R. The data lie on a straight line with good approximation, thus confirming that the process

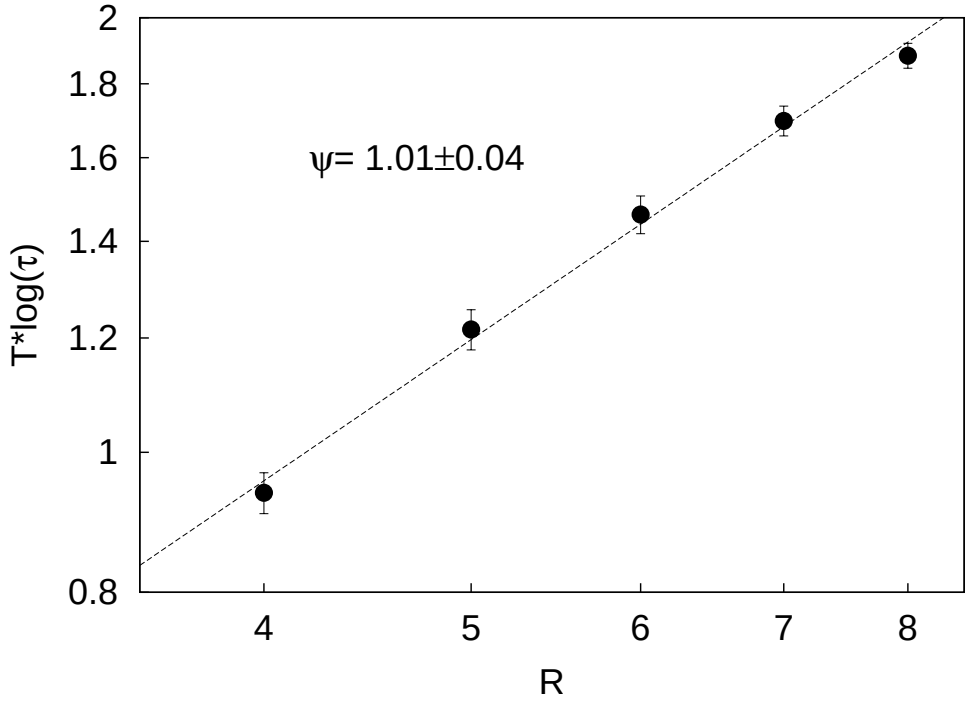

Figure 5.6: $T\log(\tau)$ *vs.* R *; the linear behaviour on log-log plot allows for a scaling ansatz* $\tau(R) \sim \exp(R/T)$.

of relaxation of the excitations does follow the Arrhenius law. A fit of the exponent gives $\psi = 1.01 \pm 0.04$, and we may therefore conclude:

$$\psi = 1. \tag{5.17}$$

Inserting our results for exponent θ [45, 76] and ψ [76] in eq.(5.15), we get back the well-known Vogel-Fulcher-Tamman law that link relaxation time and temperature in fragile glass-forming liquids:

$$\tau \sim \exp\left(\frac{A}{T - T_K}\right) \tag{5.18}$$

Free energy barriers within the RFOT. Our result, $\theta = 2$, is somewhat sensible and not particularly exciting: it is basically telling us that disorder in a supercooled liquid is not strong enough to change the leading term of the surface energy cost in any exotic way: surfaces remain surfaces, albeit a bit rough. It must be said that the value $\theta = d/2$ derived in [3], by means of RG arguments, always had its greatest appeal in the fact that, together with $\psi = \theta$, it gave back the VFT equation (5.18). The arguments used in [3] to fix θ do not belong to RFOT itself, and other values are, in principle, compatible with the conceptual structure of RFOT. Instead, the value found for ψ within RFOT regards a crucial aspect of the theory. Hence, it seems that the really interesting comparison is about the exponent ψ, after all. Value $\psi = 1$ implies that the barrier for the rearrangement of a correlated region scales linearly with its size:

$$\Delta F \sim \xi_{RFOT}. \tag{5.19}$$

Let us check if, within the theoretical scheme of RFOT, there is any theoretical constraint against this small value of the free energy barrier, i.e., $\psi = 1$. How much should pay the

system in order to rearrange a region of linear size ξ_{RFOT} ? The first expectation is that the greatest part of the energy necessary to create the excitation is stored in the interface. Hence, one may expect that the barrier scales with the same exponent as the surface energy cost, i.e. θ. This idea is deeply rooted in the theory of nucleation, which was indeed a source of inspiration for the original formulation of RFOT [3]. According to this formulation there are two competing forces: the free-energy cost to create an excitation, scaling as ΥR^{θ}, and the configurational entropy gain due to the change of state of the rearranging region, scaling as $T\Sigma R^{d}$. In these two expressions Υ is the surface tension and Σ is the configurational entropy. Hence, the total free energy for the formation of the excitation is, according to RFOT,

$$\Delta F(R) = \Upsilon R^{\theta} - T\Sigma R^{d}. \tag{5.20}$$

At this point, in perfect analogy with nucleation theory, RFOT proceeds by finding the *maximum* of such non-monotonous function (recall that $\theta < d$). This maximum provides two essential pieces of information: first, the position of the maximum, $R = \xi$, gives the critical size of the rearranging region, i.e., the mosaic correlation length:

$$\xi_{RFOT} = \left(\frac{\Upsilon}{TS_c} \right)^{\frac{1}{d-\theta}}. \tag{5.21}$$

Second, and most important in this contex, the height of the maximum, $\Delta F(R = \xi_{RFOT})$, gives the size of the free-energy barrier to be crossed to rearrange the region:

$$\Delta F(R = \xi_{RFOT}) \sim \xi_{RFOT}^{\theta}. \tag{5.22}$$

This fixes $\psi = \theta$, and coincides with the intuitive notion that the barrier should scale in exactly the same way as the interface cost.

This last result, however, is at variance with what we find here, eq.(5.19). Whatever one may think about our numerical result for θ, a value of θ as small as 1 seems rather unlikely. In any case, it is important to emphasize that $\psi = \theta$ is a consequence of the *maximization* of eq. (5.20), which, in turn, follows from the nucleation paradigm. However, as mentioned in the introductory section 2.4.2, it has been noted that nucleation is perhaps not a fully correct paradigm to describe the formation of amorphous excitations within a deeply supercooled liquid [4]. The essence of RFOT — i.e., the competition between a surface energetic term and a bulk entropic term— retains its deepest value even though we do not enclose it within the strict boundaries of nucleation theory. The value of the correlation length may come from the point where the two contributions balance, rather than from the maximum of (5.20), and (for obvious dimensional reasons) we obtain the same expression (5.21) for ξ_{RFOT} (up to an irrelevant constant), while ψ remains undetermined. These points are discussed in depth in ref. [4]. Here we simply note that our present results are quite compatible with RFOT in the form in which it was recast in ref. [4], without reference to a nucleation mechanism.

Free energy barriers in structural and spin glasses. Regarding the comparison between θ and ψ, there is a final point to be to discussed. Readers familiar with spin-glass physics will probably remember the Fisher-Huse (FH) inequality, [33]:

$$\psi \geq \theta, \tag{5.23}$$

which is plainly violated by the values we find here. The physical motivation of eq.(5.23) is basically the following: if we represent the excitation as an asymmetric one-dimensional double well, where the abscissa is the order parameter and the ordinate is the energy of the excitation, the height of the barrier (which scales as ξ^{ψ}) is always larger than (or equal to) the height of the secondary minimum (which scales as ξ^{θ}), and hence $\psi \geq \theta$. How is it, then, that we find $\psi < \theta$? The FH argument was formulated in the context of the droplet picture for spin-glasses, where there are only *two* possible ground states. In supercooled liquids, in contrast, a rearranging region can choose among an *exponentially large* number of target configurations. In these conditions, although the FH constraint still applies to the *energy* barrier, there may be a non-trivial entropic contribution that decreases the *free energy* barrier to rearrangement. We determine ψ by measuring a time, and hence a free-energy barrier, not an energy barrier, so that the FH constraint does not necessarily hold in the case of supercooled liquids. This entropic effect is absent in the original FH argument, due to the lack of exponential degeneracy of target configurations (in fact, one would expect relation (5.23) to hold even in the mean-field picture of spin-glasses, where the number of ground states is large but the configurational entropy is still zero). How the FH argument should be modified in the presence of such a large entropic contribution is, however, not clear at this point.

5.4 Surface tension and dynamical heterogeneities

In this section data are presented which put on firmer basis the phase-separated scenario described in sec. 4.3.3. In particular, it is shown that the total energy of the system, when the overlap is constrained, decreases with time according to the predictions of constrained order parameter coarsening (COP coarsening).
This is the basis allowing us to state that interfaces with a well-defined surface tension are present even between dynamically cooperative regions (DCR).

COP Coarsening Let us consider a system which has a phase transition at the critical temperature T_0, with two low-temperature equilibrium phases. If we perform a fast quench of this system from above to below T_0, domains of the two equilibrium phases start to grow until a complete phase separation is attained.
Along the transient regime where domain growth takes place, the correlation length ξ of the system actually depends on time, $\xi = \xi(t)$: this transient regime is called coarsening. The scaling of $\xi(t)$ with time along coarsening was studied for the first time in [77, 78, 79], while a comprehensive review of the subject is found in [80]. Independently Lifshitz and Slyozov [77], and Wagner [78], developed a theory which describes the growth of a nucleus of one phase in the bulk of the other phase. In this situation, the linear size $\xi(t)$ of the nucleus grows according to:

$$\xi(t) \sim (\Upsilon t)^{1/3}, \tag{5.24}$$

where Υ is the surface tension between the two phases. Eq.(5.24) is obtained when the order parameter is globally conserved and the dynamics of the system is local ($\xi(t) \sim (\Upsilon t)^{1/2}$ for non conserved order parameter).
Along coarsening, at late times, the dominant growth mechanism is the flattening of interfaces, which is carried on by the system in order to minimize surface tension, in turn proportional to interface curvature. What is very interesting for our purposes is that, on one hand, the dynamics of interfaces in the system is driven by surface tension Υ, on the

other hand, this theory yields a simple prediction fot the scaling of $\xi(t)$. Therefore, if the value of $\xi(t)$, which we measure along fixed overlap dynamic, scales like in eq.(5.24), we may state that surface tension between DCR is present.
Are we really allowed to compare our result from fixed overalap dynamics with COP coarsening? Two basic conditions are required in order to obtain the scaling law of eq.(5.24):

- The dynamics must be local.
- The order parameter must be conserved.

In our case both conditions are fulfilled: we use a local MC algorithm and have conservation of total overlap $Q(t)$, which is our order parameter. So far, so good.
Now, is the scaling law in eq.(5.24) the only signature of COP coarsening we can look for? Indeed, there is another quantity, whose time scaling is well defined along COP coarsening, and which we can study: the total energy of the system, $E(t)$. Recall that, within coarsening, domain growth is driven by the minimization of the energy stored in interfaces, therefore we can write:

$$E(t) - k_0 \sim \mathcal{S}(t), \tag{5.25}$$

where $E(t)$ is the total energy of the system, $\mathcal{S}(t)$ measures the total area of interfaces present at time t, and k_0 is a costant depending on system energy in the phase separated equlibrium. The total area of interfaces $\mathcal{S}(t)$ may be simply assumed to scale like:

$$\mathcal{S}(t) \sim n(t)\xi^{\theta}(t), \tag{5.26}$$

where $n(t)$ is the number of domains of different phases at time t and ξ^{θ} is proportional to the size of a surface enclosing a domain of linear size ξ. Considering a system confined in a fixed volume V, we also have $n(t) = V/\xi^{d}(t)$. Therefore we can rewrite eq.(5.25) as:

$$\begin{aligned} E(t) - k_0 &\sim \mathcal{S}(t) \\ &\sim n(t)\xi^{\theta}(t) \\ &\sim \xi^{\theta-d}(t). \end{aligned} \tag{5.27}$$

Let us for a moment consider as free the exponent 1/3 of eq.(5.24), assuming that its precise value may depend on the system, and call it α. Then eq.(5.27) reads as:

$$E(t) - k_0 \sim t^{\alpha(\theta-d)}. \tag{5.28}$$

Assuming that in our system $\xi(t)$ scales like:

$$\xi(t) \sim t^{\alpha}, \tag{5.29}$$

the consistency of our data with COP coarsening can be, in turn, checked in two ways:

θ and α free. Without any assumption on the values of exponents θ and α, one can study the scaling of $E(t)$ vs. $\xi(t)$, i.e., find θ from eq.(5.27). This route allows us to check the coarsening scenario independently of the particular value of α in our system, and at the same time to work out an extimate exponent θ for the surface tension between DCR. Nevertheless, while $E(t)$ can be measured accurately, the values of $\xi(t)$ has very large error bars (cfr. sec. 4.3.2). Hence estimation of θ may be plagued by relevant errors.

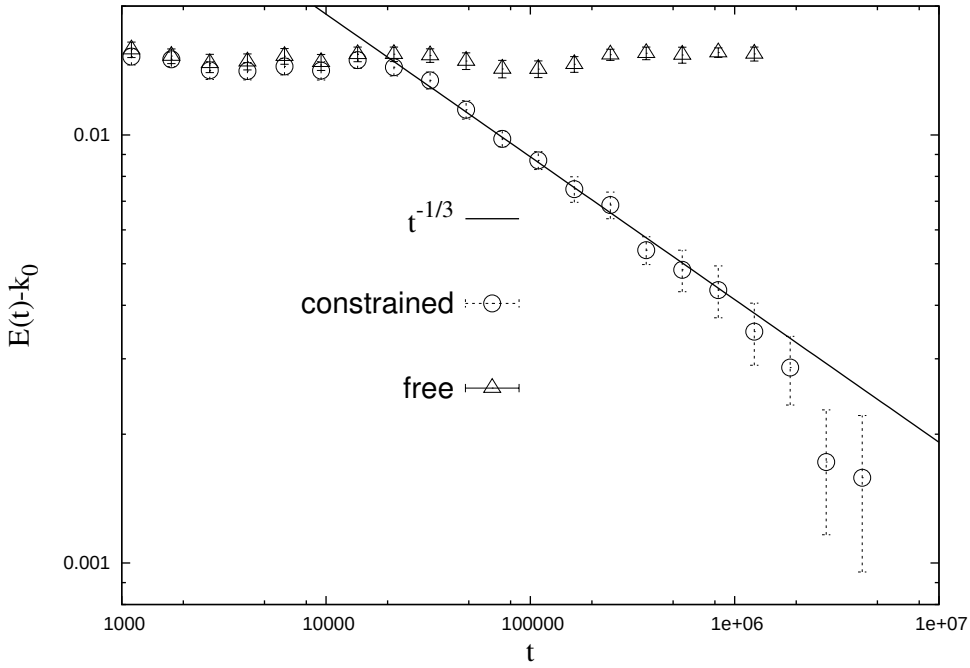

Figure 5.7: *Scaling of $\langle E(t)\rangle - k_0$ vs t; free (triangles) and constrained (circles) dynamics. k_0 is fit parameter fo $k_0 + k_1 t^{1/3}$.*

θ and α fixed. Let us assume a plain scenario, in which a good degree of universality is ascribed to the value $\alpha = 1/3$ of the coarsening exponent, and the conservative choiche $\theta = 2$ is also accepted. Evidence that the same exponent, $\theta = 2$, rules the scaling of surface tension between RFOT amorphous excitations was presented in [76] and discussed in sec.3.3.1. With θ and α fixed, only the data of $E(t)$ are needed. If energy matches with the scaling law

$$(E(t) - k_0) \sim t^{-1/3}, \tag{5.30}$$

it is enough to state that COP coarsening *is* at work. In this case we can also state that the data are compatible with the presence of interfaces between high and low overlap regions, whose energy cost is:

$$\Delta E = \Upsilon L^2, \tag{5.31}$$

with L the linear size of the interface and Υ surface tension.

Energy vs. time: checking coarsening with $\theta = 2$ and $\alpha = 1/3$. Fig.(5.7) shows the behavior of total energy $\langle E(t)\rangle$, averaged over 18 samples, along fixed overlap ($Q = 0.25$) dynamics at $T = T_c$. Data are fitted to $\langle E(t)\rangle = k_0 + bt^{-1/3}$, within the time interval where $\langle E(t)\rangle$ is decreasing, with k_0 and b fit parameters. The scaling law of eq.(5.30) fits very well our data. This analysis allows us to conclude that COP coarsening is a good model for the fixed overlap dynamics studied here.
Let us note, comparing figs. 5.7 and 4.8 in sec. 4.3.2, that $\xi(t)$ and $\langle E(t)\rangle$ saturates at different times. This may happen because $\xi(t)$ was obtained from a low-k fit of $S(k,t)$; hence, only large-scale fluctuations of the overlap field are accounted in estimating $\xi(t)$. After the moment in time when $\xi(t)$ saturates, it is still possible for the system to lower its energy by making rearrangements on small length-scales, to which the low-k tail of $S(k,t)$ is not sensitive.

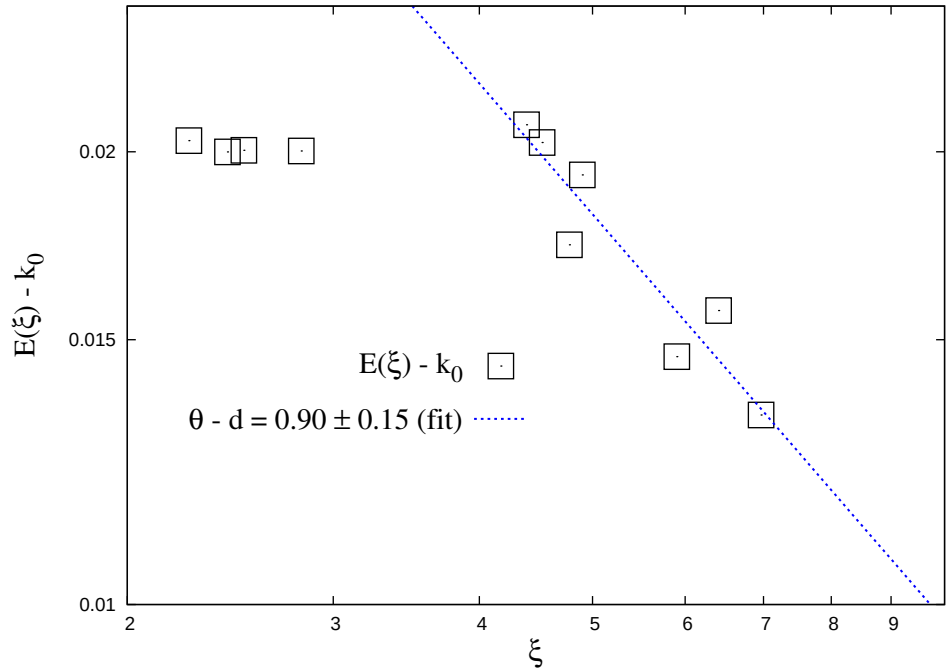

Figure 5.8: *Scaling of* $\langle E(t)\rangle - k_0$ *vs* $\xi(t)$*, squares; fit of* $(\langle E(\xi)\rangle - k_0)$ *vs* ξ^b *yields* $\theta - d = b = 1.4$*, hence, according to* $(\langle E(\xi)\rangle - k_0) \sim \xi^{\theta-d}$*,* $\theta = 1.6$ *(blue line). Data are compared to* ξ^{-1} *(red line),* $(\theta = 2)$

Energy vs. length: measuring θ. Fig. 5.8 shows the behaviour of $(\langle E(t)\rangle - k_0')$ as a function of $\xi(t)$, both considered at the same time. Hence is plotted $(\langle E(\xi)\rangle - k_0')$ vs ξ, with k_0' obtained by fitting energy data with:

$$\langle E(t)\rangle = k_0' + bt^{\alpha}. \tag{5.32}$$

Exponent α is here a fit parameter, with value $\alpha = 0.21 \pm 0.10$, which seems compatible with $\alpha = 1/3$. At early times, i.e. when $Q(t) > \hat{Q} = 0.25$, the length $\xi(t)$ is increasing whereas $\langle E(t)\rangle$ is costant, hence $(\langle E(\xi)\rangle - k_0')$ vs ξ is costant. Then is found a time interval where $\xi(t)$ is increasing and at the same time $\langle E(t)\rangle$ decreases. This is the time window in which we fit $(\langle E(t)\rangle - k_0')$ vs $\xi(t)$, finding that:

$$(\langle E(\xi)\rangle - k_0') \sim \xi^{\theta-d} \qquad \text{with} \qquad \theta - d = 0.90 \pm 0.15. \tag{5.33}$$

At larger times, while $\langle E(t)\rangle$ is still decreasing, $\xi(t)$ saturates (cfr. fig. 4.8), therefore the scaling $(\langle E(\xi)\rangle - k_0')$ vs ξ cannot be studied. From this analysis, being $d = 3$, we have $\theta = 2.10 \pm 0.15$. This direct estimate of θ, which is largely compatible with the value $\theta = 2$, yiels evidence that: 1) surface tension is present between regions with a different value of the overlap, 2) the energy cost of interfaces, which act as a drive for coarsening, scales with the size of interfaces in the same way it does in the context of RFOT excitations. Nevertheless, due to the uncertainty which plagues the estimate of $\xi(t)$ values (cfr. sec. 4.3.2), this study must be regarded with some circumspection.

Comments. If the check of COP coarsening scenario has to be considered, we regard as more reliable the test done by simply studying the scaling with time of total energy $E(t)$ along fixed overlap dynamics. The assumption that coarsening exponent is precisely $\alpha = 1/3$ also for our system appeared harmless, considering that by simply fitting energy

data is found $\alpha = 0.21 \pm 0.10$.
We can conclude that the COP coarsening scaling law:

$$(E(t) - k_0) \sim t^{-1/3}, \tag{5.34}$$

matches our data. This allows us to state that *surface tension*, at $T = T_c$, is present also between *dynamically cooperative regions*, in particular it drives a phase separation between high and low overlap regions.

Speculating a bit, we may ask why along fixed overlap dynamics something similar to coarsening —i.e., domain growth driven by surface tension— should be found. Actually, when we constrain overlap $Q(t)$, we are reducing the volume of phase space available to the system, and thus *also* total entropy is reduced. Let us call S_{constr} the entropy of the constrained system and $\Delta S = S_{free} - S_{constr} > 0$ the entropy difference between free and unconstrained system. Thus, if nothing else happens, apart the shrinking of phase space volume available, it would be:

$$\begin{aligned} f_{constr} = U - TS_{constr} &= U - TS_{free} + T\Delta S > U - TS_{free} = f_{free} \\ f_{constr} &> f_{free} \end{aligned} \tag{5.35}$$

The system, nevertheless, will always try to minimize its free-energy. Maybe, an optimization of the total energy, which compensates the loss of entropy, is the simplest way to do that. A new value of energy, U_{constr}, should be attained, $U_{constr} < U_{free}$, such that:

$$f_{constr} = U_{constr} - TS_{constr} = U_{free} - TS_{free} = f_{free}. \tag{5.36}$$

A sistem can lower its energy in many different ways. Our data are compatible with the hypothesis that interfaces with definite energy cost are present in the system, and that the total energy is decreased by reducing the size of these interfaces.

Chapter 6

Conclusions

Two competing length-scales dominated the physics of supercooled liquids along the last decade. The length-scale ξ_{DYN}, that defines the exent of dynamic correlations, and the length-scale ξ_{RFOT}. The latter, differently from ξ_{DYN}, is defined within a thermodynamic contex, the random first-order theory. Depending on the viewpoint, it is perhaps more desirable to give a thermodynamical —rather than dynamical— definition of a particular phase of matter, as it is the supercooled liquid phase. A supercooled liquid, according to RFOT, differs from a simple liquid in that it is characterized by the coexistence of many amorphous phases, each defined over the characteristic length-scale ξ_{RFOT}. These domains, being equally amorphous, are not recognizable in a snapshot of the system. Still, they are present, and moreover, according to RFOT, are divided by well defined interfaces.

We were able to measure the energy stored in these interfaces. An ad-hoc numerical method was studied and applied to circumvent the problem of locating the position of interfaces. More precisely: first, it was decided the identity of amorphous phases; second, according to this definition, an amorphous excitation was produced and its energy cost studied. This was not done arbitrarily: the identity we choosed for the phases, i.e., minima of potential energy, is deeply rooted in the physics of supercooled liquids.
The method we used to build the excitation, and in turn the interface, had two main guidelines: make it local and make it static. By exchanging particles between inherent structures, we aimed at realizing excitations which were *local* realizations of an inherent structure. Moreover, as an inherent structure is defined independently of time, its local realization appeared as a good candidate to represent a *static* excitation. This was done in order to study objects as close as possible to the excitations defined within RFOT. This set-up is also the main approximation of our work, to be accepted in order to accept, in turn, the results.

At different temperatures the system explores stationary points of the energy lanscape characterized by a different energy. As quoted in the introductory chapter, there is a well defined map between the temperature and the average energy of the inherent structures sampled by the system at that temperature. By measuring the energy stored in interfaces between IS at the same energy, and by doing this at different energies, we were able to study how surface tension Υ depends on temperature. We found that Υ decreases for increasing T and attains small values above mode coupling temperature T_c, although it is difficult to state exactly at which temperature it vanishes. The vanishing of surface tension, which marks the spinodal point for RFOT amorphous excitations, was found to be sharply defined as a function of the inherent structures energy. A spinodal energy

e_{sp} was identified where Υ vanishes. The energy e_{sp} has a value in plain agreement with the threshold energy e_{th}, which marks the saddle-minima topological crossover in the potential energy landscape. In our opinion, the coincidence $e_{th} \sim e_{sp}$ is remarkable for the following reason: whereas e_{th} is defined from a *global* feature of the system, i.e., the number of unstable directions of stationary point of energy, e_{sp} is defined studying a *local* property, i.e., the cost of an interface. This is one evidence more of how intimately the RFOT theory, which describes local activated events, and the topological crossover scenario, which describes a global property of the system, are connected. Moreover, the measure of a finite surface tension Υ, below T_c, strongly supports the "multi-state" scenario of mosaic: amorphous phases are well defined because divided by interfaces of finite energy cost.

Results on Υ fluctuations are also interesting. It is quite reasonable to imagine that, among all the mosaic states, some are more similar, others are less. Within the work of this thesis further evidence was provided that RFOT amorphous states are intimately connected with potential energy minima. Carrying on this paradigm, we can say that the definition of mosaic states is sharper the lower the temperature, as it is for configurations which are minima of potential energy landscape (PEL). As the surface tension is determined by the mismatch between mosaic states, we expect it to be defined more sharply when states are well distinguished, hence at low temperatures. Clearly, when talking about how sharply an observable is defined, we refer to the width of its distribution. Also, Υ is the average over the cost of all the unitary elements of an interface: it is therefore reasonable to expect that Υ fluctuations are smaller the larger the interface. Hence, we can expect that, the larger the linear size ξ_{RFOT} of an amorphous excitation, the smaller the fluctuations of its energy cost. Recalling that ξ_{RFOT} increases as the temperature is decreased, we can guess that two main effects are competing in determining the shrinking of surface tension fluctuations when going deeply supercooled: the more pronounced difference between phases and the larger size of droplets. By measuring the surface tension between a whole population of amorphous states, we checked that these were not only speculations. Without going further into details, we found that, for increasing sizes, the amorphous droplets show decreasing fluctuations in their surface cost.

The shape of the surface tension distribution of a size $\xi_{RFOT}(T)$ droplet, at temperature $T = 0.89\ T_c$, was found in plain agreement with the prediction already given on that in a completely different framework, i.e., by measuring the behaviour of the point-to-set correlation function [6]. This datum is particularly significative in that the point-to-set correlation function, until now, was the only one able to capture the increse of ξ_{RFOT} in the supercooled liquid phase. The simplest version of RFOT [4] predicts a sharp transition from non-ergodic to ergodic behavior at the length-scale ξ_{RFOT}. As a matter of fact this transion appeared much smoother in numerical experiments, so that surface tension fluctuations were introduced to account for this [6]. At that stage, people who are not supporters of RFOT were perhaps allowed to say that the fluctuating surface tension was an ad-hoc ingredient of the theory. Our finding of a surface tension distribution in *quantitive* agreement with the expectations from the behaviour of the point-to-set coorelation function is therefore remarkable.

Checked that surface tension is a good order parameter, in order to decide whether neighbouring bunch of particles are in the same amorphous phase or not, we used it as a tool to study the relaxational dynamics of amorphous droplets. The distinguishing feature of a supercooled liquid is its increasing relaxational time τ: succeeding in predicting a behaviour of τ in agreement with experimental data is therefore of primary importance

for RFOT. The relation between τ and ξ_{RFOT} is determined by the exponent ψ of the free energy cost ΔF to rearrange a region of linear size ξ_{RFOT}: $\tau \sim \exp(\Delta F/T) \sim \exp(\xi^{\psi}_{RFOT}/T)$. Studying the relaxation of amorphous droplets, we were able to estimate ψ. That is, we found that ΔF scales linearly with ξ_{RFOT}: $\Delta F \sim \xi_{RFOT}$, $\psi = 1$. This piece of information, together with the measure exponent $\theta = 2$, which rules the scaling of droplets energy cost, allowed us to derive the Vogel-Fulcher-Tamman law within the formalism of RFOT. The VFT law is probably the most famous phenomenological law which links time and temperature in fragile glass-forming liquids, providing good fits of experimental data. Beacause of that, there is a widespread attitude in modeling the theoretical details of RFOT theory in order to work out VFT from RFOT. The debate is precisely focused on the values of the exponents θ and ψ, which are not strictly fixed by the RFOT theory. We walked along this same path, but precisely in the opposite direction. Starting with no theoretical claims on the values of ψ and θ we fixed them from numerical simulations: they turned out to be perfectly suited to give VFT back from RFOT.

Last but no least, a comment on the interplay between surface tension and dynamical heterogeneities. The approximation of RFOT amorphous states with inherent structures, together with our method to mimic RFOT excitations, could be criticized. That is why surface tension was investigated also in a completely different framework, i.e., fixed overlap dynamics. In this framework we studied the behaviour of dynamical, rather than statical, cooperative excitations. On one hand, we lost a clear connection with RFOT; on the other hand, we studied excitations spontaneously forming in the system and detectable by means of a standard kind of correlation function, i.e., the four-point correlation function $g_4(r,t)$ —or its fourier transform $S_4(k,t)$. According to our data the lengh-scale $\xi(t)$ of dynamical correlations behaves differently whether dynamics is constrained or not; more precisely, instead of decaying with time, the extent of dynamical correlations increases and levels off at a finite value under the effect of the constraint. We propose that a phase separation between high an low overlap regions occours, driven by the surface tension stored in the interfaces between regions with a different value of overlap. This scenario is supported by the behaviour of the total energy of the system: this is in plain agreement with the predictions of conserved order parameter coarsening.
Fixed overlap dynamics was studied at mode coupling temperature T_c, at which there are indications that both dynamic, ξ_{DYN}, and static, ξ_{RFOT}, correlation lengths are finite [6, 12, 45]. First remark: although studying dynamically cooperative regions instead RFOT excitations, we found another evidence supporting the existence of interfaces with a finite surface tension in the supercooled liquid phase. Second, and last, remark: we ended up with the evidence that at T_c not only static and dynamic correlation lengths are both finite, but also both static and dynamic excitations are separated by interfaces with a finite energy cost. This is perhaps a good starting point for further investigations aimed at finding the common physical roots of static and dynamic exctitations in supercooled liquids.

Bibliography

[1] J. C. Dyre. Colloquium: The glass transition and elastic models of glass-forming liquids. *Rev. Mod. Phys.*, 78:953–972, July 2006.

[2] M. Goldstein. Viscous Liquids and the Glass Transition: A Potential Energy Barrier Picture. *J. Chem. Phys.*, 51:3728–3739, November 1969.

[3] T.R. Kirkpatrick, D. Thirumalai, and P.G. Wolynes. Scaling concepts for the dynamics of viscous liquids near an ideal glassy state. *Phys. Rev. A*, 40:1045–1054, 1989.

[4] J.-P. Bouchaud and G. Biroli. On the Adam-Gibbs-Kirkpatrick-Thirumalai-Wolynes scenario for the viscosity increase in glasses. *J. Chem. Phys.*, 121(15):7347–7354, 2004.

[5] F. H. Stillinger and T. A. Weber. Hidden structure in liquids. *Phys. Rev. A*, 25:978–989, February 1982.

[6] G. Biroli, J.-P. Bouchaud, A. Cavagna, T. S. Grigera, and P. Verrocchio. Thermodynamic signature of growing amorphous order in glass-forming liquids. *Nature Phys.*, 4:771–775, 2008.

[7] S. Whitelam, L. Berthier, and J. P. Garrahan. Dynamic Criticality in Glass-Forming Liquids. *Phys. Rev. Lett.*, 92(18):185705–+, May 2004.

[8] F. Ritort and P. Sollich. Glassy dynamics of kinetically constrained models. *Adv. Phys.*, 52:219–342, June 2003.

[9] G. Biroli and J.-P. Bouchaud. Diverging length scale and upper critical dimension in the mode-coupling theory of the glass transition. *Europhys. Lett.*, 67(1):21–27, 2004.

[10] G. Biroli, J.-P. Bouchaud, K. Miyazaki, and D. R. Reichman. Inhomogeneous Mode-Coupling Theory and Growing Dynamic Length in Supercooled Liquids. *Phys. Rev. Lett.*, 97(19):195701–+, November 2006.

[11] S. Franz and A. Montanari. Analytic determination of dynamical and mosaic length scales in a Kac glass model. *J. Phys A: Math. Gen.*, 40:251–+, March 2007.

[12] S. Karmakar, C. Dasgupta, and S. Sastry. Growing length and time scales in glass-forming liquids. *Proc. Natl. Acad. Sci.*, 106:3675–3679, March 2009.

[13] G. Adam and J. H. Gibbs. On the Temperature Dependence of Cooperative Relaxation Properties in Glass-Forming Liquids. *J. Chem. Phys.*, 43:139–146, July 1965.

[14] W. Götze. Aspects of structural glass transitions. In Hansen et al. [19].

[15] J.P. Hansen and I.R. McDonald, editors. *Theory of Simple Liquids*. Academic Press, London, 1986.

[16] W. Kob and H. C. Andersen. Testing mode-coupling theory for a supercooled binary Lennard-Jones mixture. II. Intermediate scattering function and dynamic susceptibility. *Phys. Rev. E*, 52:4134–4153, October 1995.

[17] B. W. Downs W. E. Britton and J. Downs, editors. *Lectures in Theoretical Physics*. Wiley, New York, 1961.

[18] H. Mori. Transport, Collective Motion, and Brownian Motion. *Progr. Theor. Phys.*, 33:423–455, March 1965.

[19] J. P. Hansen, D. Levesque, and J. Zinn-Justin, editors. *Liquids, freezing, and the glass transition*. Proceedings of the LI Les Houches summer school. North-Holland, 1987.

[20] J.-P. Bouchaud, L. Cugliandolo, J. Kurchan, and M. Mézard. Mode-coupling approximations, glass theory and disordered systems. *Phys. A*, 226:243–273, February 1996.

[21] T. R. Kirkpatrick and D. Thirumalai. Mean-field soft-spin Potts glass model: Statics and dynamics. *Phys. Rev. B*, 37:5342–5350, April 1988.

[22] A. Cavagna, I. Giardina, and G. Parisi. Stationary points of the Thouless-Anderson-Palmer free energy. *Phys. Rev. B*, 57:11251–11257, May 1998.

[23] A. Cavagna, I. Giardina, and G. Parisi. Role of saddles in mean-field dynamics above the glass transition. *J. Phys. A: Math. Gen.*, 34:5317–5326, July 2001.

[24] A. Cavagna. Supercooled liquids for pedestrians. *Phys. Rep.*, 476:51–124, June 2009.

[25] S. Sastry, P. G. Debenedetti, and F. H. Stillinger. Signatures of distinct dynamical regimes in the energy landscape of a glass-forming liquid. *Nature Phys.*, 393:554–557, June 1998.

[26] A. Cavagna. Fragile vs. strong liquids: A saddles-ruled scenario. *Europhys. Lett.*, 53:490–496, February 2001.

[27] T.S. Grigera, A. Cavagna, I. Giardina, and G. Parisi. Geometric approach to the dynamic glass transition. *Phys. Rev. Lett.*, 88(5):055502, Jan 2002.

[28] T.S. Grigera. Geometrical properties of the potential energy of the soft-sphere binary mixture. *J. Chem. Phys.*, 124(6):064502, 2006.

[29] A.W. Kauzmann. *Chem. Rev.*, 43:219, 1948.

[30] J.H. Gibbs and E.A. DiMarzio. Nature of the glass transition and the glassy state. *J. Chem. Phys.*, 28(3):373–383, 1958.

[31] T. R. Kirkpatrick and P. G. Wolynes. Stable and metastable states in mean-field potts and structural glasses. *Phys. Rev. B*, 36(16):8552–8564, Dec 1987.

[32] B. Derrida. Random-energy model: An exactly solvable model of disordered systems. *Phys. Rev. B*, 24:2613–2626, September 1981.

[33] D. S. Fisher and D. A. Huse. Nonequilibrium dynamics of spin glasses. *Phys. Rev. B*, 38:373–385, July 1988.

[34] A. Cavagna, T.S. Grigera, and P. Verrocchio. Mosaic multistate scenario versus one-state description of supercooled liquids. *Phys. Rev. Lett.*, 98(18):187801, 2007.

[35] C. Bennemann, C. Donati, J. Baschnagel, and S. C. Glotzer. Growing range of correlated motion in a polymer melt on cooling towards the glass transition. *Nature*, 399:246–249, May 1999.

[36] L. Berthier. Time and length scales in supercooled liquids. *Phys. Rev. E*, 69(2):020201–+, February 2004.

[37] C. Donati, S. Franz, S.C. Glotzer, and G. Parisi. Theory of non-linear susceptibility and correlation length in glasses and liquids . *J. Non-Cryst. Solids*, 307-310:215–224, September 2002.

[38] L. Berthier, G. Biroli, J.-P. Bouchaud, W. Kob, K. Miyazaki, and D. R. Reichman. Spontaneous and induced dynamic fluctuations in glass formers. I. General results and dependence on ensemble and dynamics. *J. Chem. Phys.*, 126(18):184503–+, May 2007.

[39] L. Berthier, G. Biroli, J.-P. Bouchaud, W. Kob, K. Miyazaki, and D. R. Reichman. Spontaneous and induced dynamic correlations in glass formers. II. Model calculations and comparison to numerical simulations. *J. Chem. Phys.*, 126(18):184504–+, May 2007.

[40] L. Berthier, G. Biroli, J.-P. Bouchaud, L. Cipelletti, D. El Masri, D. L'Hôte, F. Ladieu, and M. Pierno. Direct experimental evidence of a growing length scale accompanying the glass transition. *Science*, 310:1797–1800, 2005.

[41] C. Toninelli, M. Wyart, L. Berthier, G. Biroli, and J.-P. Bouchaud. Dynamical susceptibility of glass formers: Contrasting the predictions of theoretical scenarios. *Phys. Rev. E*, 71(4):041505–+, April 2005.

[42] M. M. Hurley and P. Harrowell. Kinetic structure of a two-dimensional liquid. *Phys. Rev. E*, 52:1694–1698, August 1995.

[43] A. Andreanov, G. Biroli, and J. -. Bouchaud. Mode-Coupling as a Landau Theory of the Glass Transition. *ArXiv e-prints*, March 2009.

[44] S. Franz and G. Parisi. On non-linear susceptibility in supercooled liquids. *J. Phys. Condens. Matt.*, 12:6335–6342, July 2000.

[45] C. Cammarota, A. Cavagna, G. Gradenigo, T. S. Grigera, and P. Verrocchio. Surface tension fluctuations and a new spinodal point in glass-forming liquids. *ArXiv e-prints*, April 2009.

[46] R. C. Tolman. Consideration of the gibbs theory of surface tension. *J. Chem. Phys.*, 16:758–774, 1948.

[47] F.H. Stillinger and T.A. Weber. Packing structures and transitions in liquids and solids. *Science*, 225:983–989, 1984.

[48] B. Bernu, J. P. Hansen, Y. Hiwatari, and G. Pastore. Soft-sphere model for the glass transition in binary alloys: Pair structure and self-diffusion. *Phys. Rev. A*, 36(10):4891–4903, Nov 1987.

[49] G. Parisi. Off-Equilibrium Fluctuation-Dissipation Relation in Fragile Glasses. *Phys. Rev. Lett.*, 79:3660–3663, November 1997.

[50] J.-N. Roux, J.-L. Barrat, and Jean-Pierre Hansen. Dynamical diagnostics for the glass transition in soft-sphere alloys. *J. Phys.: Condens. Matt.*, 1:7171–7186, 1989.

[51] T.S. Grigera and G. Parisi. Fast Monte Carlo algorithm for supercooled soft spheres. *Phys. Rev. E*, 63(4):045102, Mar 2001.

[52] D.C. Liu and J. Nocedal. On the limited memory BFGS method for large scale optimization. *Math. Programming*, 45:503–528, 1989.

[53] S. Boettcher. Stiffness of the Edwards-Anderson Model in all Dimensions. *Phys. Rev. Lett.*, 95(19):197205–+, November 2005.

[54] S. Franz, T. Jörg, and G. Parisi. Overlap interfaces in hierarchical spin-glass models. *J. Stat. Mech.*, 2:2–+, February 2009.

[55] E. Brézin, S. Franz, and G. Parisi. Critical interface: twisting spin glasses at T_c. *ArXiv e-prints*, August 2009.

[56] M. P. A. Fisher and M. Wortis. Curvature corrections to the surface tension of fluid drops: Landau theory and a scaling hypothesis. *Phys. Rev. B*, 29(11):6252–6260, Jun 1984.

[57] Y. Imry and S.-K. Ma. Random-Field Instability of the Ordered State of Continuous Symmetry. *Phys. Rev. Lett.*, 35:1399–1401, November 1975.

[58] D. A. Huse and C. L. Henley. Pinning and roughening of domain walls in Ising systems due to random impurities. *Phys. Rev. Lett.*, 54:2708–2711, June 1985.

[59] T. Halpin-Healy and Y. Zhang. Kinetic roughening phenomena, stochastic growth, directed polymers and all that. Aspects of multidisciplinary statistical mechanics. *Phys. Rept.*, 254:215–414, March 1995.

[60] X. Xia and P.G. Wolynes. Fragilities of liquids predicted from the random first order transition theory of glasses. *Proc. Natl. Acad. Sci.*, 97:2990–2994, 2000.

[61] M. Dzero, J. Schmalian, and P.G. Wolynes. Activated events in glasses: The structure of entropic droplets. *Phys. Rev. B*, 72(10):100201, 2005.

[62] S. Franz. First steps of a nucleation theory in disordered systems. *J. Stat. Mech.*, 2005:P04001, 2005.

[63] T. Halpin-Healy and Y. Zhang. Kinetic roughening phenomena, stochastic growth, directed polymers and all that. Aspects of multidisciplinary statistical mechanics. *Phys. Rep.*, 254:215–414, 1995.

[64] T. Halpin-Healy. Diverse manifolds in random media. *Phys. Rev. Lett.*, 62(4):442–445, Jan 1989.

[65] E. T. Seppälä, M. J. Alava, and P. M. Duxbury. Extremal statistics in the energetics of domain walls. *Phys. Rev. E*, 63(6):066110–+, June 2001.

[66] K. P. J. Kytölä, E. T. Seppälä, and M. J. Alava. Elastic manifolds in disordered environments: Energy statistics. *Europhys. Lett.*, 62:35–41, April 2003.

[67] A. Tanguy, J. P. Wittmer, F. Leonforte, and J.-L. Barrat. Continuum limit of amorphous elastic bodies: A finite-size study of low-frequency harmonic vibrations. *Phys. Rev. B*, 66(17):174205–+, November 2002.

[68] F. Léonforte, A. Tanguy, J. P. Wittmer, and J.-L. Barrat. Inhomogeneous Elastic Response of Silica Glass. *Phys. Rev. Lett.*, 97(5):055501–+, August 2006.

[69] F. Sciortino, W. Kob, and P. Tartaglia. Inherent Structure Entropy of Supercooled Liquids. *Phys. Rev. Lett.*, 83:3214–3217, October 1999.

[70] W. Cardy, editor. *Scaling and Renormalization in Statistical Phyisics*. Cambridge University Press, 1996.

[71] N. Lačević, F. W. Starr, T. B. Schröder, and S. C. Glotzer. Spatially heterogeneous dynamics investigated via a time-dependent four-point density correlation function. *J. Chem. Phys.*, 119:7372–7387, October 2003.

[72] M.E. Newman and G.T. Barkema, editors. *Monte Carlo Methods in Statistical Physics*. Oxford University Press, 1999.

[73] N. Lačević, F. W. Starr, T. B. Schröder, V. N. Novikov, and S. C. Glotzer. Growing correlation length on cooling below the onset of caging in a simulated glass-forming liquid. *Phys. Rev. E*, 66(3):030101–+, September 2002.

[74] T. Castellani and A. Cavagna. Spin-glass theory for pedestrians. *J. Stat. Mech.*, 2005(05):P05012, 2005.

[75] B. Coluzzi, M. Mézard, G. Parisi, and P. Verrocchio. Thermodynamics of binary mixture glasses. *J. Chem. Phys.*, 111(19):9039–9052, 1999.

[76] C. Cammarota, A. Cavagna, G. Gradenigo, T. S. Grigera, and P. Verrocchio. Numerical determination of the exponents controlling the relationship between time, length and temperature in glass-forming liquids. *ArXiv e-prints*, June 2009.

[77] I. M. Lifshitz. Kinetics of ordering during second-order phase transition . *Sov. Phys. JETP*, 15:939–942, November 1962.

[78] C Wagner. *Z. Elktrochem.*, 65:581, November 1961.

[79] I. M. Lifshitz and V. V Slyozov. *J. Phys. Chem. Solids*, 19:35, 1961.

[80] A. J. Bray. Theory of phase-ordering kinetics. *Adv. Phys.*, 43:357–459, May 1994.